

AN IMPLEMENTATION OF PROBABILISTIC SEISMIC HAZARD ANALYSIS
IN SELECTION OF SEISMIC COEFFICIENT FOR PSEUDO-STATIC
ANALYSIS OF SLOPE STABILITY

A THESIS SUBMITTED TO
THE GRADUATE SCHOOL OF NATURAL AND APPLIED SCIENCES
OF
MIDDLE EAST TECHNICAL UNIVERSITY

BY

KÜBRA GEDİKASLAN

IN PARTIAL FULFILLMENT OF THE REQUIREMENTS
FOR
THE DEGREE OF MASTER OF SCIENCE
IN
EARTHQUAKE STUDIES

SEPTEMBER 2017

Approval of the thesis:

**AN IMPLEMENTATION OF PROBABILISTIC SEISMIC HAZARD
ANALYSIS IN SELECTION OF SEISMIC COEFFICIENT FOR PSEUDO-
STATIC ANALYSIS OF SLOPE STABILITY**

submitted by **KÜBRA GEDİKASLAN** in partial fulfillment of the requirements for
the degree of **Master of Science in Earthquake Studies Department, Middle East
Technical University** by,

Prof. Dr. Gülbin Dural Ünver
Dean, Graduate School of **Natural and Applied Sciences** _____

Prof. Dr. Ayşegül Askan Gündoğan
Head of Department, **Earthquake Studies** _____

Assoc. Prof. Dr. Mustafa Tolga Yılmaz
Supervisor, **Engineering Science Department, METU** _____

Prof. Dr. Murat Altuğ Erberik
Co-Supervisor, **Civil Engineering Dept., METU** _____

Examining Committee Members:

Prof. Dr. Sadık Bakır
Civil Engineering Dept., METU _____

Assoc. Prof. Dr. Mustafa Tolga Yılmaz
Engineering Science Dept., METU _____

Prof. Dr. Murat Altuğ Erberik
Civil Engineering Dept., METU _____

Assoc. Prof. Dr. Sevtap Ayşe Kestel
Applied Mathematics Dept., METU _____

Assist. Prof. Dr. Ebru Akış
Civil Engineering Dept., Atılım University _____

Date: 08.09.2017

I hereby declare that all information in this document has been obtained and presented in accordance with academic rules and ethical conduct. I also declare that, as required by these rules and conduct, I have fully cited and referenced all material and results that are not original to this work.

Name, Last Name: Kübra GEDİKASLAN

Signature :

ABSTRACT

AN IMPLEMENTATION OF PROBABILISTIC SEISMIC HAZARD ANALYSIS IN SELECTION OF SEISMIC COEFFICIENT FOR PSEUDO-STATIC ANALYSIS OF SLOPE STABILITY

Gedikaslan, Kübra

MSc. in Earthquake Studies

Supervisor: Assoc. Prof. Dr. M. Tolga Yılmaz

Co-Supervisor: Prof. Dr. Altuğ Erberik

September, 2017 124 pages

The seismic coefficient, k_h , is a seismic design parameter. This parameter defines the ratio of inertial force acting on a mass to its weight, and is practically used in pseudo-static analyses of seismic slope stability. This design parameter can be assigned by the principles of performance-based design after simplifications regarding the relationship between ground displacement and probabilistic seismic hazard. A widely used simplification is to consider Newmark's sliding block analogy for estimations of seismic displacement on sloping ground. Therefore, the permanent sliding-block displacements (D) corresponding to a set of critical accelerations were computed for a sample of 70 horizontal-motion accelerograms. A prediction equation was developed by using the method of least squares. Moment magnitude, Joyner and Boore distance, style of faulting, average shear-wave velocity in top 30m were chosen as the parameters necessary for prediction of D . A probabilistic seismic hazard analysis was performed by implementing this prediction equation. A zone near Şebinkarahisar district of Giresun province was chosen as a case study. The results were used for computation of sliding (critical) accelerations corresponding to the displacements of 1 cm, 10 cm and 100 cm. The return periods of the random events that these displacement limits are exceeded were calculated. The critical

acceleration corresponding to a particular displacement threshold, related to desired performances of facilities near to sloping ground, and to a particular return period, related to intensity of ground motion to be considered in design, was supposed to be appropriate parameters for final selection of k_h . Hence, the spatial distributions of k_h on the study zone were shown. The ranges of k_h were compared with the topographical and geotechnical characteristics of the area. A criticism on the prediction equation for D was presented by putting emphasize on the variance of prediction and on the site effects.

Keywords: seismic coefficient, Newmark sliding block, slope stability, seismic hazard.

ÖZ

OLASILIKSAL DEPREM TEHLİKESİ ANALİZİ İLE ŞEV STABİLİTESİNİN PSÜDO-STATİK ANALİZİNDE KULLANILAN SİSMİK KATSAYININ BELİRLENMESİ

Gedikaslan, Kubra

Yüksek Lisans, Mühendislik Bölümü

Tez Yöneticisi: Doç. Dr. M. Tolga Yılmaz

Ortak Tez Yöneticisi: Prof. Dr. Altuğ Erberik

Eylül 2017, 124 sayfa

Sismik katsayı, k_h , sismik tasarım parametrelerinden biridir. Bu parametre kütleyle etki eden atalet yükünün kütlelerin ağırlığına oranına eşittir. Sismik katsayı deprem sırasında şev stabilitesinin psüdo-statik değerlendirmesinde kullanılmaktadır. Olasılıksal deprem tehlikesi ile deplasman ilişkilendirilerek, k_h performans temelli tasarım prensiplerine göre belirlenebilir. Sismik şev deplasmanlarının hesabı için Newmark'ın kayan blok analizi kullanılmıştır. 70 kuvvetli yer hareketi ivme kaydı ile farklı kritik ivme değerlerine karşılık gelen kalıcı blok deplasmanları, D , hesaplanmıştır. En küçük kareler yöntemi kullanılarak bir ampirik denklem oluşturulmuştur. D parametresinin tahmininde, depremin moment büyüklüğü, Joyner ve Boore mesafesi, fay tipi ve zeminde en üst 30 m içinde ortalama kesme dalgası hızının parametre olarak kullanılması gerekli görülmüştür. Bu denklem kullanılarak olasılıksal sismik tehlike analizi hesaplanmıştır. Giresun ili Şebinkarahisar İlçesi vaka bölgesi olarak belirlenmiştir. Sonuçlar, 1 cm, 10 cm ve 100 cm deplasman sınırlarının aşılmasına karşılık gelen kritik ivme değerlerinin belirlenmesi için kullanılmıştır. Yıllık tekerrür sürelerine ve kritik ivme değerlerine karşılık gelen

deplasman deęerleri hesaplanmıřtır. Kabul edilebilir deplasmana ve tekerrür süresine karşılık gelen kritik ivme deęeri ile sismik katsayı belirlenmiřtir. Bu kritik ivme deęerleri, alıřma alanının evresinde eřdeęer eęriler ile řekil üzerinde gsterilmiřtir. Elde edilen deęerler, ayrıca heyelan sahasının topografik ve geoteknik zellikleri erevesinde de deęerlendirilmiřtir. Denklemin standart sapmasının ve ortalama kesme dalga hızı parametresinin D 'ye etkisi irdelenmiřtir.

Anahtar kelimeler: sismik katsayı, Newmark analizi, řev stabilitesi, deprem tehlikesi

To My Family

ACKNOWLEDGMENTS

I would like to express my deepest gratitude to my supervisor Assoc. Prof. Dr. M. Tolga Yılmaz for his guidance, advice, criticism, encouragements and insight throughout the research.

I wish to express my deep gratitude to my co-supervisor Prof. Dr. M. Altuğ Erberik for his excitement, guidance and constant support throughout this study.

I would like to thank the Supervising Committee Members, Prof. Dr. Sadık Bakır, Assoc. Prof. Dr. S. Ayşe Kestel and Assist. Prof. Dr. Ebru Akış for their valuable suggestions and constructive criticism.

I would like to express my deepest appreciation to my parents Serpil Gedikaslan, Ergün Gedikaslan, my sisters Büşra, Şeyda and Beyza for the support, understanding and motivation that they provided me throughout my life.

Finally, I would like to express my sincere thanks to Can Gürsoy for his support and motivation.

TABLE OF CONTENTS

ABSTRACT	v
ÖZ	vii
ACKNOWLEDGEMENTS	x
TABLE OF CONTENTS	xi
LIST OF TABLES	xiv
LIST OF FIGURES	xv
LIST OF ABBREVIATIONS.....	xviii
CHAPTERS	
1 INTRODUCTION.....	1
1.1 General	1
1.2 Literature Survey.....	4
1.3 Scope	15
2 PREDICTION OF ULTIMATE DISPLACEMENT OF A SLIDING BLOCK	17
2.1 Introduction	17
2.2 Newmark's Sliding Block Analysis	17
2.3 The Empirical Prediction Equation for D	20
2.3.1 The Linear Model.....	20
2.3.2 The Sample of Accelerograms	21

2.4 The Prediction Equation for D	26
2.5 Discussion	39
3 A CASE STUDY ON THE USE OF PSHA FOR A DECISION ON SEISMIC COEFFICIENT	47
3.1 Introduction	47
3.2 Seismic Hazard Analysis.....	48
3.2.1 Integration of Hazard on a Site.....	48
3.2.1.1 Description of $f_{Ri}(m,r)$	49
3.2.1.2 Description of $f_{mi}(m)$	49
3.2.1.3 The Concept of Return Period.....	57
3.3 The Case Study of Şebinkarahisar	59
3.3.1 Seismic Activity Around Şebinkarahisar	62
3.3.2 Geometric Extends of Seismic Sources around Şebinkarahisar.....	67
3.3.3 Magnitude-Recurrence Relationships for Sources	68
3.3.4 Seismic Hazard Analysis in terms of D	71
3.3.5 The selection of Seismic Coefficient	73
3.3.6 Mapping Critical Slopes.....	81
3.4 Discussion	87
4 SUMMARY AND CONCLUSIONS.....	93
4.1 Summary	93

4.2 Conclusions	94
4.3 Future Studies.....	95
REFERENCES.....	97
APPENDICES.....	107
A. LIST OF SEISMIC EVENTS	107
B. LIST OF <i>D</i> SAMPLES	109
C. UDIM CATALOG FOR EVENTS.....	113
D. THE LIST OF DECLUSTERED EVENTS FOR BACKGROUND SEISMICITY	121

LIST OF TABLES

Table 1.1 Typical values of k_h (compiled by Melo and Sharma, 2004)	4
Table 1.2 The prediction equations for the ultimate displacement of Newmark's sliding block analogy	9
Table 2.1 The site classes according to NEHRP Provisions (BSSC, 2009).....	26
Table 2.2 Sample of D (cm) for the summary of results generated by SLAMMER.	27
Table 2.3 The functional forms considered for prediction of D (cm)	31
Table 2.4 Sample standard deviations of empirical block-displacement predictions	37
Table 2.5 P -values for a set of equation in Table 2.3	45
Table 3.1 Typical values and relationship between P_R , T_L and T_R (after Solomos, 2008)	58
Table 3.2 Importance classes and recommended values for γ for buildings (Bisch et al., 2011)	59
Table 3.3 NAF length and estimated M_W for a rupturing segment of NAF	62
Table 3.4 A sample of seismic events compiled from the catalog (UDIM, 2014)....	63
Table 3.5 The empirical linear relationships between magnitude scales	64
Table 3.6 The period of completeness for magnitude ranges.....	65

LIST OF FIGURES

Figure 1.1 Pseudo-static slope stability analysis.....	3
Figure 1.2 Newmark’s sliding block analogy for sloping ground	3
Figure 1.3 The capacity spectrum method (Freeman, 1998).....	11
Figure 1.4 The relationships between seismic intensity and performance level (National Research Council, 2003).....	13
Figure 1.5 The relationship between k_h , a_c and D (Rampello et al., 2010).....	13
Figure 1.6 The steps in PSHA (after McGuire, 2004)	14
Figure 2.1 An illustration of the Newmark’s sliding block analysis (Kramer, 1996).....	19
Figure 2.2 The sample’s histogram for SRSS of PGA in the sample	23
Figure 2.3 The sample’s histogram for M_W of events in the sample.....	23
Figure 2.4 The scattering of R_{jb} with M_W in the sample (the data for $R_{jb}=0$ is located on horizontal axis) (<i>SS</i> : Strike-slip, <i>R</i> : Reverse, <i>N</i> : Normal)	24
Figure 2.5 The histogram for style of faulting in the sample (<i>SS</i> : Strike-slip, <i>R</i> : Reverse, <i>RQ</i> : Reverse oblique, <i>NQ</i> : Normal oblique, <i>N</i> : Normal).....	24
Figure 2.6 The histogram for site conditions in the sample	25
Figure 2.7 The relationship between a_c , D and SoF in case $R_{jb}=10\text{km}$	33
Figure 2.8 The relationship between R_{jb} and D in case V_{S30} is 300 m/s, a_c is 0.10g, and SoF is <i>SS/N</i>	34
Figure 2.9 The relationship between V_{S30} and D in the case M_W is 7.0 R_{jb} is 10 km, and SoF is <i>SS/N</i>	34
Figure 2.10 The relationship between R_{jb} and D in the case that a_c is 0.10 g, V_{S30} is 300 m/s and SoF is <i>SS/N</i>	35
Figure 2.11 The plot of residuals versus (a) M_W , (b) V_{S30} , (c) R_{jb} , (d) a_c , (e) f_r , and (f) D estimated by Equation 2.3.....	38
Figure 2.12 The comparison of predictions among a set of prediction equations	41
Figure 2.13 The comparisons of predicted D with computed D for a set of prediction equations.....	41

Figure 2.14 The differences between maximum and SRSS of the two components of D	43
Figure 2.15 The comparison of predicted D with computed D according to Equation 2.4	44
Figure 3.1 The magnitude-recurrence models: (a) exponential, (b) truncated exponential and (c) characteristic	50
Figure 3.2 The determination of period of completeness according to TCEF (Nasır et a., 2013)	56
Figure 3.3 Landslide map around Şebinkarahisar (Duman et al., 2007)	60
Figure 3.4 Earthquakes since 1939 on NAF (Barka et al., 2002).....	62
Figure 3.5 The relationship between magnitude scales: (a) M_B to M_W , (b) M_S to M_W , (c) M_L to M_W , and (d) M_D to M_W	65
Figure 3.6 Declustered catalog of events around Şebinkarahisar	66
Figure 3.7 Accumulation rate of M_W around Şebinkarahisar	66
Figure 3.8 a) The area and b) fault sources used in the study	67
Figure 3.9 The magnitude-recurrence relationship used in analyses	71
Figure 3.10 The calculation (grid) points shown by triangles.....	72
Figure 3.11 The relationship between T_R , a_c and D for coordinates 38.40°E and 40.30°N a)to conversion b) to selection.....	76
Figure 3.12 The spatial distribution of k_h for $D_{all} =1$ cm, $T_R=475$ yr and $V_{S30}=300$ m/s.....	77
Figure 3.13 The spatial distribution of k_h for $D_{all} =10$ cm, $T_R=475$ yr, and $V_{S30}=300$ m/s.....	78
Figure 3.14 The spatial distribution of k_h for $D_{all} =10$ cm, $T_R= 2475$ yr and $V_{S30}=300$ m/s.....	78
Figure 3.15 The annual rate of exceedance versus a_c for $D_{all}=1$ cm, $D_{all} =10$ cm and $D_{all} =100$ cm for the coordinates 38.40°E and 40.30°N	80
Figure 3.16 The relationship between D and V_{S30} on the coordinates 38.40°E and 40.30°N in case $T_R=475$ years	80
Figure 3.17 Spatial distribution of k_h for $D=1$ cm, $T_R=475$ yr and $V_{S30}=700$ m/s.....	81
Figure 3.18 Residual shear strength of soil (after Skempton, 1964).....	82

Figure 3.19 The clayey deposits on an unstable cut on landslide zone near Şebinkarahisar.....	83
Figure 3.20 The forces acting on a section of an infinite slope	84
Figure 3.21 The limit for $\theta(\%)$ corresponding to k_h in Figure 3.13 (continuous black lines) and the spatial distribution of topographical slope (colored fill) around Şebinkarahisar.....	86
Figure 3.22 The spatial distribution of k_h for $D_{all} = 10$ cm, $T_R = 475$ yr, and $V_{S30} = 300$ m	89
Figure 3.23 The spatial distribution of k_h for $D_{all} = 10$ cm, $T_R = 2475$ yr, and $V_{S30} = 300$ m/s.....	90
Figure 3.24 The spatial distribution of k_h for $D_{all} = 1$ cm, $T_R = 475$ yr, and $V_{S30} = 300$ m/s.....	90
Figure 3.25 The relationship between T_R , a_c and D for coordinates 38.40°E and 40.30°N using Equation 2.3 and 2.4.....	91

LIST OF ABBREVIATIONS

A	: Fault area
a	: Activity parameter in Gutenberg Richter relationship
$a(t)$: Acceleration
a_c	: Critical acceleration
AS95	: Ambraseys and Srbulov (1995)
b	: Relative rate of different magnitudes
BG09	: Bozbey and Gundogdu (2009)
BT07	: Bray and Travararou (2007)
c	: Cohesion
C	: Constant
D	: Permanent sliding-block displacement
D_{all}	: Specific displacement limit
D_x	: Displacement of x direction
D_y	: Displacement of y direction
D_{SRSS}	: Displacement of square root of sum of squares
D_{5-95}	: Significant duration
f_r	: Dummy term for reverse and reverse oblique fault
f_N	: Dummy term for strike-slip, normal and normal-oblique fault
FS	: Factor of safety
f_{Mi}	: Probability density function for magnitude
f_{Ri}	: Probability density function for distance
g	: Gravity
GMPE	: Ground motion prediction equations
HF84	: Hynes-Griffin and Franklin (1984)
J107	: Jibson (2007) for equations i in Table 1.2
J207	: Jibson (2007) for equations ii in Table 1.2
I_a	: Arias intensity
k	: Slope of the hazard curve

k_h	: Seismic coefficient
M_L	: Local (Richter) magnitude
M_{max}	: Minimum magnitude
M_{min}	: Maximum magnitude
MTA	: General Directorate of Mineral Research and Exploration
M	: Event magnitude
M_D	: Duration magnitude
M_S	: Surface-wave magnitude
M_W	: Moment magnitude
N	: Normal fault
N_{eq}	: Equivalent uniform number of cycles
NAF	: North Anatolian Fault
NQ	: Normal oblique fault
P -value	: Observed significance level
PGA	: Peak ground acceleration
PGV	: Peak ground velocity
PSHA	: Probabilistic seismic hazard analysis
PI	: Plasticity index
PL	: Plastic limit
P_R	: Probability of exceedance
R_r	: Source-to-site distance
R	: Reverse fault
r^2	: Coefficient of determination
R_{jb}	: Joyner and Boore distance
R_{rup}	: Closest distance to fault rupture
RQ	: Reverse oblique fault
SRSS	: Square root of sum of squares
SS	: Strike-slip fault
SR08	: Saygili and Rathje (2008)
SRL	: Surface rupture length
SLAMMER	: Seismic Landslide Movement Modeled using Earthquake Records
SoF	: Style of faulting
PEER	: Pacific Earthquake Engineering Research Center

T	: Natural period
T_D	: Predominant period of motion
T_L	: Time span
T_{LR}	: Implicit return period
T_R	: Return period
USGS	: U.S.Geological Survey
V_{S30}	: Average shear-wave velocity in top 30 m
W	: Weight of the sliding mass
x_k	: Predictors
Y	: Strong motion parameter
\hat{y}	: Predicted value
y	: Dependent variable
λ_y	: Annual rate of exceedance
ϕ_r	: Residual friction angle
ϕ	: Internal friction angle
ν_{Mmin}	: Annual rate of events with magnitudes greater than M_{min}
μ	: Shear rigidity of the crust
σ	: Standard deviation
σ_n	: Normal stress
β	: Parameter of the exponential magnitude distribution

CHAPTER 1

INTRODUCTION

1.1 General

Seismic slope stability is generally analyzed by a pseudo-static approach, such that transient inertial loads are converted to equivalent static loads for simplified comparisons of resisting forces with driving forces acting on masses. This simplification is supposed to provide reasonably safe conclusions about slope stability. The simplicity in analyses is necessary for faster assessments of numerous sites involving severe uncertainties about material behavior and ground-water conditions. The slope stability is usually expressed by the factor of safety, FS , against failure,

$$FS = \frac{\text{available shear strength}}{\text{shear stress required to maintain equilibrium}} \quad (1.1)$$

The vertical action of seismic ground motion is generally ignored for practical reasons because its effects can be both beneficial and detrimental for slope stability due to the altering direction of load vector (Kramer, 1997). The earliest document on a pseudo-static seismic slope stability analysis was attributed to Terzaghi (1950) by Seed (1979). The total horizontal inertial load acting on a possible slip surface (or, hypothetical failure plane) is proportional to the weight of the sliding mass (W) as shown in Figure 1.1. The seismic coefficient, k_h , depends on the desired level of safety, the allowable slope displacement, and the mechanical properties of geological materials forming the sloping ground (Hynes-Griffin and Franklin, 1984; Bray et al., 1995). There is not any general consensus on the rule for selection of an appropriate

k_h for design. Considerable judgement is required for the selection of this parameter (Kramer, 1996; Bakır and Akış, 2005). Table 1.1 shows several design recommendations. Hence, this seismic-analysis parameter is frequently considered as a fraction of peak ground acceleration (PGA), or it is empirically related to the intensity of ground motion.

If the total inertial load acting on the mass above a sliding surface becomes larger than the ultimate resistance on sliding surface, this mass will be accelerated by the unbalanced inertial load. In practice, a range of residual displacement on sloping ground is allowable during severe seismic events, so that k_h can be related to a displacement limit, and to seismic hazard on a site of interest. Hence, k_h can be determined by the philosophy of performance based design, which is based on a comparison between the likelihoods of seismic actions and the specific limits for a performance parameter (Bray and Travasarou, 2011). This approach requires a reliable relationship between system properties and performance parameter of interest for any given ground-motion intensity. This performance parameter can be the total seismic displacement of unstable mass if the seismic performance of sloping ground is of concern.

The simplest method for estimation of seismic displacement of sloping ground is the use of the sliding block analogy of Newmark (1965) as shown in Figure 1.2. The threshold horizontal acceleration that will initiate sliding is named as critical acceleration, a_c . This parameter can be considered as a constant, if vertical component of transient seismic load and strength degradation of material are both disregarded. Computation of block displacements for any given a_c requires appropriate selections of ground-motion accelerograms that are related to characteristics of seismic hazard on a particular site. This is not a feasible procedure for quick assessments of sloping ground.

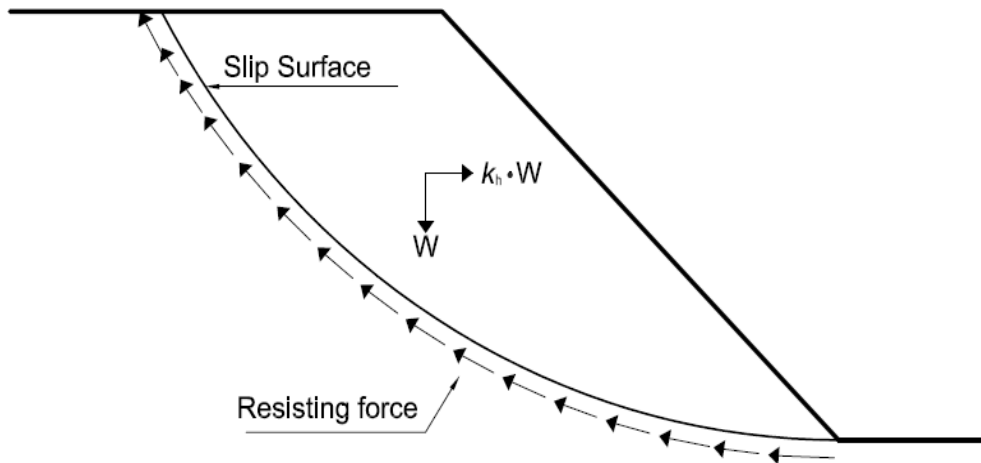


Figure 1.1 Pseudo-static slope stability analysis

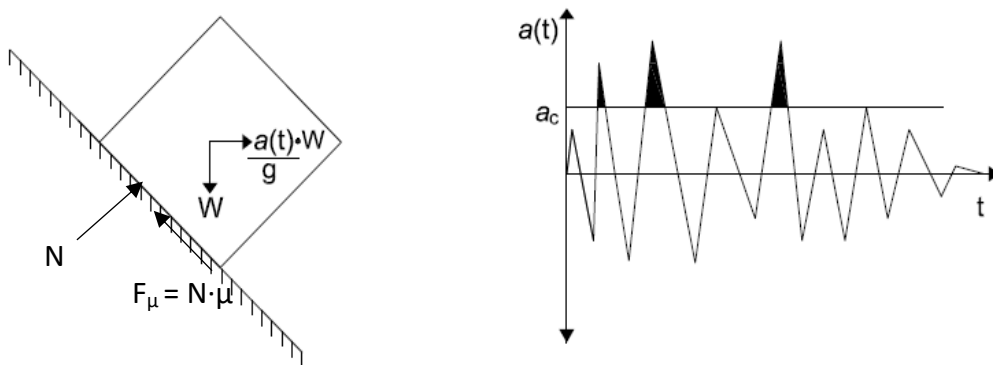


Figure 1.2 Newmark's sliding block analogy for sloping ground

In this study, a probabilistic procedure to specify k_h is discussed. It is supposed that Newmark's analogy is appropriate for estimation of total displacement of sloping ground. The basic principles of performance based design are adopted, such that k_h is defined as a function of the annual rate of exceedance for any given limit for displacement. This rate is computed by a conventional probabilistic seismic hazard analysis (PSHA). A prediction equation that is suitable for PSHA for block displacement (D) is developed by using a sample of ground-motion records. A zone

around the city of Şebinkarahisar in Turkey is chosen as a case study, because this particular zone has both severe landslide susceptibility and severe seismic hazard.

Table 1.1 Typical values of k_h (compiled by Melo and Sharma, 2004)

k_h	FS	Comments	Source
0.1		Severe earthquakes	Terzaghi (1950)
0.2		Violent destructive earthquakes	
0.5		Catastrophic earthquakes	
0.15	>1.15	With a 20% strength reduction	Seed (1979)
0.10	>1.00	Major earthquake	U.S Army Corps of Engineers (1982)
0.15	>1.00	Great earthquake	
1/3 to 1/2 PGA/g	>1.00		Marcuson and Franklin (1983)
1/2 PGA/g	>1.00	With a 20% strength reduction	Hynes-Griffin and Franklin (1984)
0.05-0.15	>1.00	Standard of practice, somewhat larger for critical conditions	Usually in the United States
0.15-0.25	>1.00	Standard of practice, somewhat larger for critical conditions	Usually in Japan

1.2 Literature Survey

Newmark's (1965) sliding-block analogy is the simplest method to estimate the total displacement of sloping ground during a seismic event (Figure 1.2). The rigid block is mobilized when the component of inertial load parallel to sliding surface exceeds the frictional resistance on inclined surface. In case the horizontal component of

ground motion is solely taken into consideration in analyses, the threshold (or, critical) acceleration, a_c , should be exceeded for mobilization of the block. Hence, a_c is the unique model parameter necessary for computation of total block displacement D . The accumulating block displacement is related to the difference between the peaks of transient-acceleration history and a_c . Hence, a_c should be equal to the peak ground acceleration (PGA) acting on the mass, if sliding is to be prevented. Otherwise, the total (or, ultimate) displacement should be computed by numerical integration. Newmark's analogy is most appropriately applied to the landslides in fairly stiff material or to relatively thin soil masses that move as a coherent mass along a well-defined slip surface. The deformability of sliding mass can have a significant effect on D for deep and soft deposits, such that D due to the assumption of rigid sliding block can reach to values about two times of the ones computed by considering the deformability of sliding block (Kramer and Smith, 1997; Gipprich et al., 2008).

More sophisticated analyses were suggested in literature to account for the fact that sliding masses are not rigid bodies, but deform internally when subjected to seismic shaking. A reasonably simple method is decoupled analysis, which involves two steps of calculation. First, the average seismic acceleration acting on sloping ground is computed by ignoring yielding. Second, D is computed for any given a_c by numerical integration as it is in the Newmark's method (Clague and Stead, 2012). The empirical design charts of Makdisi and Seed (1978) are based on decoupled analyses of earth structures. These charts are used for estimation of co-seismic displacements as a function of slope geometry, earthquake magnitude and a_c . The studies using linear viscoelastic sliding mass models have shown that decoupled approximation is unconservative. Lin and Whitman (1983) showed that the decoupled analyses yield 20% more conservative results than the coupled analyses. However, Gazetas and Uddin (1994), and Rathje and Bray (2000) showed that this level of conservatism depends on D , and on the oscillation period of deformable mass. The decoupled approximation can be particularly unconservative for intense ground motions for deep soft soil deposits (Kramer and Smith; 1997). Hence, more

accurate estimations of D are possible by using the coupled analyses rather than the decoupled analyses, but the modeling of hysteretic material behavior can hinder the simplicity in estimation of D in regional studies. On the other hand, these analyses may provide site-specific correction factors for the results of simpler sliding-block analyses.

Several prediction equations to estimate D were proposed in literature. The sliding of mass in upward direction and the vertical component of ground motion were usually ignored. These relationships, summarized in Table 1.2, were empirically determined by using results of a relatively large number of analyses. Since Newmark (1965), D has been conventionally expressed as a function of the ratio of a_c to PGA. D was shown to be dependent on the earthquake magnitude (M) as well (Yegian et al., 1991; Bray and Travarasou, 2007; Jibson, 2007). D also depends on peak ground velocity (Newmark, 1965; Whitman and Liao, 1985; Cai and Bathurts, 1996), on significant duration, (D_{5-95} - Makdisi and Seed, 1978; Bray et al. 1998), on equivalent uniform number of cycles N_{eq} and on predominant period of motion (T_D -Sarma, 1988; Yegian et al., 1991), on source-to-site distances (Ambraseys and Srbulov, 1995; Romeo, 2000), on site conditions (Romeo, 2000), and on Arias Intensity (I_a - Jibson et al., 1998; Hsieh and Lee, 2011). Particularly the parameters D_{5-95} , N_{eq} , T_D and I_a are related to M (Seed et al., 1969; Yegian et al., 1991; Wilson, 1993; Kempton and Stewart., 2006).

The prediction of D requires an estimation of PGA according to the studies presented in Table 1.2. The variability of the relationships between D and the other set of site-specific parameters hinders practical estimation of D for any specific level of seismic hazard. On the other hand, PGA is correlated with a set of seismic parameters such as event magnitude (M), source-to-site distance (R_r), style of fault rupture (SoF), and seismic site conditions (e.g., Sharma et al., 2009; Bommer et al., 2007). Therefore, a relationship between D and a_c may not require an estimation of PGA , if the seismic parameters R , M , SoF , and a site parameter are used together as predictors for D .

Probabilistic distribution of D can be computed by a conventional seismic hazard analysis.

Rathje and Saygili (2009) implemented two prediction equations (Table 1.2) in a seismic hazard analysis. Because PGA and PGV are the two predictors of these empirical relationship, these relationships were coupled with the GMPEs of Boore and Atkinson (2009) in the hazard analysis. Annual probability of exceeding a level of displacements were computed for a set of a_c . The uncertainty in geotechnical (yield strength) parameters were finally introduced in selection of k_h by applying the probabilistic logic (event) tree approach on a theoretical infinite slope. Bray and Travorou (2011) stated that k_h used in pseudostatic slope-stability analyses should be related to seismic hazard, and to seismic displacements that satisfy the seismic-safety objectives for sloping ground. k_h also depends on the source-to-site distance, and on the magnitude of design earthquake. Therefore, the principles of performance-based design should be considered in determination of k_h . Gülerce and Balal (2016) proposed a procedure to compute the seismic hazard in terms of D , by joining an empirical relationship between D , a_c and PGA, with a ground-motion prediction equation (GMPE) for PGA, in a probabilistic seismic hazard analysis. The direction of computed ground motion parameter is also of concern in seismic hazard analysis. The hazard studies are often performed for geometric mean of two horizontal components of motion at a site due to the preferences for GMPEs (Baker and Cornell, 2006a). The standard deviation of logarithm of arbitrary component of ground motion amplitude is generally larger than that of the logarithm of geometric mean of two directions (Baker and Cornell, 2006b).

The concept of performance-based seismic design is based on achieving a set of seismic performance objectives for different levels of ground-motion intensity. Priestley (2000) suggested four performance levels regarding the limits for structural damage: fully operational structure (negligible damage), the limited damage on nonessential services (minor damage), substantially protected life safety (moderate to extensive damage), and the near-collapse state (extensive damage). The performance

level of a structure for particular ground-motion intensity is calculated by simplified methods which are based on relationships between displacement of a control point and overall structural performance. Then, a relationship between spectral amplitudes of seismic-loading and displacement on a control point of structure is considered. This relatively simple procedure is known as the capacity spectrum method (Freeman, 1998). The simplified load vs. displacement relationship for a structure, namely the capacity (or, pushover) curve, is intersected with the demand spectrum that is representing a ground-motion intensity to estimate the ultimate displacement of control point as shown in Figure 1.3. The displacement-based design method of Kowalsky et al., (1995) provides another simplified procedure. In this method, the nonlinear response of a structure is reduced to the response of a viscoelastic single-degree-of-freedom oscillator to compute the seismic displacements.

The conceptual checkerboard for defining acceptable performance levels for any given intensity of seismic ground motion is shown in Figure 1.4. Levels 1 to 4 depict seismic performances. The performance objectives for buildings carrying different levels of risks are also shown in Figure 1.4. Similar objectives can be defined for the use of performance-based engineering in seismic slope stability, if Newmark's sliding block analogy is employed for estimation of ultimate slope displacement during a seismic event. Hynes-Griffin and Franklin (1984) stated that the total displacement will be limited to figures less than 100 cm, if a_c is respectively around 0.17 times PGA. Bozbey and Gundogdu (2011) concluded that this limit will be 30 cm if a_c is around 0.50 times PGA. Hence, k_h to be used in pseudo-static stability analyses can be related to a_c as shown in Figure 1.5 by supposing that the allowable displacement for a sloping ground is D_{all} (Rampello et al., 2010). A justified set of D_{all} pertinent to specific performance levels is necessary for this approach.

Table 1.2. The prediction equations for the ultimate displacement of Newmark's sliding block analogy

Reference	Expected ultimate displacement (D) due to the sliding block analogy
Newmark (1965)	$D = (V^2 \cdot (2 \cdot g \cdot a_c)^{-1}) (1 - (a_c / PGA))$
Richard and Elms (1979)	$D = 0.087 \cdot V^2 \cdot PGA^{-1} \cdot (a_c / PGA)^{-4}$
Whitman and Liao (1985)	$D = 37 \cdot V^2 \cdot PGA^{-1} \cdot \exp(-9.4 \cdot (a_c / PGA))$
Sarma (1988)	$\log\left(\frac{4 \cdot D}{c \cdot PGA \cdot g \cdot T^2}\right) = 1.07 - 3.83 \cdot \left(\frac{a_c}{PGA}\right)$
Ambraseys and Menu (1988)	$\log(D) = 0.90 + \log\left[1 - a_c / PGA\right]^{2.53} \cdot (a_c / PGA)^{-1.09}$
Yegian et. al. (1991)	$\log(D / (N_{sp} \cdot PGA \cdot T^2)) = 0.22 - 10.12 \cdot (a_c / PGA) + 16.38 \cdot (a_c / PGA)^2 - 11.48 \cdot (a_c / PGA)^3$
Ambraseys and Srbulov (1995)	$\log(D) = -2.41 + 0.47 \cdot M_s - 0.01 \cdot \log\left(\sqrt{R_f^2 + h^2}\right) + \log\left[1 - a_c / PGA\right]^{2.91} \cdot (a_c / PGA)^{-1.02}$
Cai and Bathurst (1996)	$\log(D) = 9.2 \cdot PGV^2 \cdot (g \cdot PGA)^{-1} \cdot \exp\left[-5.87 \cdot a_c / PGA\right] \cdot (a_c / PGA)^{0.49}$
Jibson et al. (1998)	$\log(D) = 1.521 \cdot \log(I_a) - 1.993 \cdot \log(a_c) - 1.546$
Romeo (2000)	$\log(D) = -1.281 + 0.648 \cdot M_L - 0.934 \cdot \log\left(\sqrt{R_c^2 + 3.5^2}\right) - 3.669 \cdot (a_c / PGA) + 0.225 \cdot s$
Stewart et al. (2003)	$\log(D \cdot (k_{\max} \cdot D_{5-95})^{-1}) = 1.87 - 3.477 \cdot a_c / PGA$
Bray and Travarasrou (2007)	$\ln(D) = -0.22 - 2.83 \cdot \ln(a_c) - 0.333 \cdot [\ln(a_c)]^2 + 0.566 \cdot \ln(a_c) \cdot \ln(PGA) + 3.04 \cdot \ln(PGA) - 0.244 \cdot [\ln(PGA)]^2 + 0.278 \cdot (M - 7)$

Table 1.2 (continued)

Reference	Expected ultimate displacement (D) due to the sliding block analogy
Jibson (2007)	
(i)	$\log(D) = 0.215 + \log\left[\left(a_c/PGA\right)^{-1.438} \cdot \left(1 - a_c/PGA\right)^{2.341}\right]$
(ii)	$\log(D) = -2.710 + \log\left[\left(1 - a_c/PGA\right)^{2.335} \cdot \left(a_c/PGA\right)^{-1.478}\right] + 0.424 \cdot M_w$
(iii)	$\log(D) = 2.401 \cdot \log(I_a) - 3.481 \cdot \log(a_c) - 3.23$
(iv)	$\log(D) = 0.561 \cdot \log(I_a) - 3.833 \cdot \log(a_c/PGA) - 1.474$
Saygili and Rathje (2008)	
(i)	$\ln(D) = 5.52 - 4.43 \cdot (a_c/PGA) - 20.39 \cdot (a_c/PGA)^2 + 42.61 \cdot (a_c/PGA)^3 - 28.74 \cdot (a_c/PGA)^4 + 0.72 \cdot \ln(PGA)$
(ii)	$\ln(D) = 2.39 - 5.24 \cdot (a_c/PGA) - 18.78 \cdot (a_c/PGA)^2 + 42.01 \cdot (a_c/PGA)^3 - 29.15 \cdot (a_c/PGA)^4 - 1.56 \cdot \ln(PGA) + 1.38 \cdot \ln(I_a)$
(iii)	$\ln(D) = -0.74 - 4.93 \cdot (a_c/PGA) - 19.91 \cdot (a_c/PGA)^2 + 43.75 \cdot (a_c/PGA)^3 - 30.12 \cdot (a_c/PGA)^4 - 1.3 \cdot \ln(PGA) + 1.04 \cdot \ln(PGV) + 0.67 \cdot \ln(I_a)$
Rathje and Saygili (2009)	
(i)	$\ln(D) = 4.89 - 4.85 \cdot (a_c/PGA) - 19.64 \cdot (a_c/PGA)^2 + 42.49 \cdot (a_c/PGA)^3 - 29.06 \cdot (a_c/PGA)^4 + 0.72 \cdot \ln(PGA) + 0.89 \cdot (M - 6)$
(ii)	$\ln(D) = -1.56 - 4.58 \cdot (a_c/PGA) - 20.84 \cdot (a_c/PGA)^2 + 44.75 \cdot (a_c/PGA)^3 - 30.5 \cdot (a_c/PGA)^4 - 0.64 \cdot \ln(PGA) + 1.55 \cdot \ln(PGV)$
Bozbey and Gundogdu (2011)	$\log(D) = -4.39 \cdot (a_c/PGA) + 1.94$
Hsieh and Lee (2011)	
(i)	$\log(D) = 0.847 \cdot \log(I_a) - 10.62 \cdot a_c + 6.587 \cdot a_c \cdot \log(I_a) + 1.84$
(ii)	$\log(D) = 11.287 \cdot a_c \cdot \log(I_a) - 11.485 \cdot a_c + 1.948$

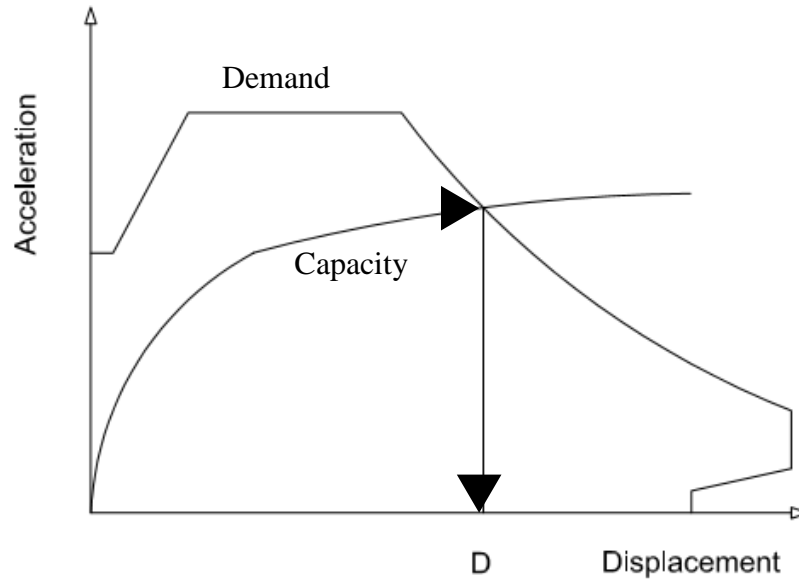


Figure 1.3 The capacity spectrum method (Freeman, 1998)

Wieczorek et al. (1985) suggested 5 cm as D_{all} for San Mateo County in California, because the settlement limit that typical buildings can withstand is between 10 and 30 cm. Keefer and Wilson (1989; quoted by Jibson and Keefer, 1993) suggested 10 cm for southern California, because the shear strength of soil will be almost reduced to its residual shear strength, which is usually much lower than the ultimate shear strength in undisturbed state. According to the State of Alaska's geotechnical evaluation criteria, the block displacements of 15 and 90 cm respectively correspond to minor and major ground adjustments for natural slopes, whereas $D = 300$ cm means catastrophic ground failure (Matasovic, 1991). Hence, D_{all} can be related to the desired seismic performance of facilities and structures near to the sloping ground. k_h is specified as the limit for a/g that satisfies the performance objective $D < D_{all}$ for any specific level of ground-motion intensity.

The procedure for prediction of the design parameters related to seismic ground motion is called Seismic hazard analysis. This procedure can be either deterministic or probabilistic. In the deterministic procedure, a particular earthquake scenario is considered (Krinitzsky, 1995). In the probabilistic procedure, the likelihoods of different scenarios are considered for computation of a weighted average. The probabilistic seismic hazard analysis (PSHA) basically includes five steps as shown in Figure 1.6 (Cornell, 1968; McGuire, 1978). The first step consists of identification of seismic sources around the site of interest (Figure 1.6.a). The probabilistic distributions of earthquake magnitude on each seismic source are modeled in the second step (Figure 1.6.b). In the third step, the probabilistic distribution of distance between site and fault rupture is modeled for each event magnitude (Figure 1.6.c). The fourth step involves the use of ground-motion prediction equations (GMPE's) to compute probabilistic distribution of a ground-motion parameter for each set of event magnitude and distance (Figure 1.6.d). Alternatively, this probability-integration problem can be solved by Monte Carlo simulation of the source activity, and by stochastic modelling ground motion (Sisi et al., 2017). The final step is the integration of uncertainties in distance, magnitude, and ground-motion parameter to the probability that a specific level of ground-motion parameter will be exceeded on a specific site during a presumed interval of time (Figure 1.6.e). The GMPE's are empirical regressions of recorded data to predict a ground-motion parameter as a function of a set of predictor parameters related to properties of seismic event, such as magnitude of earthquake (M), its distance to site (R_r), and site conditions. The model coefficients are empirically determined by using sample gathered from strong motion datasets. The site conditions also effect the ground-motion parameters. The site term generally depends on near-surface shear-wave velocity, usually expressed by the average shear-wave velocity in top 30 m of geological layers (V_{s30}). This average is calculated by considering the travel time of vertically incident waves (Borcherdt, 1994).

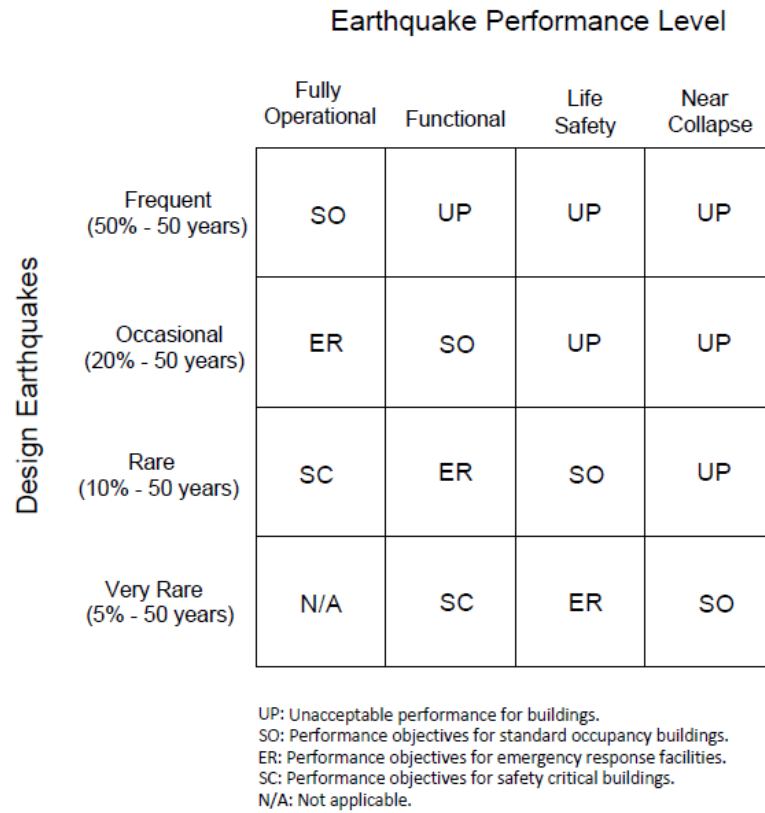


Figure 1.4 The relationships between seismic intensity and performance level (National Research Council, 2003)

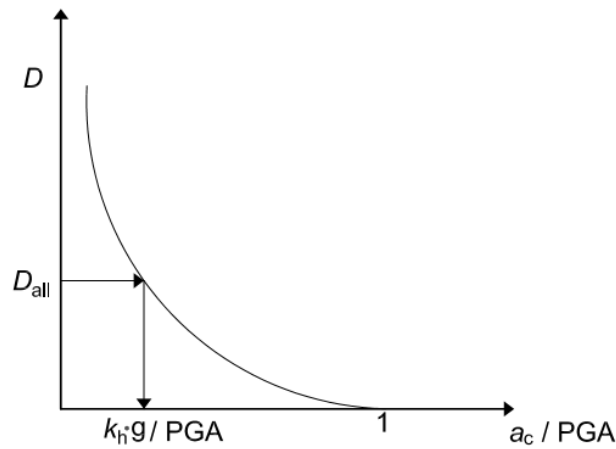


Figure 1.5 The relationship between k_h , a_c and D_{all} (Rampello et al., 2010)

In summary, it is possible to estimate the design value of k_h , by considering a specific level of seismic hazard and performance objectives for a sloping ground. The sliding-block analogy of Newmark can be a tool for simplification of response of a sloping ground, so that a relationship between k_h and the probability of exceeding D_{all} can be simply generated by seismic hazard analyses. This procedure requires a prediction equation for D that is functionally similar to GMPEs used in seismic hazard analyses.

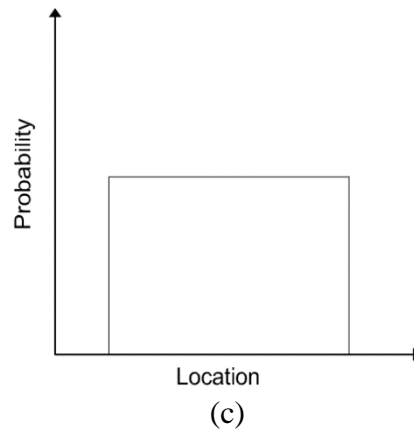
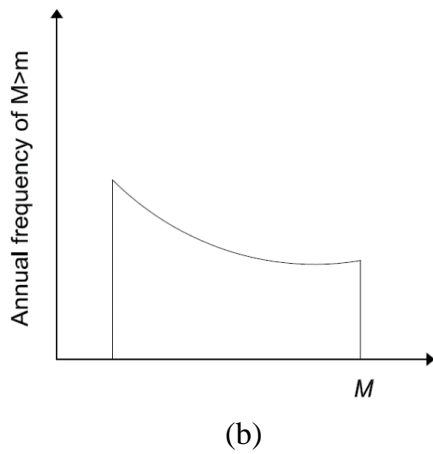
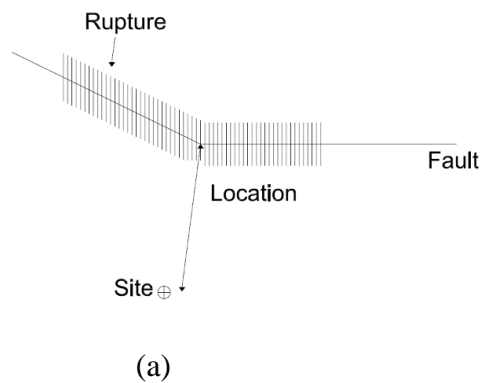


Figure 1.6 The steps in PSHA (after McGuire, 2004)

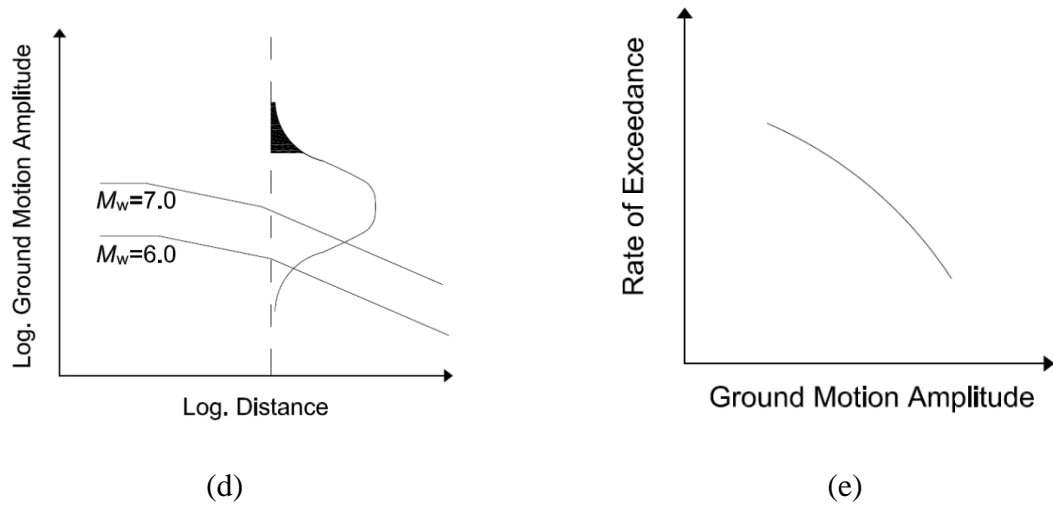


Figure 1.6 (continued)

1.3 Scope

In this study, a procedure for determination of design parameter k_h is developed. For this purpose, a prediction equation for total displacement of a sliding block (D) is empirically derived by using a sample of ground-motion accelerograms. This equation is implemented in a PSHA to produce seismic hazard curves for D . It is shown that the design parameter k_h can be derived from this hazard curve for a specific annual probability of exceedance and for a specific D_{all} , so that the concept of performance based design can be used for simplified seismic assessments of sloping ground. The application of this procedure is shown for the region around the city of Şebinkarahisar in Turkey, because the levels of landslide and seismic hazard are severely high in this region.

In chapter 1, the scope of this study is presented. A literature review on the methods and concepts that are related to the simplified assessment of seismic slope stability are presented.

In chapter 2, the Newmark's sliding block analysis is summarized. The studies that yield empirical relationships between the displacement of sliding block (D) and a set of predictor parameters are presented. Because these relationships cannot be simply implemented in a seismic hazard analysis, a new empirical relationship that is related to source and distance parameters is developed.

In chapter 3, the procedure for selection of k_h for a specific displacement limit (D_{all}) is explained, so that a performance objective can be met. The steps of probabilistic seismic hazard analysis are explained in detail. The seismic hazard is computed for a grid of coordinates around the city of Şebinkarahisar. The probabilistic modeling of seismic events on North Anatolian Fault and that of the seismic events on unmapped faults are explained. The contour maps of k_h for specific probabilities of exceedance in 50 years, and for a set of displacement limits are developed. These contours are compared with the spatial distribution of topographical slope around the city. Particular emphasize is put on the uncertainty of GMPE.

In chapter 4, a summary of this study and its conclusions are presented. The limitations of the study are discussed. Consequently, the possible future studies are suggested.

CHAPTER 2

THE PREDICTION OF ULTIMATE DISPLACEMENT OF A SLIDING BLOCK

2.1 Introduction

In this chapter, a new prediction equation for estimation of the ultimate displacement of sliding block according to the Newmark's analogy for seismic displacement of slopes was developed. The functional form and predictor parameters of this relationship are consistent with those of GMPEs used for seismic hazard analysis, so that a computer program on seismic hazard analysis can be run in order to express the hazard in terms of D . For this purpose, a sample of ground motion records was compiled. Then, the coefficients of this equation were estimated by the principle of least squares.

2.2 Newmark's Sliding Block Analysis

The total displacement of a block (D) with respect to the frictional surface can be calculated by a numerical integration of relative acceleration and velocity of sliding mass with respect to the frictional plane on rigid support (Newmark, 1965). The integration scheme is demonstrated in Figure 2.1. The acceleration history of frictional plane is defined by $a(t)$. $a(t)$ is equal to a_c , the threshold acceleration for initiation of sliding block, during sliding. A sample of $a(t)$ recorded during severe earthquakes is used for computation of D .

The characteristics of ground motion records used in the studies about the estimation of D show significant variability. For instance, Hynes-Griffin and Franklin (1984) conducted sliding block analyses with two horizontal components of 348 ground-motion and 6 synthetic records. M was smaller than 8.0 for all records. a_c was in the range from 0.05 to 0.20g. Ambraseys and Menu (1988) used 50 earthquake records to compile a sample for D . The range of M was from 6.6 to 7.3. Jibson (1993) used 11 strong motion records with I_a ranging from 0.2 m/sec to 10 m/sec. a_c was ranging from 0.02g to 0.4g. In a sequent study, Jibson (2007) used 555 strong-motion records with PGA ranging from 0.03g to 1.78g. Romeo (2000) used two horizontal components of 95 ground motion records after baseline correction and digital filtering to expel the noise in the records. The band-pass frequencies were between 0.2 and 0.5 Hz for high pass filtering. The figures were 25 and 30 Hz for the low pass filtering. M_W was between 4.6 and 6.8. Watson-Lamprey and Abrahamson (2006) used 6158 scaled records with M_W ranging between 4.5 to 7.9. Bray and Travararou (2007) used 688 ground motion records from 41 earthquakes. M_W was ranging from 5.5 to 7.6. The maximum rupture length of fault was limited to 100 km. Consequently, PGA was ranging between 0.002g and 2.7g. Bray and Travararou (2007) did not explicitly state any information about digital filtering, but they stated that the frequency range from 0.25 to 10 Hz had not been filtered out. Saygili and Rathje (2008) used the two horizontal components of 2000 scaled ground motion records with a_c ranging from 0.05g to 0.3g. Amplitude out frequencies smaller than 0.25 Hz or greater than 10 Hz were removed. Hsieh and Lee (2011) used two horizontal components of 746 ground motion records. a_c was ranging from 0.01 to 0.40g. The database was processed with baseline correction and band-pass filtering, but no further information on corner frequencies of digital filters was provided. Possibly, the corner frequencies were similar to those stated in the studies of Watson-Lamprey and Abrahamson (2006), that of Bray and Travararou (2007), and that of Saygili and Rathje (2008), because the ground motion records used in these studies extracted from same library records, namely PEER database.

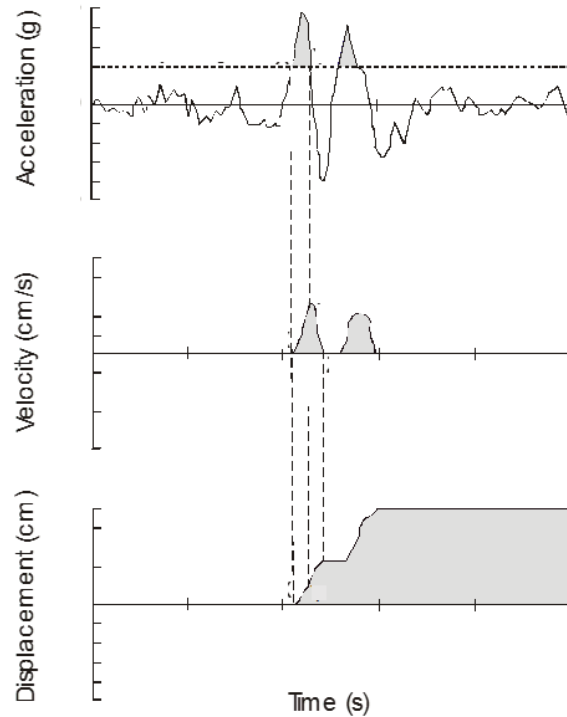


Figure 2.1 An illustration of the Newmark's sliding block analysis (Kramer, 1996)

Several mathematical procedures were followed to estimate the coefficients of predictor functions. Jibson (1993) used linear regression to estimate D by using I_a and a_c . Bray and Travararou (2007) used a probit regression model, because $D = 0$ in case $a_c \geq \text{PGA}$. The model coefficients were estimated by the method of maximum likelihood. Bray and Travararou (2007) stated that the range $D < 1$ cm is negligible for all practical purposes and considered the conditional probability that this 1 cm limit is exceeded in the prediction of D . Nonetheless the data with $D < 1$ cm was lumped at $D = 1$ cm in statistical analysis. This limit of 1 cm was also supported by Hynes-Griffin and Franklin (1984), stating that the sliding block model yield poor predictions of displacements smaller than 1 cm. These observations may be related to possible high frequency noise in the records as well. Hence, a lower limit for PGA can be necessary to limit the bias in predictions. The consequences of this limit is discussed in Section 2.5.

2.3 The Empirical Prediction Equation for D

A sample of accelerograms and the method of least-squares were used to develop an empirical prediction equation for D . This reasonably simple relationship was used for the computation of seismic hazard for sloping ground in Chapter 3. The sample properties and the linear model used for the regression of the relationship between D and a set of seismic source, distance and site parameters are presented in the following sections.

2.3.1 The Linear Model

The general objective of regression analysis is to develop a statistical relationship between a set of parameters (predictors) and a variable (Devore and Berk, 2007). In general, an additive linear regression model equation is

$$Y = \beta_0 + \beta_1 x_1 + \beta_2 x_2 + \dots + \beta_k x_k + \varepsilon \quad (2.1)$$

where β_k are model coefficients, x_k are predictors, Y is the (response) variable and ε represents random deviations. The mean and standard deviation of ε is zero and σ respectively. ε is supposed to be uncorrelated with the predictor parameters. The coefficient of determination (r^2), which is computed after estimation of model coefficients, is interpreted as the proportion of observed variation in Y that can be attributed to the changes in predictors. r^2 is between 0 and 1, and becomes closer to 1 by increasing strength of correlation. The sample size necessary for reasonable estimations of coefficients is another important question. It is recommended that the number of observations (x_k vs. y_k) should be at least 10 to 20 times the number of parameters (Devore and Berk, 2007).

Strasser et al. (2009) stated that the variability in Y , depicted by the random term ε , has a very pronounced effect on the results of seismic hazard analysis. A limited change in variability in Y can significantly change the seismic hazard, particularly the ground-

motion amplitudes pertinent to lower probability ranges for being exceeded (Bommer and Abrahamson, 2006). The statistical properties of ε are estimated by computing the statistics of residuals, which are the differences between predicted Y and observed Y for any given set of x_k . Therefore, ε is not only related to the variability in observations, but also to the choice for predictor parameters, to the functional form of empirical relationship, and to the method used for estimation of coefficients.

2.3.2 The Sample of Accelerograms

The ground-motion accelerograms were gathered from PEER strong motion database (<http://ngawest2.berkeley.edu/> last access: June 23rd 2013). The PEER database was providing 3551 three-component ground-motion accelerograms recorded during 173 shallow crustal earthquakes. The event magnitudes were ranging from 4.2 to 7.6. Each acceleration time series has been corrected by filtering out the high and the low frequency noise. The lowest limit of usable spectral frequency was determined based on the type of filter and the filter's corner frequency. A simple baseline correction was applied to the records in case the filtering could not remove non-physical trends in the displacement time series (Chiou et al., 2008). This database was chosen to compile a coherent sample of accelerograms, since it had been used in a number of studies regarding Newmark's sliding block analysis as explained in Section 2.2.

The records compiled for this study were not scaled. Only the records of which PGA of at least one of two horizontal components is greater than 0.05g was used for this study. Hence, a significant proportion of records can yield the ranges of D that are important in engineering applications. The histogram for the distribution of PGA in the sample is shown in Figure 2.2. The square root of sum of squares (SRSS) of two horizontal components of each ground-motion record was considered in the statistical analyses of the parameters related to strong ground motion records. 70 accelerograms recorded during 46 events between the years 1900 and 2013 were compiled. The catalog

information about these seismic events are presented in Appendix A. M_W of these events is ranging from 4.5 to 7.6. The histogram of M_W was shown in Figure 2.2. The median PGA, 0.31g, and the median M_W , 5.85, shows that a significant part of the sample constitutes a set of destructive ground-motion records. A reasonable uniform distribution of PGA and that of M_W in the sample is not possible because of the limitations of the sample size. R_{jb} , the closest distance to surface projection of rupture plane (Joyner and Boore, 1981), was used as the distance parameter in compilation of sample. This distance parameter is coherent for estimation of ground motion amplitudes, because it inhibits the artificial significance of hanging wall effect in the events of reverse faults (Abrahamson and Somerville, 1996). This effect was stated as the tendency of ground-motion amplitudes recorded on hanging-wall sites of reverse faults to be significantly greater than the amplitudes on footwall sites (Chang et al, 2004). The upper limit for R_{jb} was chosen as 200km. The range for R_{jb} is narrower for lower M_W because of the limitation for PGA. The scattering of R_{jb} with M_W is shown in Figure 2.4. Another parameter related to the properties of seismic source is the style of faulting, SoF . The events of database were categorized by five different classes of SoF . Figure 2.5 shows the sample's histogram for this source parameter. The sample for events on normal faults is rather limited, which is increasing the uncertainty related to the SoF parameter. The non-uniform distribution of this parameter in the sample can be attributed to the likelihood of each SoF among significant seismic events.

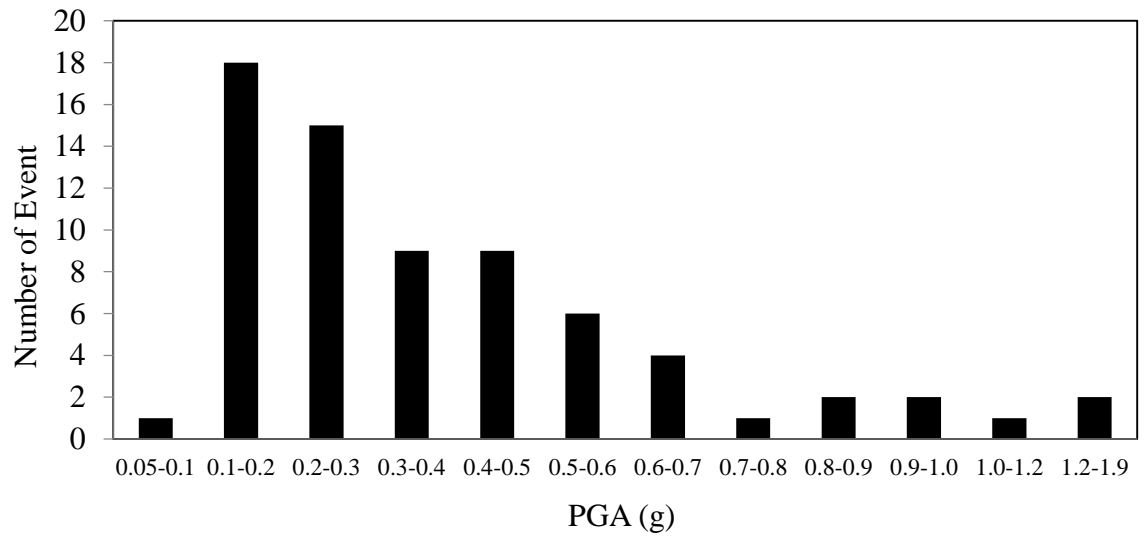


Figure 2.2 The sample's histogram for SRSS of PGA in the sample

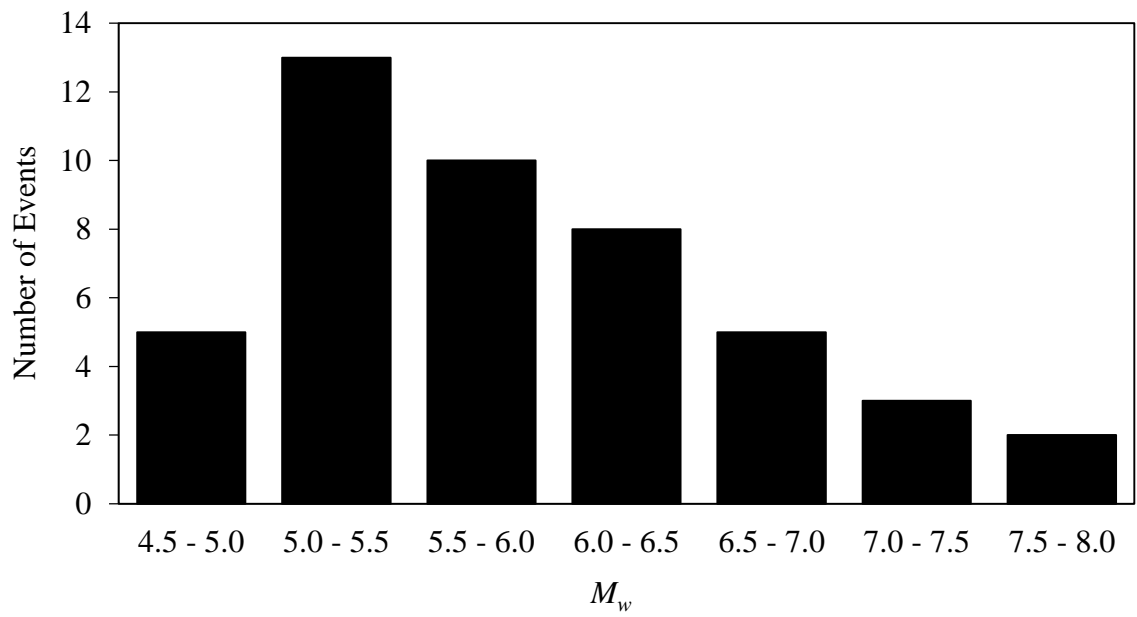


Figure 2.3 The sample's histogram for M_w of events in the sample

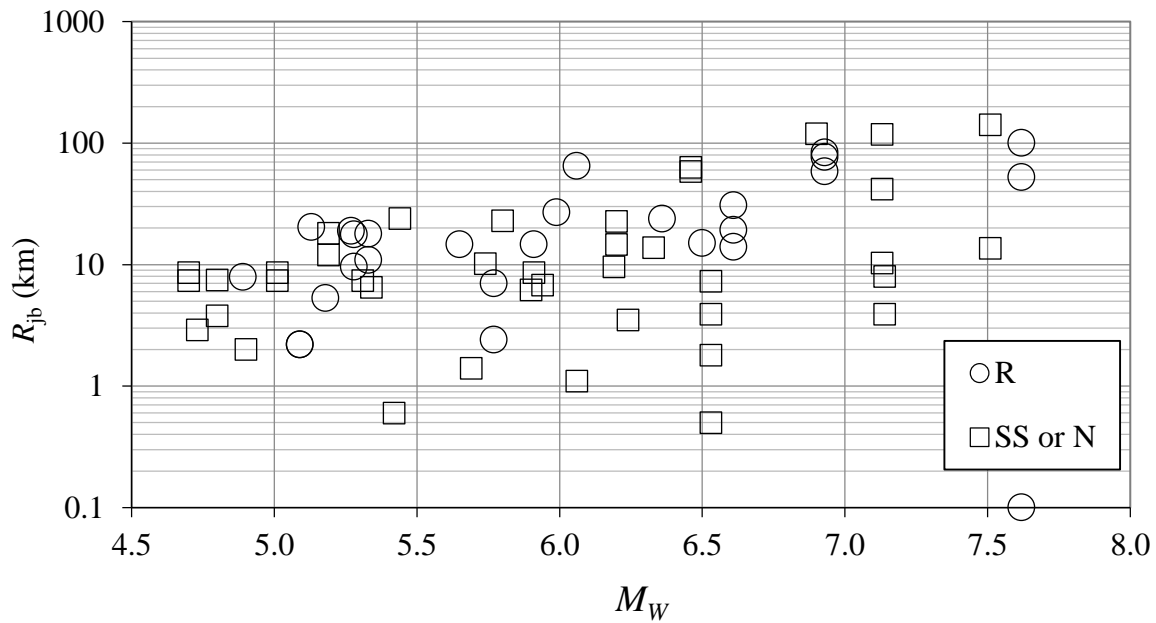


Figure 2.4 The scattering of R_{jb} with M_W in the sample (the data for $R_{jb}=0$ is located on horizontal axis. *SS*: Strike-slip, *R*: Reverse, *N*: Normal)

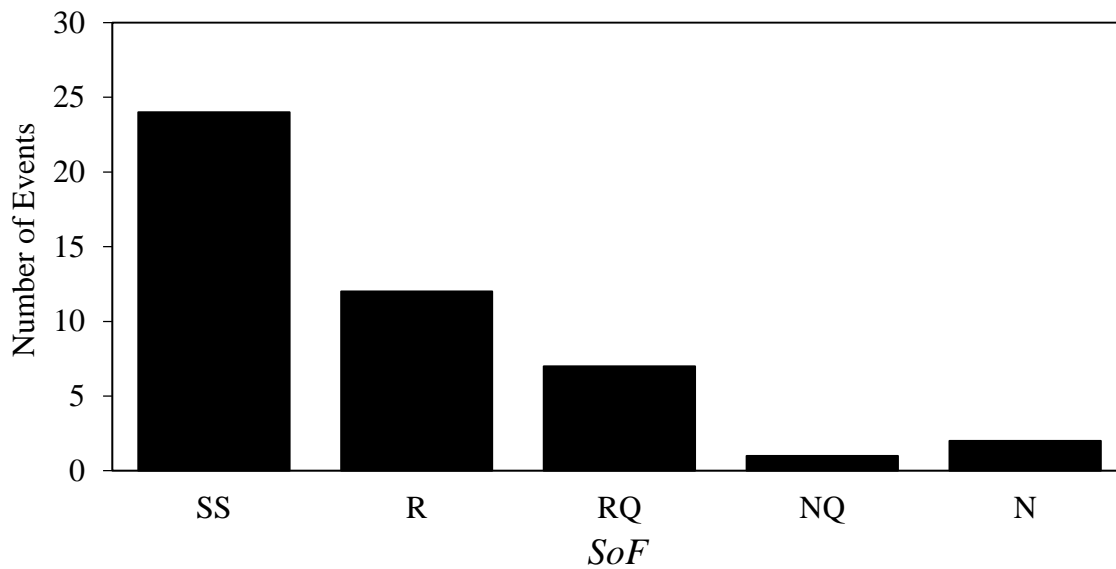


Figure 2.5 The histogram for style of faulting in the sample (*SS*: Strike-slip, *R*: Reverse, *RQ*: Reverse oblique, *NQ*: Normal oblique, *N*: Normal)

V_{S30} is the parameter depicting the site conditions for the records in PEER database. Figure 2.6 shows the histogram for V_{S30} in the sample, such that the class intervals are assigned according to the document *NEHRP Provisions* (BSSC, 2009). This site classification system shown in Table 2.1. Almost all site classes in the sample belong to class D or C, which are consistent with the applicability of Newmark’s analogy (Section 1.2). Class-E sites are on soft soils which may show rapid degradation in yield strength during severe seismic excitation. The class-A and class-B are respectively pertinent to rocks and hard rock, which are less likely to be encountered in formations susceptible to massive slope failures.

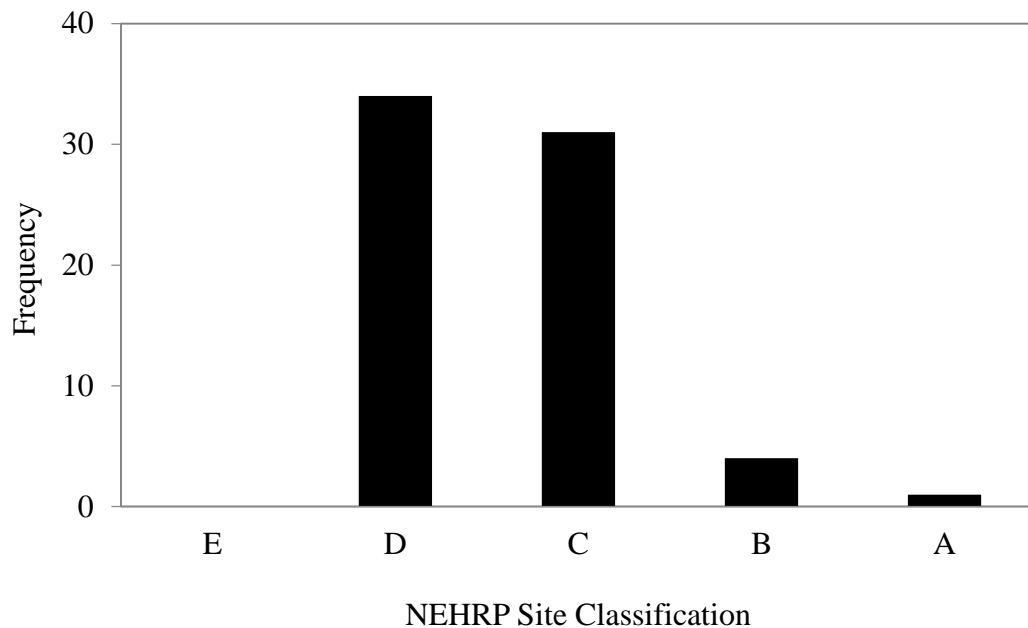


Figure 2.6 The histogram for site conditions in the sample

Table 2.1. The site classes according to NEHRP Provisions (BSSC, 2009)

Site Class	Soil Profile	Range of V_{S30} (m/s)
A	Hard Rock	$V_{S30} > 1500$
B	Rock	$760 < V_{S30} \leq 1500$
C	Very dense soil and soft rock	$360 < V_{S30} \leq 760$
D	Stiff soil profile	$180 < V_{S30} \leq 360$
E	Soft soil profile	$V_{S30} < 180$

2.4 The Prediction Equation for D

Sliding block analysis was performed by the computer program SLAMMER—Seismic Landslide Movement Modeled Using Earthquake Records (Jibson et al., 2013). SLAMMER was used for building a dataset on the relationship between D and a_c . The sample of strong-motion records were used for sliding block analysis. The ground-motion files should contain only acceleration values in units of g (the acceleration of Earth’s gravity) sampled at a constant time interval (digitization interval). A set of a_c ranging from 0.05 g to 1.20 g was entered in the program. First, the total (final) displacement of a sliding block was individually computed for two horizontal components of each ground-motion record. Then, SRSS of two horizontal displacement components was calculated. This combined displacement was supposed as a sample observation of D for any given a_c . A set of results computed by SLAMMER is shown in Table 2.2. First column shows identification numbers of earthquake records. The column headers, starting with 0.05 and ending with 1.20, depict the set of a_c in units of g . The numbers on each column shows computed D in units of cm for any record and a_c . All data for D less than 0.0001 cm were truncated to zero. The results of SLAMMER are

presented in Appendix B. Only the data for $D > 0$ was used for development of predictive equations, because the functional forms that were chosen for analyses cannot yield $D = 0$, and because the inclusion of the data for zero displacement in the sample is expected to cause excessive bias in estimations due to the relative scarcity of the data for $D > 0$ in the practical range of a_c . Consequently, a sample size of 259 was generated for SRSS of D before the estimation of model coefficients. This final sample size is supposed to be sufficient for functional forms that involve 6 prediction parameters at most.

Table 2.2. A sample of D (cm) generated by SLAMMER

No.	a_c (g)										
	0.05	0.10	0.15	0.20	0.30	0.40	0.50	0.60	0.70	1.00	1.20
1	1.89	0.07	0.00	0.00	0.00	0.00	0.00	0.00	0.00	0.00	0.00
2	0.22	0.00	0.00	0.00	0.00	0.00	0.00	0.00	0.00	0.00	0.00
3	15.17	7.84	4.35	2.05	0.08	0.00	0.00	0.00	0.00	0.00	0.00

The functional forms of a number of GMPE's were investigated to choose a set of reasonably simple predictor functions (e.g., Sarma and Free, 1995; Gulkan and Kalkan, 2002; Akkar and Boomer 2007). The distance parameters, R_{jb} and R_{rup} ; the source parameters, SoF and M_W ; and the site parameter V_{S30} are provided in the PEER database for each ground-motion record. These parameters and a_c are considered as possible predictors for D . These parameters are positive real numbers, except for SoF . This categorical parameter was represented by a binary function, f_r . f_r was set to 1 for reverse

and reverse-oblique faults, and to 0 for strike-slip, normal and normal-oblique faults. This two-class system had been used by Crouse and McGuire (1996). Further separation in these classes of *SoF* was not possible due to the limitations in data. Particularly the records originating from normal faults could not be considered in a separate class, because of the scarcity of these records. The two distance parameters, R_{jb} , widely known as the Joyner and Boore distance, and R_{rup} , the closest distance to fault rupture (Kaklamanos et al., 2011) were compared to maximize R^2 . The unit of distance parameters are km. A constant term was also added to these distance parameters, such as $\log(R_{jb}+C)$ or $\log(R_{jb}^2+C^2)^{1/2}$, in order to increase R^2 (Cornell et al., 1979; Faccioli, 1979; Abrahamson and Youngs, 1992; Joyner and Boore, 1981; Akkar et al., 2013). The constant C was determined by changing this number until R^2 was maximized such that C was truncated to the nearest 1 km.

Several additive linear regression models were examined to maximize r^2 . These models are shown in Table 2.3. The model coefficients were determined by the method of least squares. The number of coefficients to be estimated was limited to 6. Hence, the sample size of 70 ground motions records were deemed as sufficient. The regression tool of the computer program MS-Excel version 14 (Microsoft Corporation, 2010) was used for the analyses. The equations involving the parameter $\log(R_{jb})$ systematically yielded r^2 greater than the equations involving $\log(R_{rup})$. Therefore, $\log(R_{jb})$ was supposed to be a more efficient parameter than $\log(R_{rup})$. It was observed that, the improvement of R^2 due to the estimator $\log(R_{jb}^2+C^2)^{1/2}$ is not very significant with respect to the estimator $\log(R_{jb}+C)$. For instance, r^2 is 0.720 and 0.716 due to the functional forms #2 and #3 in Table 2.3 respectively. Therefore, the simpler predictor $\log(R_{jb}+C)$ was preferred for the final empirical relationship to be used in case study. A number of functions modeling the possible interaction between estimator parameters were also considered. This interaction was modeled as the product of two parameters, such as $M_W \cdot \log(V_{S30})$. However, no significant increase in r^2 was obtained. Table 2.3 also presents the conventional r^2 and r^2

that is adjusted according to the number of predictors in each functional form. Because r^2 can be artificially increased by adding unrelated parameters in the estimator function, the adjusted r^2 is a more useful parameter in comparisons prediction equations with different numbers of predictors (Devore and Berk, 2007). Consequently, the coefficients of prediction equation with the highest adjusted R^2 are

$$\log(D) = 2.753 \cdot M_w - 1.595 \cdot \log(V_{S30}) - 0.872 \cdot \log(R_{jb}^2 + 3^2) - 2.441 \cdot \log(a_c) + 0.557 \cdot f_r - 0.147 \cdot M_w^2 - 7.756 \quad (2.2)$$

σ was estimated as 0.561 for this prediction equation. Nonetheless, a number of equations, that have a simpler functional form, yield similar figures for r^2 . Hence, the contribution of some of the parameters in Equation 2.2 to $\log(D)$ is insignificant. For instance, the adjusted r^2 of the 4th Equation in Table 2.3 is 0.71, which is very close to that of 1st equation. The coefficients of this equation are

$$\log(D) = 0.933 \cdot M_w - 1.797 \cdot \log(V_{S30}) - 2.230 \cdot \log(R_{jb} + 6) - 2.409 \cdot \log(a_c) + 0.539 \cdot f_r - 0.747 \quad (2.3)$$

σ was estimated as 0.572 for this prediction equation. Equation 2.3 was chosen for the seismic hazard analysis (Chapter 3) because of its simplicity, so that only the most significant parameters were used in estimation. The effect of differences of two functional forms on the estimation was supposed to be insignificant and to be sensitive to the sample size. This equation was further investigated by plotting the response of D to the changes in predictor parameters.

Figure 2.7 shows the significance of SoF for D . The displacement estimated for reverse and reverse-oblique type fault ruptures is almost 3.5 times larger than that estimated for strike-slip, normal and normal-oblique ruptures. This is much larger than the plausible ranges for spectral acceleration, which are discussed by Bommer et al. (2003). The reverse faults are generating higher amplitudes for higher frequencies according to Choi

and Youngs (2008). The effect of *SoF* on spectral amplitudes is sensitive to event magnitude, to distance, and to distance measure. Because *SoF* is sensitive to the duration of ground motion, the spectral amplifications may not be simply correlated with *D*. Nonetheless, Sharma et al. (2009) developed a GMPE that was increasing spectral accelerations by a factor of 2 approximately for events originating from reverse faulting with respect to the events on strike-slip earthquakes. This rather extreme amplification may depict the importance of limitations in data, or the sensitivity of results to the choices for functions used for prediction equations. On the other hand, observations supporting the importance of *SoF* for landslides have been reported in literature.

Kieffer et al. (2006) studied landslides triggered by 2004 Niigata Ken Chuetsu Earthquake ($M_W=6.6$) on a thrust fault (a thrust fault is a reverse fault with a low dip angle; Bolt, 1993). It was stated that the source characteristics of this earthquake show similarities to those of 1994 Northridge earthquake ($M_W = 6.7$) in many ways. Great landslides occurred on the hanging wall (ground above a reverse fault) during both earthquakes. In both events, most of the triggered landslides were shallow failures. This observation can be explained by the high frequency shaking (Kieffer et al., 2006), which is consistent with the arguments of Choi and Youngs (2008). Chen et al. (2012) analyzed four large landslides triggered by 2008 Wenchuan Earthquake ($M_S = 8.0$) in China by using Newmark's sliding block analysis. The change of style of faulting from reverse-dominated slip to dextral slip in two segments of fault rupture was observed to have a significant effect on the maximum distance between the large landslides and the fault. It was concluded that a reverse fault could cause large landslides in a wider region than a strike-slip fault.

Table 2.3. The functional forms considered for prediction of D (cm)

No	Functional Form	r^2	Adjusted r^2
1	$\log(D) = \beta_0 M_w + \beta_1 \log(V_{S30}) + \beta_2 \log(R_{j_b}^2 + 9) + \beta_3 \log(a_c) + \beta_4 f_r + \beta_5 M_w^2 + \sigma$	0.728	0.721
2	$\log(D) = \beta_0 M_w + \beta_1 \log(V_{S30}) + \beta_2 \log(R_{j_b} + 6) + \beta_3 \log(a_c) + \beta_4 f_r + \beta_5 M_w^2 + \sigma$	0.723	0.717
3	$\log(D) = \beta_0 M_w + \beta_1 \log(V_{S30}) + \beta_2 \log(R_{j_b}^2 + 9)^{1/2} + \beta_3 \log(a_c) + \beta_4 f_r + \sigma$	0.720	0.715
4	$\log(D) = \beta_0 M_w + \beta_1 \log(V_{S30}) + \beta_2 \log(R_{j_b} + 6) + \beta_3 \log(a_c) + \beta_4 f_r + \sigma$	0.716	0.711
5	$\log(D) = \beta_0 M_w + \beta_1 \log(V_{S30}) + \beta_2 \log(R_{j_b} + 6) + \beta_3 \log(a_c) + \beta_4 f_r + \beta_5 M_w \cdot \log(R_{j_b} + 6) + \sigma$	0.716	0.710
6	$\log(D) = \beta_0 M_w + \beta_1 \log(V_{S30}) + \beta_2 \log(R_{j_b} + 6) + \beta_3 \log(a_c) + \beta_4 f_r + \beta_5 f_N + \sigma$	0.700	0.700
7	$\log(D) = \beta_0 M_w + \beta_1 \log(V_{S30}) + \beta_2 \log(R_{rup}) + \beta_3 \log(a_c) + \beta_4 f_r + \beta_5 M_w^2 + \sigma$	0.676	0.668
8	$\log(D) = \beta_0 M_w + \beta_1 \log(V_{S30}) + \beta_2 \log(R_{rup}) + \beta_3 \log(a_c) + \beta_4 f_r + \sigma$	0.667	0.660
9	$\log(D) = \beta_0 M_w + \beta_1 \log(V_{S30}) + \beta_2 \log(R_{rup}) + \beta_3 \log(a_c) + \beta_4 f_r + \beta_5 M_w \cdot \log(R_{rup}) + \sigma$	0.667	0.659
10	$\log(D) = \beta_0 M_w + \beta_1 \log(V_{S30}) + \beta_2 \log(R_{j_b} + 6) + \beta_3 \log(a_c) + \sigma$	0.660	0.655
11	$\log(D) = \beta_0 M_w + \beta_1 \log(V_{S30}) + \beta_2 \log(R_{rup}) + \beta_3 \log(a_c) + \beta_4 f_r + \beta_5 f_N + \sigma$	0.657	0.649
12	$\log(D) = \beta_0 M_w + \beta_1 \log(V_{S30}) + \beta_2 \log(R_{rup}) + \beta_3 \log(a_c) + \sigma$	0.580	0.574

Still, a well-supported explanation for the significance of SoF in prediction of D cannot be given in this study. The hanging-wall effect is not expected to be an explanation, because the distance parameter was chosen as R_{jb} . A possible bias in data may be another reason. Figure 2.4 shows that the distance parameter R_{jb} is generally greater for the records of reverse faults. The figures for the median R_{jb} are 15 km for the reverse and reverse-oblique faults, and 5 km for other styles of faulting respectively. On the other hand, the median magnitudes for these two SoF classes are almost equal. The number of ground motion records from strike-slip or normal ruptures is 41, whereas the figures are 29 for reverse faults. Hence, the ratios of two SoF in sample are reasonably similar, and their difference is not expected to cause significant bias in the results. Hence, unless this partial difference in ranges of R_{jb} provides a better explanation for the effect of SoF on D , the richer high-frequency content of ground motion after the events of reverse faults (Choi and Youngs, 2008) may be a sole explanation. This richness is expected to yield an increase in PGA, which is in turn reducing the a_c/PGA ratio, and eventually increasing D according to the studies shown in Table 1.2. Another reason can be the sensitivity of significant duration of ground motion to SoF , which is not investigated in this study. Hence, the sample size should be increased to clarify the reason of this observation, and further studies are necessary.

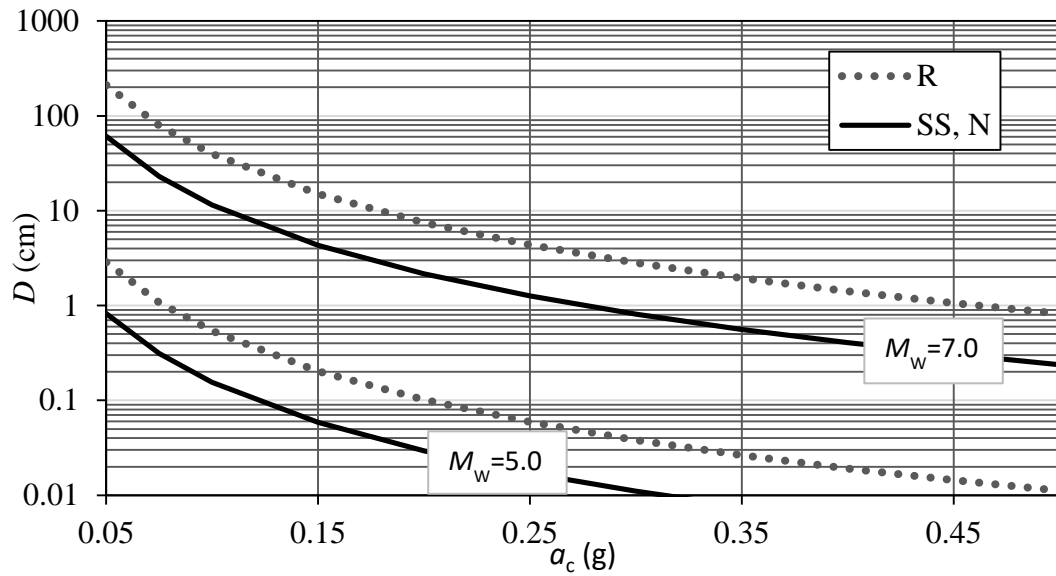


Figure 2.7 The relationship between a_c , D and SoF in case $R_{jb}=10\text{km}$

Figure 2.8 shows the relationship between R_{jb} and D in the case that V_{S30} is 300 m/s, $a_c=0.1$ g, and SoF is strike-slip or normal (SS, N). D decreases with increasing R_{jb} and with decreasing M_w . Both parameters are observed to have a very pronounced effect on D . For instance, if M_w increases from 5.5 to 6.0m, D is increased by a factor of 2.9. Figure 2.9 shows that the effect of V_{S30} on D is also very significant. Therefore, it is more likely to observe excessive seismic displacements of sloping ground on deep and relatively soft/loose soils than those on stiffer geological formations. A sloping loose soil layer resting on excessively weathered rock is expected to accumulate more seismic displacements than that on hard rock. For instance, if V_{S30} increases from 360 m/s to 760 m/s, which are the limits for the site-class C (Table 2.1), D will be decreased by a factor of 3.8. a_c is also a critically important parameter. Figure 2.9 shows the relationship between a_c and D , in the case that M_w is 7.0, R_{jb} is 10 km, and SoF is strike slip. D will decrease by 81% in case a_c is doubled.

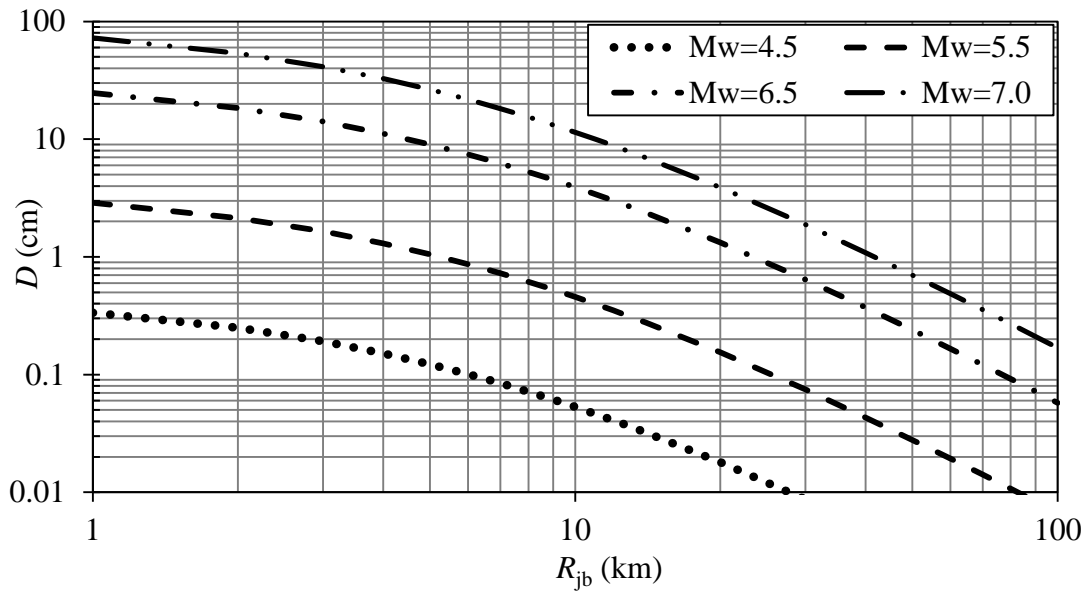


Figure 2.8 The relationship between R_{jb} and D in case V_{S30} is 300 m/s, a_c is 0.10g, and SoF is SS/N

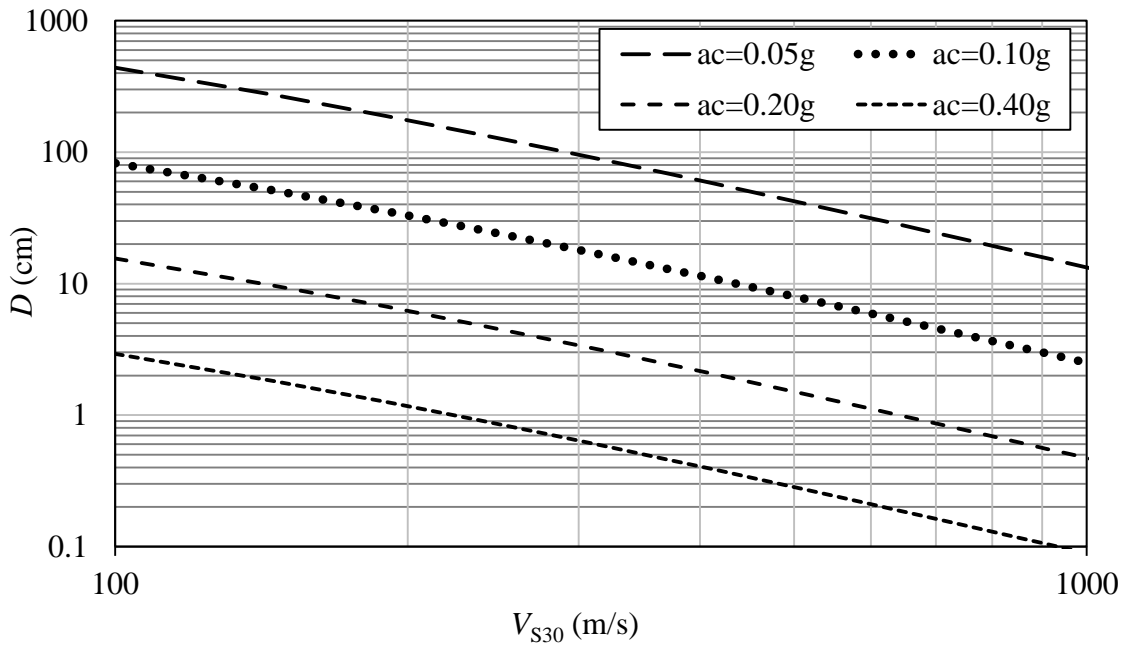


Figure 2.9 The relationship between V_{S30} and D in the case M_w is 7.0 R_{jb} is 10 km, and SoF is SS/N

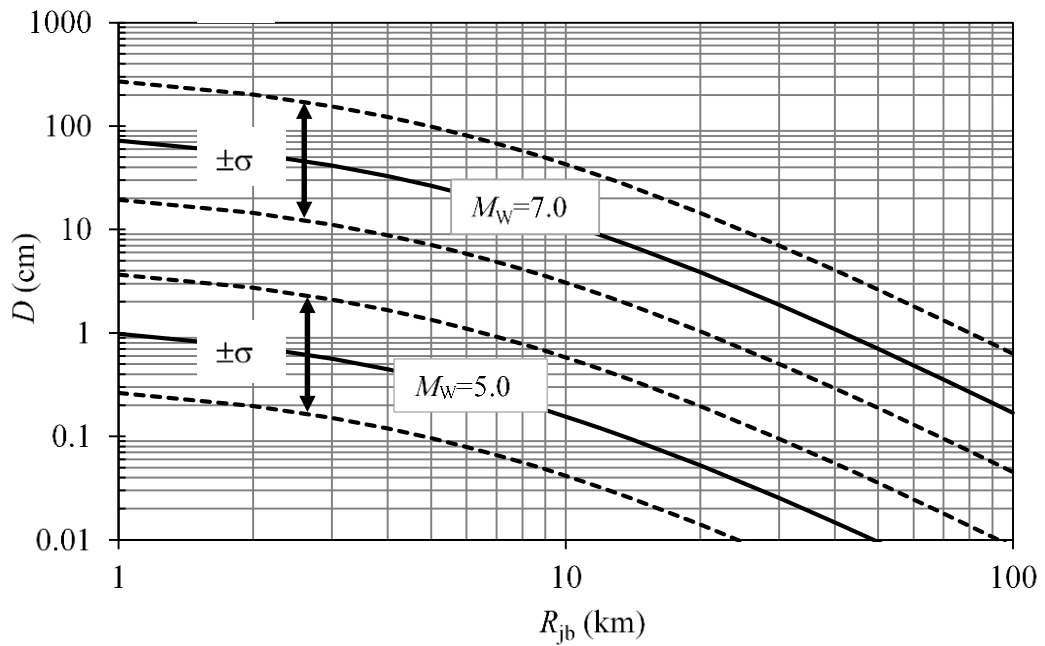


Figure 2.10 The relationship between R_{jb} and D in the case that a_c is 0.10 g, V_{S30} is 300 m/s and SoF is SS/N

The uncertainty in prediction of D appears to be more important than the sensitivity of D to the prediction parameters. Figure 2.10 shows the variability of D by two curves enveloping the expected value of D . These curves are obtained adding and subtracting one σ to the predicted value of $\log(D)$. σ was estimated as 0.572 for predictions of $\log D$ by Equation 2.3. The figures for σ according to the equations in Table 1.2 are presented in Table 2.4. A number of studies yield to the figures for σ that are reasonably close 0.572. Particularly Jibson (2007) report figures significantly exceeding 0.572. Lower ranges for σ reported in literature are supposed to be more reasonable, because these prediction equations are based on the presumption that PGA is definitely known before estimation of D , or ignore the relationship between the variance of PGA and that of D in case PGA is supposed as a variable. On the other hand, σ is ranging almost from 0.28 to 0.55 according to a number of published studies on GMPEs for $\log(\text{PGA})$ (e.g., Joyner and Boore, 1981; Sarma and Free, 1995; Özbey et al., 2004; Bragato, 2005; Marin et al., 2004). Parameter σ for $\log(D)$

is more similar to the figures reported for the logarithm of peak ground velocity (PGV). Parameter σ was reported as 0.50 by Boore and Atkinson (2007), possibly due to higher sensitivity of PGV to low-frequency content of ground motion with respect to PGA. Arias intensity is another parameter used for estimation $\log(D)$. This variable is also very sensitive to duration of ground motion. A number of GMPE studies on Arias intensity yielded similar ranges for σ . The figures for standard deviation of $\log I_A$ are 0.994 according to Lee et al. (2002). These figures are 0.534 and 0.539 respectively for class C and class D sites (Table 3) according to Hwang et al. (2004), they are 0.679 and 0.520 sites classified as rock and stiff soil respectively according to Tselentis et al. (2005). The recent study of Sandikkaya and Akkar (2016) reported (total) σ for $\log I_a$ as 0.624 for the equation employing R_{jb} as the distance parameter. Hence, the similarity between variances of I_a and D shows the importance of duration dependence of D for its variability, and explains why the variability of D is generally greater than those of the ground-motion amplitude parameters. An investigation of residuals will depict further information about the variability of D .

The residuals are shown in Figure 2.11. A residual is the difference between the observed and the predicted value of response variable (i.e., $\log(D)$ in Equation 2.3) for a given set of parameters. The sum of all residuals is equal to zero. A linear regression model is not always appropriate for the data, because the deviation for the expected (mean) may not be completely random, and may show significant dependence on predictors. Therefore, an examination of the residuals is important (Devore and Berk, 2007).

A limited relationship between residuals and some of the prediction parameters was observed. The decrease in the variability of residuals in lower ranges of R_{jb} (Figure 2.11.c) and higher ranges of a_c (Figure 2.11.d) may be explained by the scarcity of data in these ranges. Figure 2.11.f shows a relationship between σ and D . The variability of residuals is greater in the range $D > 1$ cm than that in the range $D < 1$ cm. Table 2. presents findings supporting this relationship. Saygili and Rathje

(2008, 2009) reported the relationships that show increasing variability in $\log D$ by increasing a_c/PGA . An increase in the ratio a_c/PGA implies a consequent decrease in $\log D$. Nonetheless, these observations can be explained by the limitations of sample, particularly about its size. An alternative transformation of D instead of $\log(D)$, or weighted least-squares can be used to decrease possible bias in estimated model coefficients (Devore and Berk, 2007), unless the relationship between $\log(D)$ and σ is explained by the limitations of the sample.

Table 2.4. Sample standard deviations of empirical block-displacement predictions

Reference	σ
Yegian et. al. (1991)	0.450
Ambraseys and Srbulov (1995)	0.580
Jibson et al. (1998)	0.375
Romeo (2000)	0.418
Stewart et al. (2003)	0.350
Bray and Travararou (2007)	0.286
Jibson (2007) (i)	0.510
Jibson (2007) (ii)	0.454
Jibson (2007) (iii)	0.656
Jibson (2007) (iv)	0.616
Saygili and Rathje (2008) (i)	0.490
Saygili and Rathje (2008) (ii)	$0.199+0.243 \cdot (a_c/PGA)$
Saygili and Rathje (2008) (iii)	$0.086+0.343(a_c/PGA)$
Rathje and Saygili (2009) (i)	$0.317+0.342 \cdot (a_c/PGA)-0.234 \cdot (a_c/PGA)^2$
Rathje and Saygili (2009) (ii)	$0.175+0.227 \cdot (a_c/PGA)$
Hsieh and Lee (2011) (i)	0.295
Hsieh and Lee (2011) (ii)	0.357

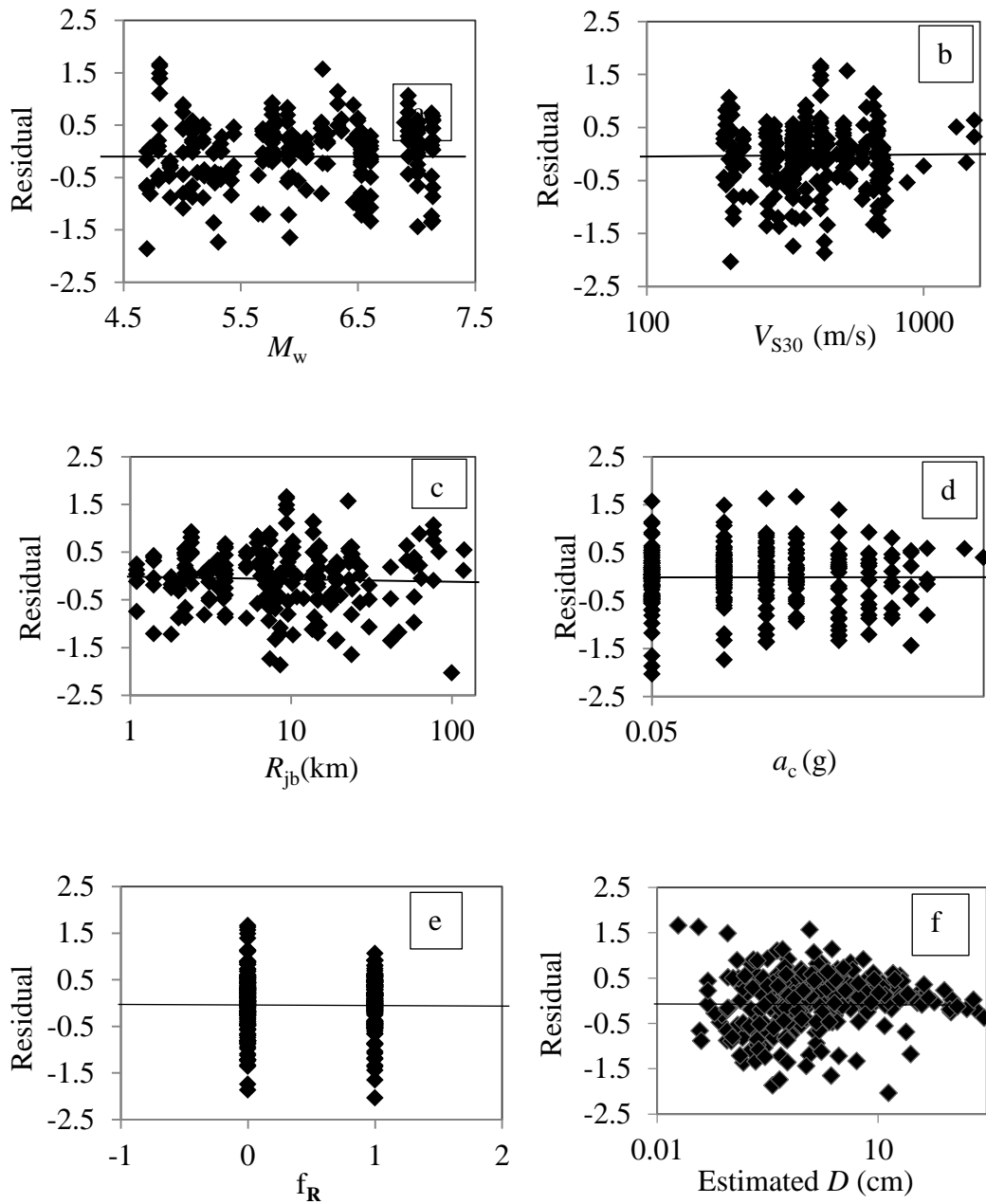


Figure 2.11 The plot of residuals versus (a) M_w , (b) V_{S30} , (c) R_{jb} , (d) a_c , (e) f_R , and (f) D estimated by Equation 2.3

2.5 Discussion

Equation 2.3, which involves a reasonably simple functional form, can be easily implemented in a conventional probabilistic seismic hazard analysis in order to develop a relationship between the annual probability of exceedance and D for any given a_c . Hence, a_c can be considered as a parameter defining a mechanical system property, such as the natural period (T) of oscillator considered in prediction of spectral acceleration. A limitation of Equation 2.3 is that, predicted D is always a positive real number, so $D=0$ is never possible. On the other hand, the predicted D can be as small as 0.01 cm, which can be practically presumed as zero.

Equation 2.3 is also compared with a number of empirical predictors for D in Figure 2.12. Although two horizontal components of D are joined by using different functions in these studies, it is supposed that all yield to figures practically close to SRSS of D . The reasonability of this assumption is discussed later in this section. The prediction equations of Hynes-Griffin and Franklin (1984, abbreviated as HF84), Ambraseys and Srbulov (1995, abbreviated as AS95), Jibson (2007, abbreviated as J107 and J207 for equations i and ii respectively in Table 1.2), Saygili and Rathje (2008, abbreviated as SR08 for equations i in Table 1.2), Bray and Travarasrou (2007, abbreviated as BT07), and Bozbey and Gundogdu (2011, abbreviated as BG11) are based on the assumption that PGA is known, so that the fraction a_c/PGA is a predictor of D . The empirical relationships shown in Figure 2.12 use different approaches to join the two components of D computed for each ground motion record in their databases. For the sake of simplicity, each pair of D components were joined in the sample shown in Figure 2.12. The geometric mean of PGA was considered for calculation of the prediction parameter a_c/PGA for each record. Therefore, the variability of predictions shown in Figure 2.12 may be biased. The magnitude limits were also considered in Figure 2.12. These limits are $5.5 \leq M_w \leq 7.6$ for BT07, $5.0 \leq M_w \leq 7.9$ for SR08, and $5.3 \leq M_w \leq 7.6$ for J207. Displacements smaller than 1 cm were disregarded in the sample for BT07. By considering the significance of variability among these relationships, it can be concluded that the predictions of

Equation 2.3 are similar to the predictions of other relationships in the range $a_c / \text{PGA} < 0.55$, and are particularly located around the predictions calculated by the relationships BG11 and J207. However, in the range of a_c greater than 55% of PGA, the predicted range of D is significantly different from the predictions of other relationships, except those of BT07. This is explained by the uncertainty in parameter PGA, which is supposed to be known before the use of other six relationships that are converging to zero as a_c/PGA reaches to one. The predictions of BT07 converges to 1 cm as a_c / PGA reaches to 1.0, because of the truncation of D at 1 cm (Bray and Travararou, 2007).

The accuracy of Equation 2.3 is also compared with those of five equations in Figure 2.13. Unlike Figure 2.12, PGA of each component was used for calculation of the parameters a_c/PGA for individual predictions of D , except for the prediction equation BT07. These predictions were limited by the range of estimations stated by the researchers. The predictions according to Equation 2.3 tend to overestimate D in the range $D < 1$ cm. On the other hand, the prediction errors for Equation 2.3 in the range $D > 1$ cm are generally smaller than those for SR08 and BG11, and comparable to those according to BT07, BG11, J207. The significant bias that yields underestimation of D in predictions of BT07 can not be explained. Nevertheless, the figures show that accuracy of predictions of Equation 2.3 is comparable to other prediction relationships presented in literature, although former estimations of PGA are not necessary for this equation.

Figure 2.14 shows the difference between the maximum and SRSS of two horizontal components of D . The largest difference between the SRSS and the maximum is 25%. The average difference is about 9%. The difference between the two sets of estimations is negligible with respect to the variability of D as shown in Figure 2.10. Therefore, a more rigorous method to join the two horizontal components of D is not practically feasible. The consideration of two components of D in analyses separately will yield a lower prediction for D . This observation is also supporting Equation 2.3 for its practical implementation in seismic hazard analyses. Nevertheless, the

improvements in functional forms, those in estimation of model coefficients, and in the sample of accelerograms can decrease σ significantly.

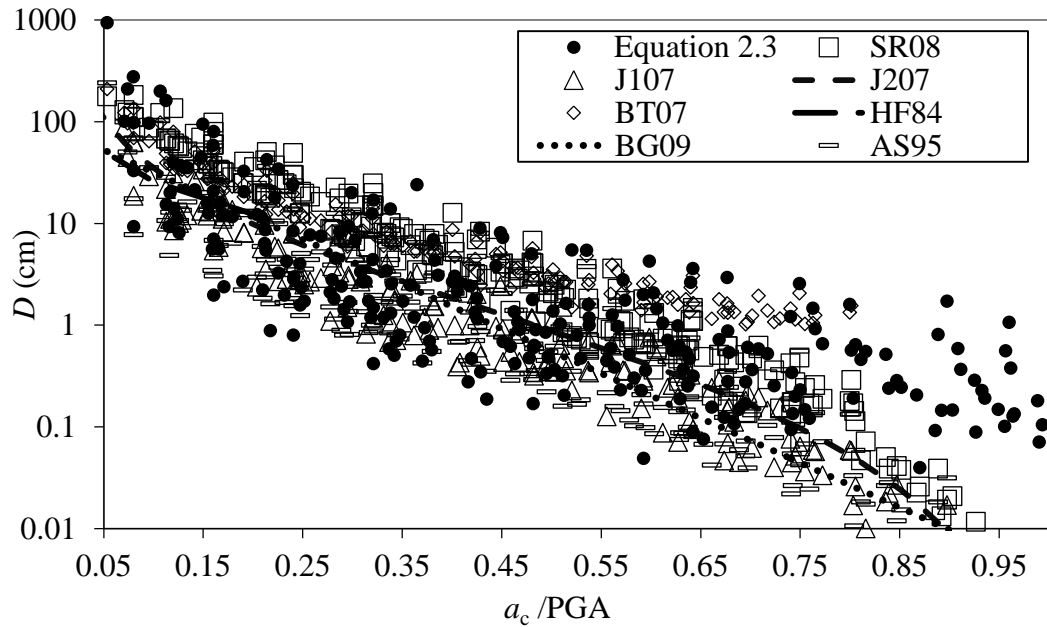


Figure 2.12 The comparison of predictions among a set of equations

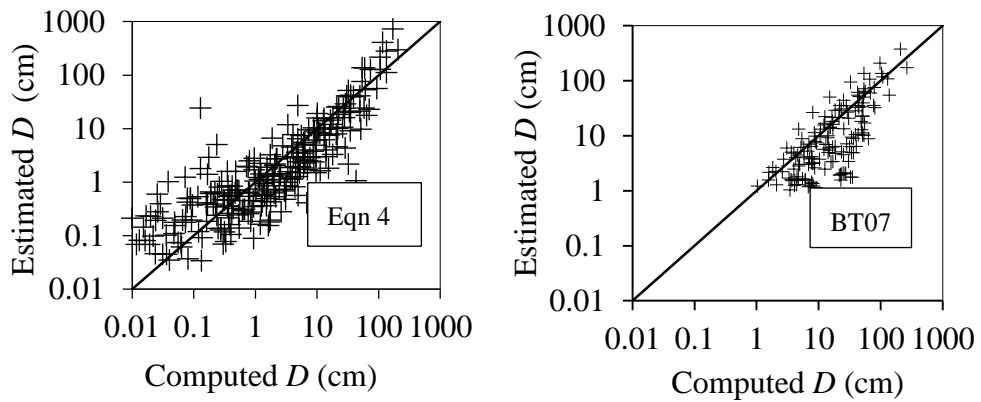


Figure 2.13 The comparisons of predicted D with computed D for a set of prediction equations

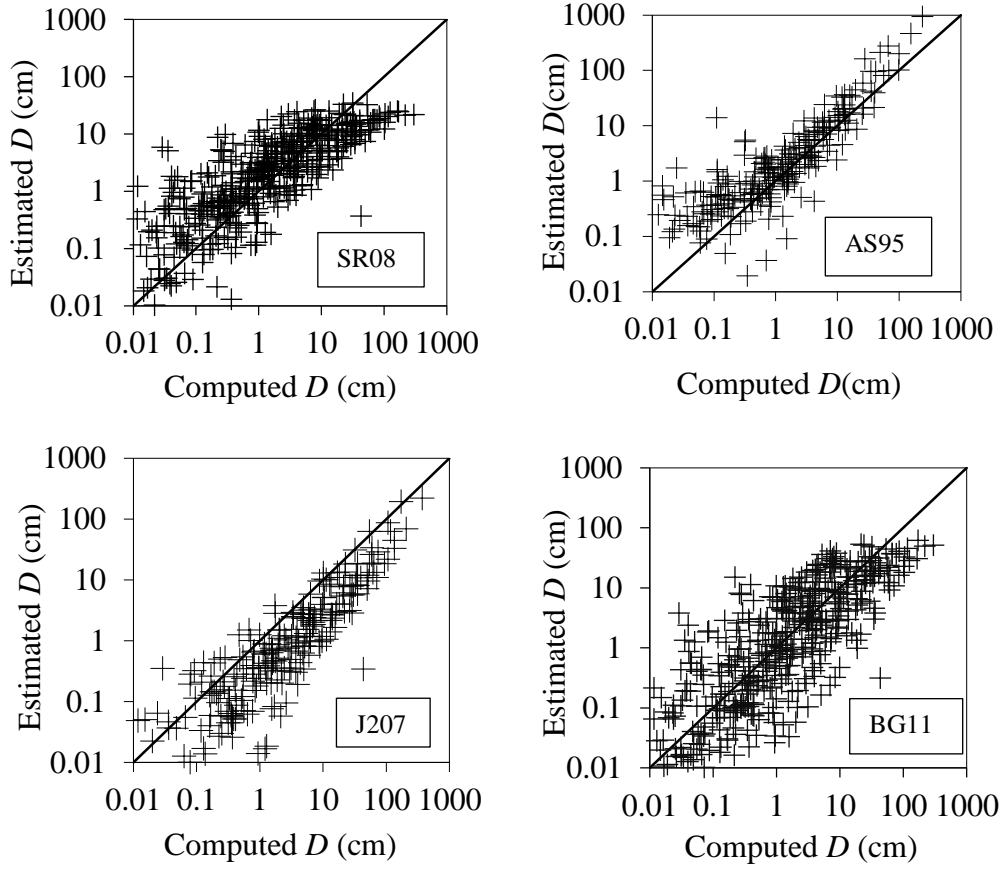


Figure 2.13 (continued)

The effect of truncation of D at 1 cm as considered by Bray and Travararou (2007) needs further investigation to understand the variability in the results of this study. In case $D < 1$ cm is eliminated from the sample, the functional form of Equation 2.3 yields a new set of coefficients, such as

$$\log(D) = 0.652 \cdot M_w - 1.032 \cdot \log(V_{s30}) - 1.372 \cdot \log(R_{jb} + 6) - 1.532 \cdot \log(a_c) + 0.262 \cdot f_r - 0.649 \quad (2.4)$$

The comparisons of D predicted by Equation 2.4 with D computed by SLAMMER are shown in Figure 2.15. Equation 2.4 yields smaller residuals in the range (SRSS) $D > 1$ cm. r^2 and σ were respectively computed as 0.761 and 0.294. When the data for (SRSS) $D < 1$ cm in the sample is eliminated, σ becomes similar to the figures reported by Bray and Travararou (2007). On the other hand, the number of seismic

events reduces from 46 to 35, and the number of ground-motion records reduces from 70 to 48 after this elimination. Therefore, it is not clear whether the reduction in σ is due to the reducing number of useful records in greater ranges of D , or due to limitations of the functional form of prediction equation. Therefore, it was concluded that the use of Equation 2.4 can yield to underestimation of seismic hazard, unless alternative rigorous statistical methods, such as weighted least squares method are able to suppress the possible relationship between σ and $\log D$. This conclusion is also supported by the variances reported after similar studies on prediction of D , and by the variances of parameter predictions that are expected to be related to D (Section 2.4). Therefore, Equation 2.3 was primarily used for computation of seismic hazard in Chapter 3. Nonetheless, Equation 2.4 was also used for computation of seismic hazard at specific coordinates to examine the significance of σ in these analyses.

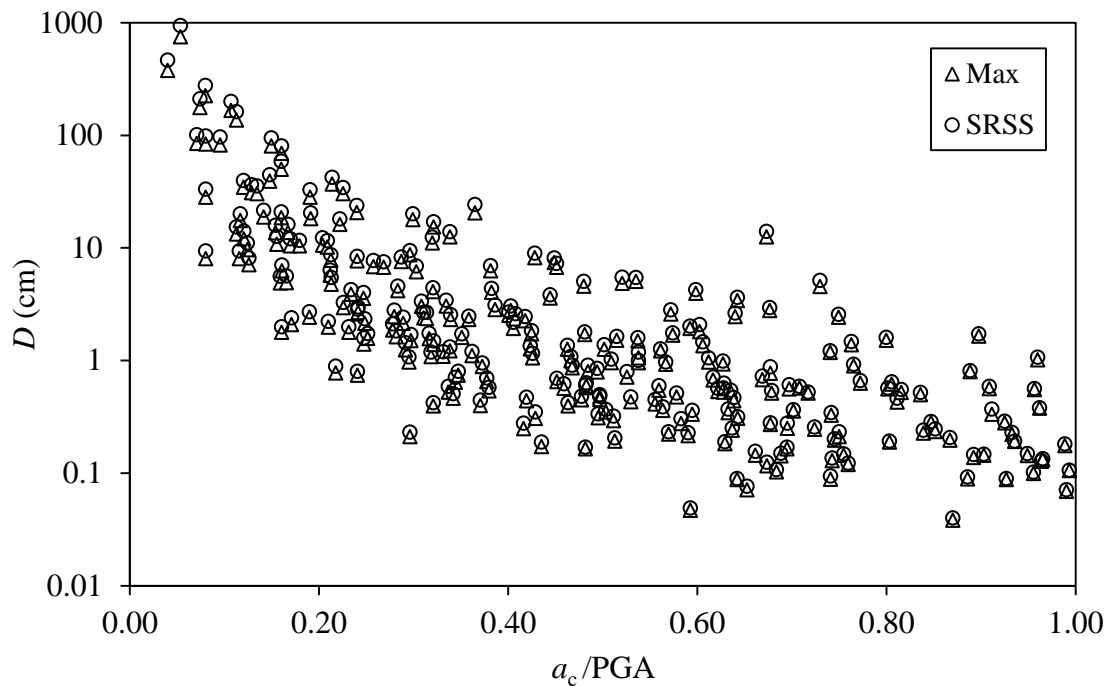


Figure 2.14 The differences between maximum and SRSS of the two components of D

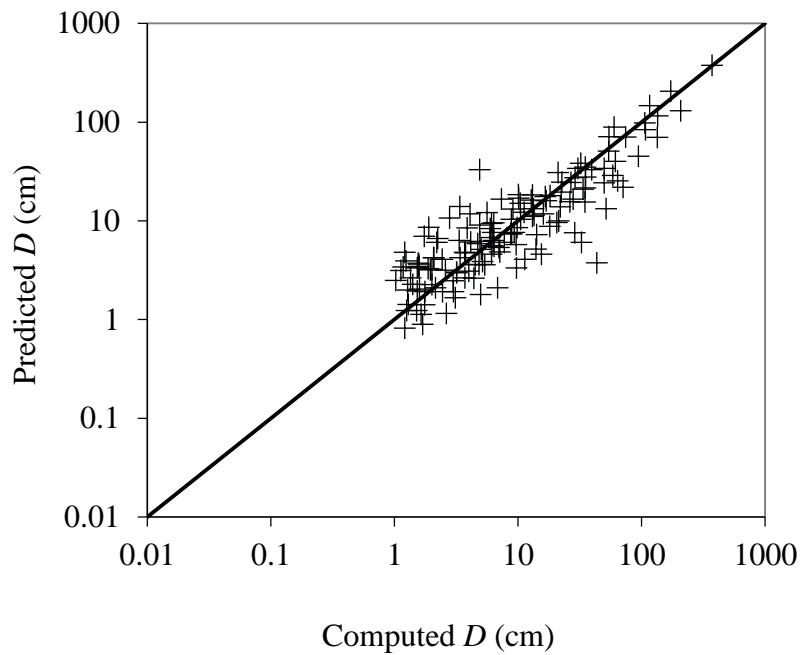


Figure 2.15 The comparison of predicted D with computed D according to Equation 2.4

The significance of parameters were also investigated by testing the null hypothesis $H_0: \beta_i=0$, against the alternative $H_a: \beta_i \neq 0$. Hence the null hypothesis suggests that the i^{th} does not have any effect on the prediction. The P -value, observed significance level of the test, is the smallest level of significance at which H_0 would be rejected by a given sample (Devore and Berk, 2007). The level of significance is usually between 0.01 and 0.10 in practical applications. Hence, the rejection of H_0 will be a strong conclusion if P -value is in this range or close to zero (Devore and Berk, 2007). The regression tool of the computer program MS-Excel is also reporting the P -values for this test. Those P -values are shown in Table 2.5 for a set of equations in Table 2.3. No.4 corresponds to Equation 2.3. The P -values shows that H_0 should be rejected for all parameters, and each parameter has a significant contribution in prediction of D . The highest P -value in Table 2.5 was obtained for M_w^2 Equation

No.1 and No.2. Nonetheless, the P -value is rather small, and it was concluded that the relationship between $\log D$ and M_w^2 is rather significant. On the other hand, the use of M_w^2 in prediction equations does not improve r^2 significantly, and the term M_w^2 can be ignored until a larger sample is available.

Table 2.5. P -values for a set of equation in Table 2.3

Parameters	P -value		
	No.1	No.2	No.4
M_w	$7.40 \cdot 10^{-5}$	$1.58 \cdot 10^{-4}$	$5.86 \cdot 10^{-39}$
$\log(V_{S30})$	$5.38 \cdot 10^{-13}$	$1.40 \cdot 10^{-13}$	$3.93 \cdot 10^{-16}$
$\log(R_{jb}^2+9)$	$3.43 \cdot 10^{-45}$		
$\log(R_{jb}+6)$		$3.04 \cdot 10^{-44}$	$3.98 \cdot 10^{-43}$
$\log(a_c)$	$6.01 \cdot 10^{-54}$	$4.09 \cdot 10^{-53}$	$4.25 \cdot 10^{-52}$
f_r	$1.79 \cdot 10^{-12}$	$1.06 \cdot 10^{-11}$	$1.49 \cdot 10^{-11}$
M_w^2	$8.44 \cdot 10^{-3}$	$1.35 \cdot 10^{-2}$	

CHAPTER 3

A CASE STUDY ON THE USE OF PSHA FOR A DECISION ON SEISMIC COEFFICIENT

3.1 Introduction

The procedure for determination of k_h by a probabilistic seismic hazard study (PSHA) is explained by a case study near to the town of Şebinkarahisar in Giresun province of Turkey. The prediction equation for D (Section 2.4) was implemented in PSHA to develop hazard curves in terms of D . Then the hazard curves were converted to relationships between k_h and return period, T_R , according to the relationship explained in Figure 1.5. Consequently, the return period of the event that D exceeds D_{all} will be equal to T_R , if the slope is marginally stable under the action of k_h . This return period will become greater by improving stability. Finally, the spatial distribution of k_h around Şebinkarahisar for a set of D_{all} and T_R was shown. An assessment of stability is presented by comparing the allowable slope angles and the existing slope angles around Şebinkarahisar.

3.2 Seismic Hazard Analysis

The procedure of PSHA used in this study is based on the frame explained by McGuire (2004). It is assumed that earthquakes occur randomly within a time interval. The random occurrences of seismic events are modeled either as Poisson or as non-Poissonian processes (Cornell and Winterstein, 1986). In a Poisson process the events are supposed to lack memory, and the probabilistic distribution of these events is stationary in any interval of time (Devore and Berk, 2007). The Poisson process is widely used in PSHA because of its mathematical simplicity. On the other hand, it is an over simplification of consequences of physical processes in tectonics (Anagnos and Kiremidjian, 1988). This simplification is used in this study to keep the comprehensibility and comparability in calculation of k_h by PSHA.

3.2.1 Integration of Hazard on a Site

PSHA determines the annual probability of exceeding a specific level (y) of a ground-motion parameter (Y) in a specific time interval at a site of interest. This probability can be computed by using the total probability theorem. In most theoretical models, the probabilistic distribution of Y is basically supposed to be limited to earthquake magnitude (M), and to distance between site and seismic source (R). The probability density functions for M and R , are defined by the functions $f_{Mi}(m)$ and $f_{Ri}(m,r)$ respectively. The hazard integral is defined as (Cornell, 1968)

$$\lambda_y = \sum_{i=1}^{N_s} v_i \cdot \int \int P[Y > y | m, r] \cdot f_{mi}(m) \cdot f_{Ri}(m, r) \cdot dm \cdot dr \quad (3.1)$$

where Y is a strong ground motion parameter of concern, y is a threshold value for Y , $f_{Ri}(r)$ represents the probability of occurrence of a given earthquake in i^{th} seismic source and at the distance r from the site of interest, $f_{mi}(m)$ describes the probability of occurrence of each earthquake magnitude in i^{th} seismic source, N_s is the number of sources to be considered in seismic hazard analysis, v_i is occurrence rate of the earthquakes in i^{th} seismic source in a specific interval of time, and λ_y describes the

frequency of exceeding y by Y in a specific interval of time. This specific interval of time is usually supposed to be a year, so that λ_y represents the annual rate of exceedance. The integral in Equation 3.1 is computed by a number of computer programs. Some of the widely known programs are EQRISK (McGuire, 1976), FRISK (McGuire, 1978), SEISRISK II and III (Bender and Perkins, 1982 and 1987), CRISIS (Ordaz et al., 2003). The continuous relationship between λ_y and y for a site is usually presented as a graphical function, namely the hazard curve (McGuire, 1993).

3.2.1.1 Description of $f_{Ri}(m,r)$

PSHA requires characterization of all known earthquake sources that can cause significant ground-motion amplitudes at the site of interest. It is necessary to model probabilistic distribution of distance between a site and seismic events for estimation of ground motion parameter. This distance parameter (R_r) is dependent on geometric properties of a source, and on possibilities for geometrical extends of a seismic event, because an event magnitude is dependent on dimensions of a fault rupture (Wells and Coppersmith, 1994). Basically, two source types considered in source characterization are line and area.

A line source is generally used for modeling earthquake occurrences on a mapped fault, in case R is not sensitive to the width of rupture in vertical direction. Faults are modelled by area sources otherwise. The area sources are also used for modeling seismic activity which cannot be associated with any mapped fault. In the latter case, it is assumed that source produces earthquakes randomly at equal likelihood anywhere within its geometrical extends. Whereas, the probabilistic distribution of R depends on the magnitude of seismic event in case of a line source (McGuire, 2004).

3.2.1.2 Description of $f_{mi}(m)$

A basic assumption of PSHA is that the past seismicity is convenient for the prediction of future seismicity on a region of interest. Expected number of

earthquake magnitudes occurring in a given period of time is described by a density function, namely the magnitude-recurrence relationship. These events are generally supposed to constitute a Poisson (or memoryless) process. There are three general models of magnitude density functions that are typically considered in PSHA: exponential model (Gutenberg-Richter), truncated exponential model, and characteristic-magnitude model as shown in Figure 3.1 (McGuire, 2004).

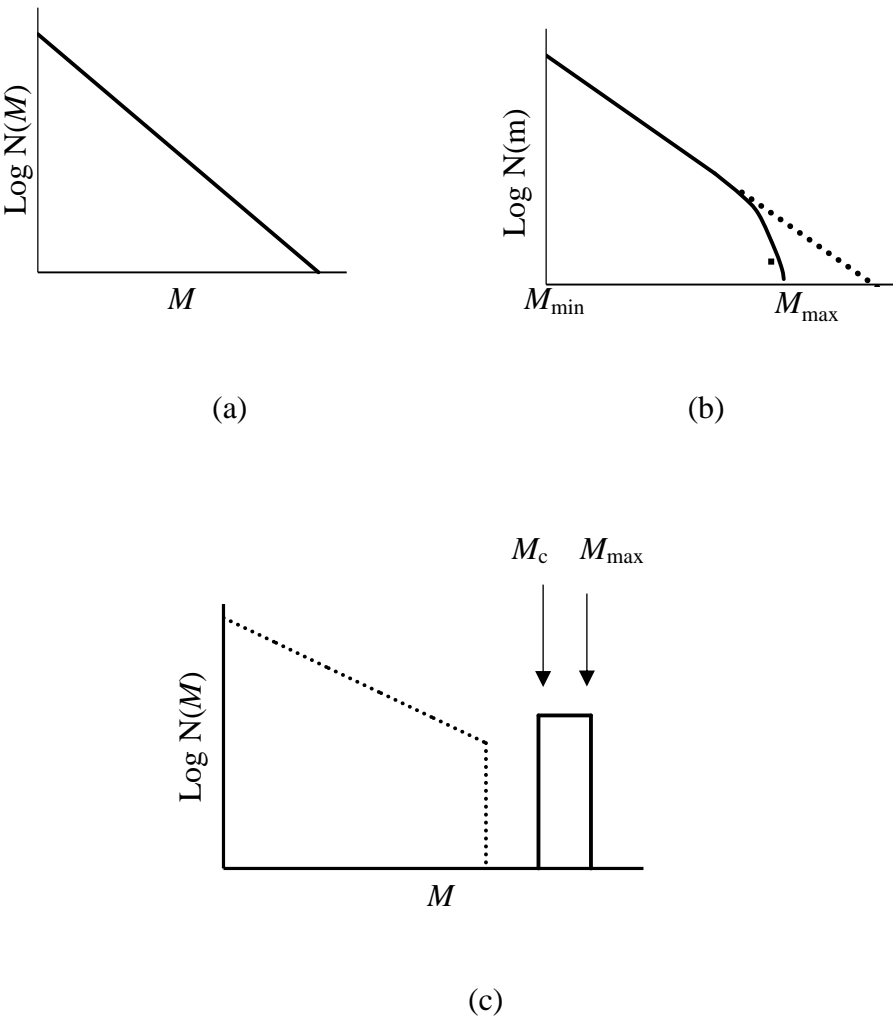


Figure 3.1 The magnitude-recurrence models: (a) exponential, (b) truncated exponential and (c) characteristic

The exponential model is based on Gutenberg-Richter (1944) magnitude-recurrence relationship. Basically, $N(M)$, the expected number of earthquakes with magnitudes

greater than M in a specific duration is estimated by

$$\log N(M) = a - b \cdot M \quad (3.2)$$

or,

$$N(M) = v_0 \cdot e^{-\beta \cdot M} \quad (3.3)$$

where $v_0 = 10^a$, and $\beta = b \cdot \ln(10)$. Usually, $N(M)$ is normalized, so that this specific duration is taken as a year. The exponential model assumes that there is no limit on the maximum possible magnitude, whereas a seismic source, occupying a finite area on earth's crust, should have a limit for earthquake magnitude. An improvement to solve this problem is the truncated exponential model expressed as

$$N(M) = v_{M_{\min}} \cdot \left(1 - p + p \cdot e^{-\beta \cdot (M - M_{\min})}\right) \quad M_{\min} \leq M \quad (3.4.a)$$

where,

$$p = \left(1 - e^{-\beta \cdot (M_{\max} - M_{\min})}\right)^{-1} \quad (3.4.b)$$

Such that, M_{\max} is the maximum magnitude that can be hypothetically recorded on a source modeled by the truncated exponential model, and M_{\min} is the minimum magnitude of concern in analysis and $v_{M_{\min}}$ is a rate of events with magnitudes greater than M_{\min} . M_{\max} is related to the maximum magnitude of events recorded in past, and to the geometrical characteristics of fault. M_{\min} is practically related to the level of ground motion that cannot cause any type of damage on structures. The normalization of Equation 3.4.a by $v_{M_{\min}}$ yields the complementary-cumulative distribution function for M , and the derivative of this function yields the probability density function for the truncated exponential model (McGuire, 2004).

$$f_m^{(M)} = p \cdot \beta \cdot e^{-\beta \cdot (M - M_{\min})} \quad (3.5)$$

The relationship between $v_{M_{\min}}$, M_{\min} , M_{\max} and the slip rate on a fault is (McGuire, 2004)

$$v_{M_{\min}} = \frac{\mu \cdot A \cdot s \cdot c \cdot \ln(10) \cdot \left(1 - \frac{\beta}{c \cdot \ln(10)}\right) \cdot \left(M_{0,\max}^{1 - \frac{\beta}{c \cdot \ln(10)}} - M_{0,\min}^{1 - \frac{\beta}{c \cdot \ln(10)}}\right)}{p \cdot \beta \cdot e^{\beta \cdot \left(M_{\min} + \frac{d}{c}\right)}} \quad (3.6)$$

where, A is fault area, s is the slip on fault surface, μ is the shear rigidity of the crust (typically $3 \cdot 10^{10}$ N/m²), $M_{0,\max}$ and $M_{0,\min}$ are upper and lower bound seismic moments. These seismic moments respectively correspond to $M=M_{\max}$ and $M=M_{\min}$ by the relationship

$$\log(M_0) = c \cdot M + d \quad (3.7)$$

c and d are the constants of Equation 3.7. These constants are equal to 1.5 and 16.05 dyne·cm respectively, in case scale of M the is moment magnitude, M_w (Hanks and Kanamori, 1979).

The geological investigations on number of active faults show that the displacement on number of successive segments during a fault rupture is historically repeated. This is showing that the magnitude of successive major events on a fault is rather uniform due to the relationship between rupture displacement and M (Schwartz and Coppersmith, 1984). An event with a magnitude ranging from M_c to M_{\max} on a particular fault is widely named as characteristic earthquake. M_c is supposed to be the minimum possible magnitude of a characteristic earthquake. Any M smaller than M_c is supposed to be pertinent to non-characteristic earthquakes. These events are generally modeled by a truncated exponential model as shown in Figure 3.1.c. Equation 3.6 can also be used for characteristic earthquake modeling after substitution of $\beta=0$ and $M_{\min}=M_c$ (McGuire, 2004). M_c and M_{\max} can be related to dimensions of a fault rupture by the relationships of Wells and Coppersmith (1994), or they can be estimated by using the catalog of historical earthquakes (Frankel,

1995). The contribution of magnitudes less than M_c on accumulation of seismic moment on a fault is relatively small because of the logarithmic relationship shown in Equation 3.7.

The parameter β and the rate of low-magnitude events (i.e., $\nu_{M_{\min}}$), is usually estimated by the catalog data of earthquakes. The uncertainty regarding the location and magnitude was considerable for the events before the period of seismic instrumentation. Therefore, the use of a catalog of seismic events in the instrumental period is necessary for estimation of β . Nonetheless, there are several important issues to consider before employing a catalog to develop magnitude-recurrence relationships. The first is that the magnitude scales used for reporting each event may not be homogeneous in catalogs. Although recent ground-motion prediction equations are based on moment-magnitude scale (M_w), this magnitude scale is not reported for each event in the catalogs. The second is the incompleteness of lower magnitude ranges particularly in early periods because of the insufficiency of instrumentation. The third aspect is the clustering of aftershocks or foreshocks around the location of a significant seismic event. These clusters violate the assumption of statistical independence of earthquakes which is a property of Poisson processes. So, the catalog should be declustered, and the aftershocks and foreshocks should be eliminated before estimation of model parameters.

When compiling an earthquake catalog for a PSHA, it is also important to take magnitude conversions into account to build a homogeneous dataset. Magnitude scales have been developed in the past as a response to different instrumentation problems in seismology. Local or Richter Magnitude (M_L), surface wave magnitude (M_S), duration magnitude (M_D), body-wave magnitude (M_B), and moment magnitude (M_w) are among widely used magnitude scales (McCalpin, 2009). M_w scale is related to the moment magnitude of a seismic event by substituting $c=1.5$ and $d=16.05$ dyne·cm in Equation 3.7 (Hanks and Kanamori, 1979). Because M_w was considered in the development of predictor equation for D in Chapter 2, the other magnitude scales should be converted to M_w in the absence of a report on this magnitude scale.

A number of empirical relationships between M_S , M_L , M_B and M_W were reported in literature (e.g., Stromeyer et al., 2004; Castellaro et al., 2006). Hence, the correlations between M_W and other magnitude scales can be statistically estimated by the regional data, and can be used for estimation of M_W to provide homogeneity in magnitude scale. On the other hand, the magnitude scales other than M_W have upper (saturation) limits which hinder the use of these relationships in greater ranges of earthquake magnitude. M_B , M_L , M_S and M_d scales saturate almost at magnitudes 7.3 (Chung and Bernreuter, 1979), 7.0, 8.0 (Hanks and Kanamori, 1979) and 6.0 (Yenier et al., 2008) respectively.

After converting a catalog to M_W scale, the clusters of aftershocks and foreshocks can be eliminated. The total seismic moment of each cluster of events should be added to the moment of its main (independent) event to preserve the seismic moment accumulating in a seismic source. The process of identification and elimination of these clusters in a catalog is known as declustering analysis (Stiphout et al., 2012). ZMAP (Wiemer, 2001) is one of the computer programs that can be used for declustering of seismic catalogs. The algorithm of Gardner ve Knopoff (1974), which is based on the limitations for inter-event distances in time and space, is implemented in ZMAP for the declustering. The events that are located in these limits are supposed to build clusters, and are eliminated by ZMAP. The event with the maximum magnitude in each cluster is supposed to be the main event. It's moment magnitude is updated according to the computed total seismic moment of event declusters.

Once dependent evens have been removed from a homogeneous catalog, the catalog can be assessed for completeness for different magnitude ranges. An earthquake catalog is complete for magnitude M_z within a specific time interval, provided that all events with magnitude M_z is recorded in this interval (McGuire, 2004). The determination of period of completeness can be rather subjective. The method of Stepp (1973) is a well-known method on estimation of periods of completeness for magnitude ranges. Since the sequence of earthquakes is supposed as a Poissonian

process, the mean rate of occurrence for a magnitude interval should be a constant in a complete period. This period range is identified by graphically investigating the relationship between the variance of average rate of occurrences and the time interval for earthquake records. Alternatively, Nasir et al. (2013) suggested plotting cumulative number of earthquake-intensity versus time (years) in order to identify the period of completeness of the earthquake catalog for this particular intensity. A conceptual explanation of this method, named as “Temporal Course of Earthquake Frequency” (TCEF), is shown in Figure 3.2. The complete recording of Poissonian events are expected to yield a linear relationship between cumulative number of earthquakes and time with a slope steeper than the slope in the period of incomplete data.

Since statistical estimation of a parameter is sensitive to missing data, β should be estimated by taking the period of completeness of each magnitude range into account. The study of Weichert (1980) presents a method to estimate β in case the observation periods of magnitude ranges are not equal. Hence, β can be estimated by the relationship

$$\frac{\sum_i t_i \cdot M_i \cdot e^{-\beta \cdot M_i}}{\sum_i t_i \cdot e^{-\beta \cdot M_i}} = \frac{\sum_i M_i \cdot z_i}{\sum_i z_i} \quad (3.8)$$

where, z_i is the number of earthquakes with magnitudes in the interval $[M_i - \Delta M_i / 2, M_i + \Delta M_i / 2]$ that are completely recorded during a period of time, t_i (years). Then, the total (annual) rate of events with magnitudes greater than M_{min} is

$$v_{M_{min}} = \frac{\sum_i e^{-\beta \cdot M_i} \cdot \sum_i z_i}{\sum_i t_i \cdot e^{-\beta \cdot M_i}} \quad (3.9)$$

Bender (1983) argued that Equation 3.8 will yield biased estimations, and suggested a method to estimate β by considering M as a continuous variable. Or, the bias can be minimized by setting $\Delta M = 0.1$, which is applicable for most earthquake catalogs.

The magnitude-recurrence relationships in a region can also be justified by historical records of events, since the duration of instrumental period is considerably short with respect to the duration between destructive earthquakes. A number of well-known historical catalogs for seismic events in Anatolia were compiled by Ambraseys and Jackson (1998), UDIM (2016) and SHARE-CET (Stucchi et al., 2012). The first record in the historical catalog of Ambraseys and Jackson (1998) involving events on Turkey was dated as 17 AD. UDIM historical earthquake database provides 98 seismic events between the years 222 BC and 1899 AD. Another historical catalog is provided by the SHARE-CET database. This database involves earthquake catalogue for Central and Eastern Turkey between years AD 1000 and AD 2006. The catalog involves 241 events until 1899 AD, before the instrumental period (Stucchi et al., 2013). The sizes of historical events are explained by M_S in the catalog of Ambraseys and Jackson (1998), by their intensity in UDIM catalog, and by M_W in the SHARE-CET database.

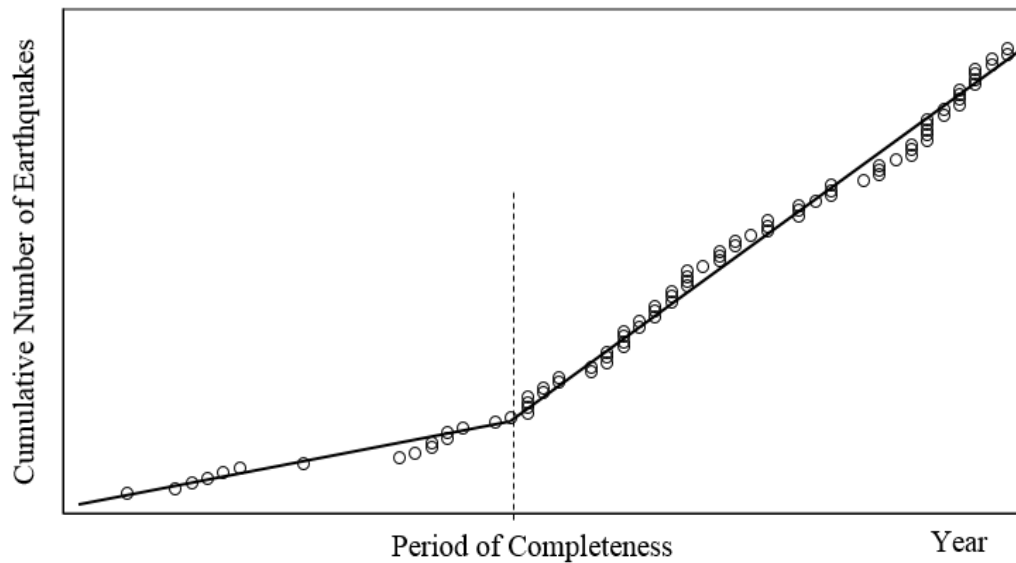


Figure 3.2 The determination of period of completeness according to TCEF

(Nasır et a., 2013)

3.2.1.3 The Concept of Return Period

An alternative and widely used parameter that is expressing the likeliness of the event that Y exceeds y is the return period, T_R . This parameter can be calculated by (EN 1998-1, 2004)

$$T_R = \frac{1}{\lambda_y} \quad (3.10)$$

by supposing that the occurrences of event $Y > y$ constitute a Poissonian process. Then, the probability that the first event will be observed within a specified duration T_L is

$$P_R = 1 - e^{-\lambda_y T_L} \quad (3.11)$$

due to probabilistic exponential distribution (Kramer, 1996) The substitution of Equation 3.10 in Equation 3.11 yields

$$T_R = -\frac{T_L}{\ln(1 - P_R)} \quad (3.12)$$

which relates the return period of the event $Y > y$ to the probability P_R . T_L is usually related to the average life span of a structure. A duration of 50 years is commonly specified for buildings, and P_R is set to a reference probability of exceedance. For instance, a return period of 475 years is calculated by supposing $P_R=10\%$, which is widely used for design of ordinary buildings accommodating people. For the design of critical structures, such as nuclear power plants, dams, and bridges; smaller ranges of P_R are employed (Solomos et al., 2008). A set of combinations of P_R and T_L , and T_R frequently considered in seismic-design practice is shown in Table 3.1.

Table 3.1. Typical values and relationship between P_R , T_L and T_R
(after Solomos, 2008)

P_R	T_L	T_R
10%	10 years	95 years
20%	50 years	224 years
10%	50 years	475 years
5%	50 years	975 years
2%	50 years	2475 years
10%	100 years	949 years
5%	100 years	1950 years
2%	100 years	4950 years

According to Bisch et. al. (2011), the document EN 1998-1 proposes two levels of seismic actions for ordinary building-type structures. (These actions correspond to seismic intensity in performance based design, explained in section 1.2) The first is defined by the 10% probability of exceedance in 50 years, which is for prevention of local collapse in structures. This pair of P_R and T_L corresponds to a return period of 475 years (Table 3.1). The second is defined by $P_R=10\%$ and $T_L=10$ years, and shall be considered for the damage limitation (i.e., serviceability) level. Instead of specifying different sets of T_R for buildings that impose various post-event risks on society, EN 1998-1 assigns scaling factors for seismic actions according to the importance of buildings. This importance factor, γ , corresponds to a range of T_R and depends on the slope of hazard curve. A simplified relationship between logarithm of λ_y and that of y is

$$\log(\lambda_y) = k \cdot \log(y) + c_1 \quad (3.13)$$

where k is the slope of the hazard curve, and c_1 is a constant. k is dependent on magnitude distribution of events around the site (McGuire, 2004). Substitution of Equation 3.10 and the definition $\gamma = y(T_R) / y(T_R=T_{LR})$ in Equation 3.13 yields,

$$\gamma \cong \left(\frac{T_{LR}}{T_R} \right)^{-1/k} \quad (3.14)$$

T_{LR} is namely implicit return period, and is taken as 475 years for $\gamma = 1.0$ (Bisch et al., 2011). The relationship between the parameter γ , k and T_R are shown for a range of importance classes in Table 3.2. T_R for buildings of minor importance is in the range from 200 to 250 years. T_R is between 800 and 1.000 years for buildings such as schools, assembly halls, cultural institutions. T_R for hospitals, fire stations and power plants are between 1.100 and 1.800 years (Bisch et al., 2011). This concept is also employed in Turkish seismic design code (Ministry of Public Works, 2007). γ is 1.0 and 1.5 respectively for dwellings and for hospital on this document. T_R is supposed to be equal to 475 years and 2475 years respectively on this document. These γ and T_R can depict reasonable figures for selection of k_h in assessment of seismic stability of slopes.

Table 3.2. Importance classes and recommended values for γ for buildings (Bisch et al., 2011)

Importance class	γ	T_R (years)		
		$k=2.5$	$k=3.0$	$k=4.0$
I	0.8	272	243	195
II	1	475	475	475
III	1.2	749	821	985
IV	1.4	1102	1303	1825

3.3 The Case Study of Şebinkarahisar

A specific zone involving an extensive territory of severe landslide hazard is chosen for computation of k_h by PSHA. The zone is around Şebinkarahisar town in Giresun Province of Turkey, which is located on the south of Black Sea. The town is located on the coordinates $38^{\circ}25'E$ and $40^{\circ}17'N$. According to the General Directorate of Mineral Research and Exploration (MTA, 2007), town is close to wide zones that are

prone to landslide hazard, marked by red and yellow colors on the map shown in Figure 3.3. According to Aral et al. (1991) the geotechnical index properties of the soil specimens recovered from landslides show that the soils prone to landslide hazard is typically classified as SM, SC, MH and CL according to the U.S. Geological Survey (USGS). The neotectonic activity of North Anatolian Fault (NAF) and relatively steep topographical slopes played prominent roles in slope failures (Aral et al., 1991). The average annual precipitation between the years 1981 and 2010 in Giresun is 786.9 mm. Whereas, the average between the years 1981 to 2010 annual precipitation is 574 mm in Turkey (Meterological Service of Turkey, 2017). Hence, the average precipitation in Giresun has been only 37% higher than the country average in this period.

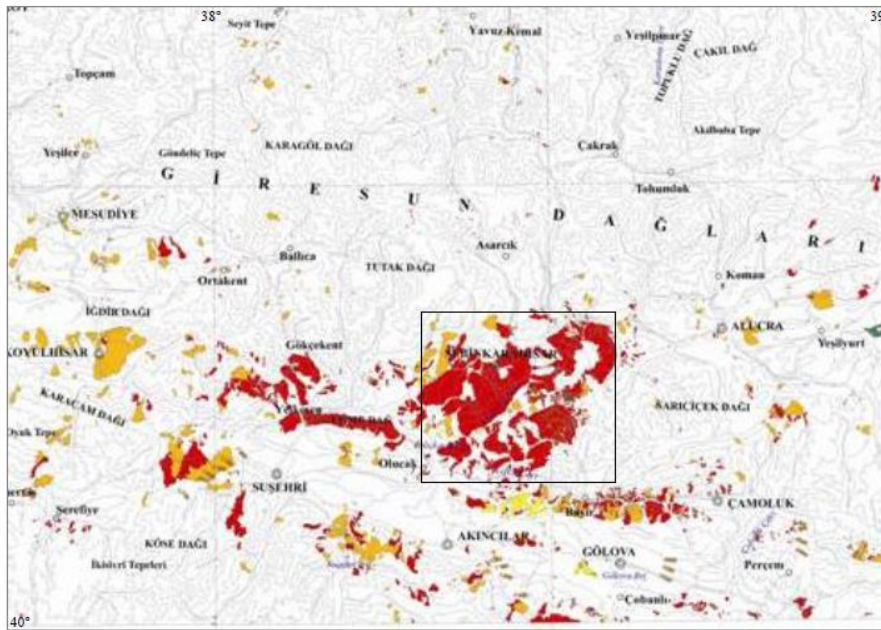


Figure 3.3 Landslide map around Şebinkarahisar (Duman et al., 2007)

Şebinkarahisar is located of a distance of 20 km approximately from North Anatolian Fault (NAF). The dextral strike-slip NAF is the most significant active tectonic structure in Turkey. The fault extends from east of Anatolia to the north of Aegean Sea. The faults consists of several segments, and it has an approximate length of

1200 km (Barka, 1992). Barka (1992) stated that the age of NAF is a controversial topic, but it is between the late Miocene and the early Pliocene (~8-4 Ma) according to the most researchers. Whereas, according to Armijo et al. (1999), this age is between 5 and 7 Ma. NAF forms the border between Eurasian Plate in the north and Anatolian Plate in the south. According to Barka (1992), the slip rate between Erzincan and Niksar is 0.7-0.8 cm/year, and is 0.5-0.6 cm/year between Niksar and Bolu. Tatar et al. (2012) used remote sensing technique to investigate the slip rate along the eastern part of the NAF. They concluded that the locking depth of fault increases from 8.1 km in Erzincan to 12.8 km nearby Niksar. According to their measurements, the slip rates on the NAF is increasing from 16.3 mm/year on the east to 24.0 mm/year on the west of fault segments between Erbaa and Niksar. Poyraz (2016) estimated the locking depth as 12.72 km between Erzincan and Tokat.

During 20th century, a number of destructive earthquakes on NAF were recorded. The extends of fault rupture during these events are shown in Figure 3.4. The first two events were located on the west of NAF, namely on its Ganos segment in 1912 ($M_W7.4$). This is later followed by a sequence of major events beginning from the eastern segments and proceeding towards the western segments located on the Sea of Marmara. These events were namely the 1939 Erzincan ($M_W7.9$), the 1942 Niksar-Erbaa ($M_W6.9$), the 1943 Tosya-Ladik ($M_W7.7$), the 1944 Gerede ($M_W7.5$), the 1957 Abant ($M_W6.8$), the 1967 Mudurnu Valley ($M_W7.1$). The 1999 Izmit ($M_W7.6$) and the 1999 Düzce ($M_W7.2$) earthquakes are the most recent destructive events on the NAF (Barka et al., 2002; Syngellakis, 2015). 1939 Erzincan earthquake is the closest rupture for the study area, and it is also one of the largest earthquakes on NAF. The magnitude of this event was estimated as 7.9 by Barka (1996) magnitude scale is unspecified, it was $M_S7.9$ according to UDIM, or it was $M_S8.0$ according to Tan et al (2008). The segments of 1939 Erzincan earthquake suggested by Barka (1996) are shown in Table 3.3. Total fault length was reported 360 km.

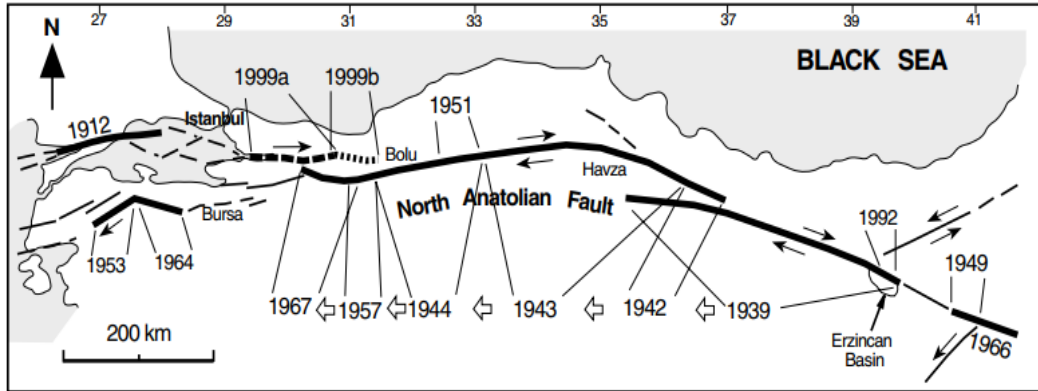


Figure 3.4 Earthquakes since 1939 on NAF (Barka et al., 2002)

Table 3.3. NAF length and estimated M_w for a rupturing segment of NAF

Segment	Length (km)	Estimated M_w
Ezinepazarı	90	7.3
Kelkit Valey	100	7.4
Ortaköy Su Şehri	45	7.0
Mihar Tümekear	65	7.2
Erzincan	60	7.2
Total	360	8.0

3.3.1 Seismic Activity Around Şebinkarahisar

The catalog of earthquakes in the instrumental period (i.e., after the year 1900) is compiled from UDIM. The database presents the catalog information about events, including date, time, latitude and longitude of epicenter, depth of hypocenter, magnitude of event according to the scales M_D , M_L , M_S , M_B , and a description about the location of the event. All events in this catalog have magnitudes (for any scale) greater than or equal to 4.0. The events that have epicenters located within 200 km radius of the coordinates 38.40°E and 40.20°N between the dates January 1st, 1990 and December 28th, 2013 were selected to compile a reduced set of events. This

reduced catalog involves 245 events. The information on depth was ignored during selection. A sample of catalog events that are compiled from the UDIM database are shown in Table 3.4. The complete catalog of selected events is presented in Appendix C.

M_w for 162 events are not reported in the compiled catalog. The duration magnitude (M_D 6.0) of the event located in Erzincan province on 08.11.1941 is considered as questionable due to possible saturation of this magnitude scale. No other magnitude scale is reported for this record. On the other hand, any record that can be associated with this event could not be found in other earthquake databases available on the web, such as SHARE-CET (Sesetyan et al., 2013) and the catalog of United States Geological Survey (2014). Therefore, this significant event was eliminated from the reduced catalog before the hazard analysis.

Table 3.4. A sample of seismic events compiled from the catalog (UDIM, 2014)

Time	Lat. (deg.)	Long. (deg.)	Depth (km)	M_D	M_L	M_w	M_S	M_b
2014	39.2	38.7	4.4	0	4.3	4.1	0	0
2014	39.5	37.4	5	0	4.3	4.2	0	0
2013	38.4	38.9	8.4	0	4.1	4.0	0	0
2013	38.6	37.3	5	0	4.0	4.0	0	0
2013	40.8	36.3	10	0	4.2	4.0	0	0
2012	39.5	39.9	5	0	4.2	0	0	0
2012	39.5	39.9	5	0	4.0	0	0	0
2012	39.5	40.0	5	0	4.2	0	0	0

In the absence of M_w , this magnitude scale was estimated by developing linear relationships between M_w and the other magnitude scales presented in the catalog of events around Şebinkarahisar. Figure 3.5 shows the best-fit linear relationships according to the principle of least squares (Devore and Berk, 2007). The upper limit for magnitude range shown on each axis in Figure 3.5 depicts the saturation magnitude for that particular scale. These linear relationships were ranked according

to the coefficient of determination (r^2), and are presented in Table 3.5. M_W reported for 83 earthquakes in this dataset. These records were used for developing relationships. Whereas, only one magnitude scale other than M_W is reported for 115 events. The solely available magnitude scale was used for estimation of M_W . Two or more of magnitude scales other than M_W were available in the remaining data, so M_w was estimated for these events by using the equation having a higher rank (r^2) in Table 3.5. The estimations for M_w were rounded up or down to the closest multiple of 0.1.

The aftershocks in the dataset of events were eliminated by declustering analysis. The dataset of events around Şebinkarahisar was declustered by using the computer program ZMAP (Wyss et al., 2001) and the method of Gardner and Knopoff (1974). The declustering method identified 18 clusters of earthquakes, and a total of 49 events out of 144 as foreshocks and aftershocks. Figure 3.6 displays the declustered catalog containing 95 main events. The seismic moment released by the clusters of fore/aftershocks is about 1.8% of the total seismic moment of the earthquakes involved in the analysis.

The declustered catalog of events is presented in Appendix D. The range of magnitudes in the catalog is assessed for completeness according to the method of Albarello et al. (2001). The annual accumulation of events in each magnitude interval is shown in Figure 3.7. The period of completeness for each magnitude range is presented in Table 3.6. The rate of accumulation of events before these periods of completeness are observed to be significantly lower than the rate in these periods.

Table 3.5. The empirical linear relationships between magnitude scales

Linear Relationship	r^2
$M_W = 0.81 \times M_S + 1.10$	0.986
$M_W = 1.03 \times M_D + 0.03$	0.982
$M_W = 1.12 \times M_B - 0.41$	0.978
$M_W = 1.06 \times M_L - 0.12$	0.973

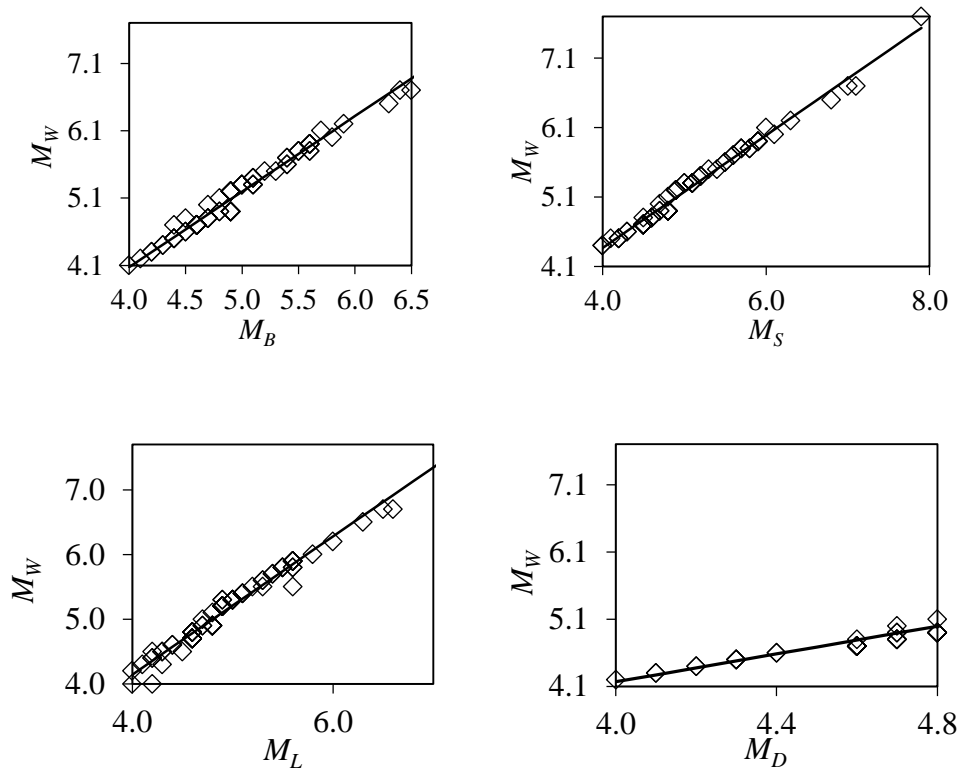


Figure 3.5 The relationship between magnitude scales: (a) M_B to M_W , (b) M_S to M_W , (c) M_L to M_W , and (d) M_D to M_W

Table 3.6. The period of completeness for magnitude ranges

M_{\min}	M_{\max}	Complete after
4.5	4.9	1954
5.0	5.4	1952
5.5	5.9	1938
6.0	7.7	1904

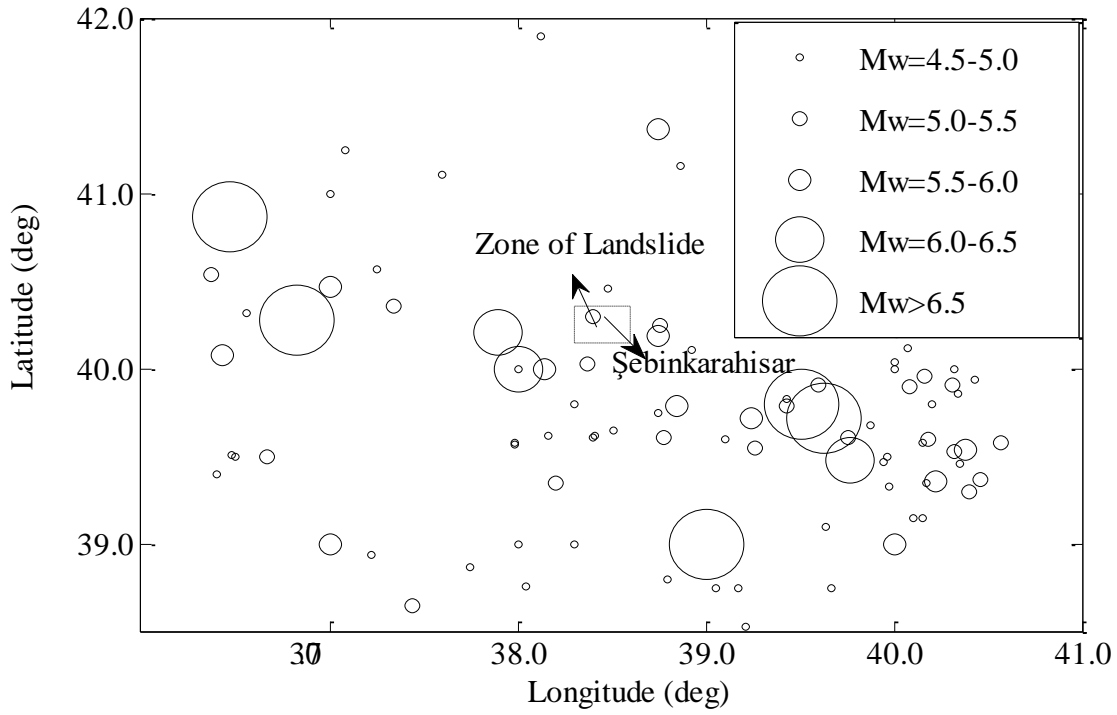


Figure 3.6 Declustered catalog of events around Şebinkarahisar

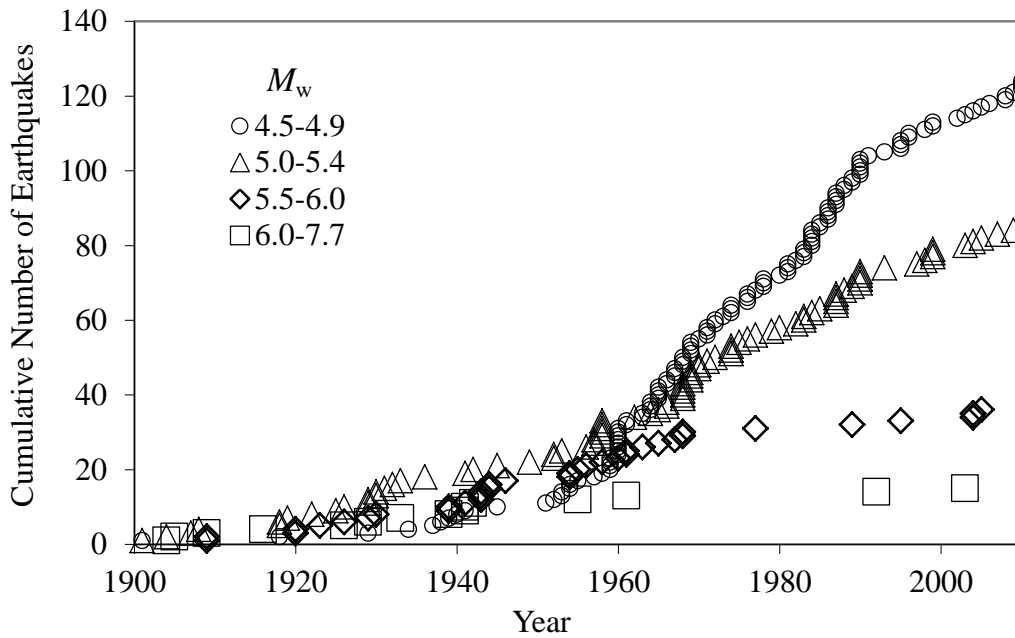


Figure 3.7 Accumulation rate of M_w around Şebinkarahisar

3.3.2 Geometric Extends of Seismic Sources around Şebinkarahisar

Line and area sources shown in Figure 3.8.a and 3.8.b were used in this study. Line sources approximately delineate the location of NAF shown on the active-fault map of Turkey that was presented by Emre et al. (2011). The modeling of each fault segment distinctly and consideration of probabilities of cascading ruptures will improve the accuracy of PSHA, provided that accurate information on the segmentation and on the distribution of total moment rates on segments is available (Erdik et al., 2004). However, a simplified continuous model of NAF was preferred to avoid complexity in analysis due to absence of accurate analysis on the probabilities of cascading ruptures on eastern NAF. Therefore, it was supposed that the source of large magnitude events in the region is solely the 352 km-long continuous linear model of NAF extending between Koyulhisar, Sivas, Refahiye, Erzincan. It was assumed that the relatively small magnitudes originate from rupturing of unmapped faults modeled by a relatively large area source.

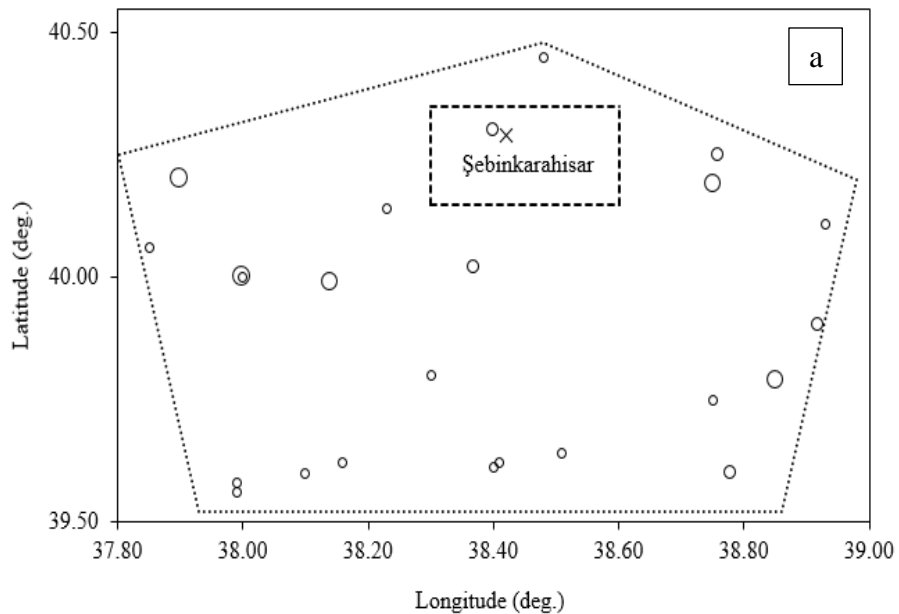


Figure 3.8 a) The area, and b) fault sources used in the study.

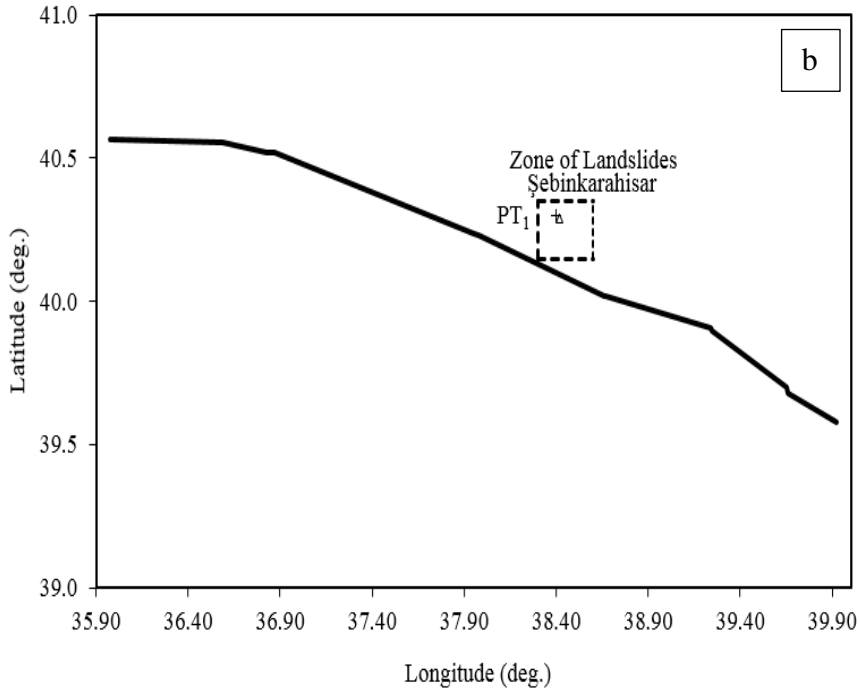


Figure 3.8 (continued)

3.3.3 Magnitude-Recurrence Relationships for Sources

An important parameter to be defined for truncated magnitude-recurrence relationships is M_{max} . M_{max} on NAF segments close to Şebinkarahisar is estimated by considering two methods. In the first method, the geometric properties of fault segments were taken into consideration. According to Wells and Coppersmith (1994), the average relationship between surface rupture length (SRL , in km) on a strike-slip fault, and moment magnitude of an event is

$$M_W = 5.16 + 1.12 \cdot \log(SRL) \quad (3.15)$$

SRL for each segment was estimated by considering the segmentation of 1939 Erzincan rupture suggested by Barka (1996). The estimated M_W for each segment, shown in Table 3.5, was supposed to be representative for M_{Max} on each segment.

The second method used was based on the historical data on earthquakes. The list of most significant earthquakes around Şebinkarahisar is presented by Table 3.7. The 26 December 1939 Erzincan earthquake ruptured number of segments that are consisting about a length of 360 km on NAF (Barka, 1996). M_w 8.0 estimated for a total length of 360 km is reasonable consistent with the figures (M_s 8.0) reported in section 3.3. Therefore, it was supposed that the maximum earthquake magnitude on the line source can reach to M_w 8.0. Although the sample used for derivation of Equation 2.3 does not involve events $M_w \geq 7.6$. It was supposed that this equation is applicable in the range of M_w from 7.6 to 8.0.

Table 3.7. The historical and recent destructive earthquakes on the east of NAF

Date	Place	Magnitude	Reference
499	Niksar	7.0	Ambraseys and Jackson, 1998
1045	Erzincan	6.8	SHARE-CET
1668	Amasya	7.9	Ambraseys and Jackson, 1998
1939	Erzincan	7.9	Syngellakis, 2015
1942	Niksar Erbaa	6.9	Syngellakis, 2015
1943	Tosya	7.7	Syngellakis, 2015

The minimum limit for magnitude of significant earthquakes on line source (NAF) is assigned similarly by using the geometric properties of fault segments, and by using the historical data. The estimated M_w for rupture of 45 km long Ortaköy Su Şehri fault is 7.0. On the other hand, the estimated M for the historical event in the year 499 is as low as 6.0 according to the study of Ambraseys and Jackson (1998). Considering the uncertainty in magnitudes reported for historical events, M_w 6.5 is supposed to be a reasonable lower limit for significant earthquakes on the line model of NAF. The magnitudes of characteristic events on line source were supposed to range from 6.5 to 8.0. The details of segmentation and probabilities of cascading fault ruptures were not considered. The recurrence relationship on the line source was modeled by using truncated exponential function (Equation 3.4.a), after substituting $\beta=0$. The slip rate is supposed as 20 mm/yr for 360 km long successive

segments of NAF around Şebinkarahisar, and width of faulting (or, interlocking width) was supposed as 10 km. These figures are reasonably consistent with slip rate and locking depth on Giresun according to the study of Tatar et al. (2012). At first, the seismic activity has been calculated by Equation 3.6. However, it was observed that the annual rates of large-magnitude events become much larger than the rates depicted by historical events. This can be explained by the almost continuous creep of the mature fault that does not result in seismic moment accumulation on fault, which was observed by remote sensing on western segments of NAF (Çakir et al., 2012; Rousset et al., 2016). A better agreement among the historical events and magnitude recurrence relationships was observed in case the rates on line source was decreased by about 40%. Hence v_{Mmin} for line source was estimated as $6.0 \cdot 10^{-3}$. This 40% decrease in estimation of seismic moment accumulation on active faults has been also suggested by Paradisopoulou et al. (2010) in a study on seismic hazard assessment in western Turkey. The magnitude recurrence relationship is compared on the catalog data of earthquakes in Figure 3.9.

The recurrence relationship on area source was modeled by using truncated exponential function (Equation 3.4). The seismic activity within 100km radius of Şebinkarahisar was considered for the area source. The magnitudes on the area source was supposed to range from 4.5 to 6.4. Hence, the events with magnitudes less than 4.5 were supposed to have an insignificant contribution to seismic hazard. There are 26 earthquakes with $M_w \geq 4.5$ in the dataset of declustered events which are located within 100 km radius area around Şebinkarahisar. The parameter β was determined according to method of Weichert (1980), and by supposing a magnitude interval of $\Delta M=0.1$ in the use of formulas of Bender (1983). β and v_{Mmin} were respectively computed as 1.84, and 1.43. All events were supposed to be shallow earthquakes. Figure 3.9 compares the theoretical magnitude recurrence relationship for area source with the declustered catalog of events.

The relatively small difference between the magnitude-recurrence relationship of area source and the declustered events can be explained by the incompleteness of

catalog data particularly in the lower ranges of M_W . The magnitude-recurrence relationship is slightly conservative for the rates of large magnitude events modelled by line source. This can be explained by the uncertainty regarding M_W of historical events, which consequently effects M_{\min} of characteristic model. Hence, the model for total seismic activity (Figure 3.9) around Şebinkarahisar was supposed to model rate of large magnitudes reasonable but can be improved by further detailing of seismic activity.

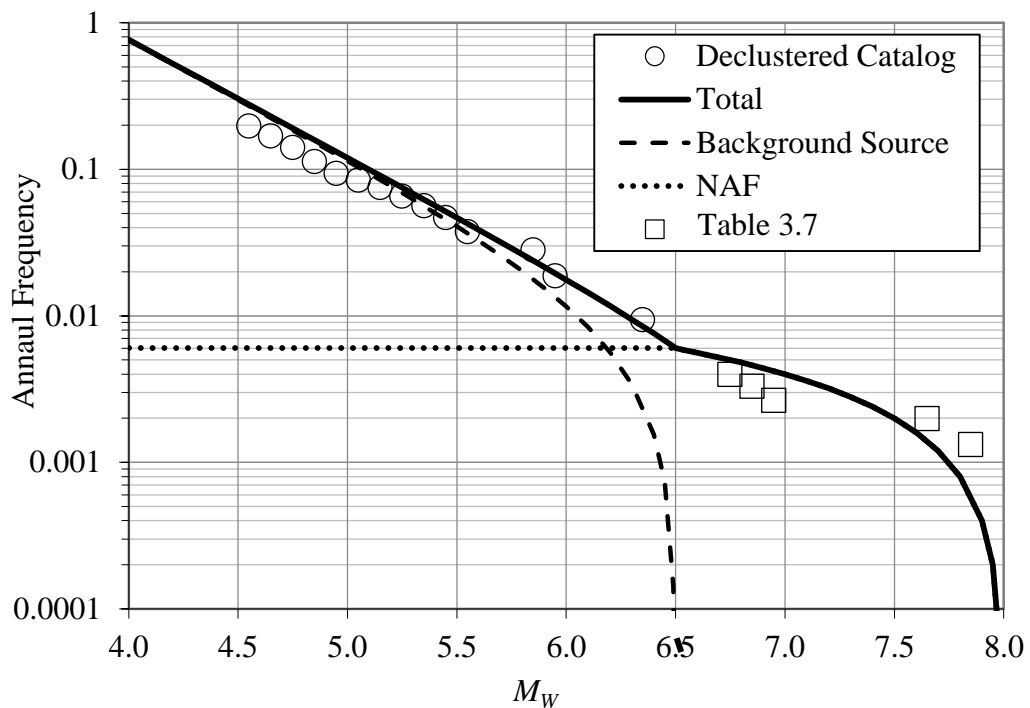


Figure 3.9 The magnitude-recurrence relationship used in analyses

3.3.4 Seismic Hazard Analysis in terms of D

In this study, the computer program CRISIS 2007 (Ordaz et al., 2007) was used for PSHA. In this program, the seismic sources can be geometrically defined as a point, a fault (combination of lines), and an enclosed area. The seismic source model can be Poissonian, and the magnitude recurrence relationships can be truncated exponential

(Equation 10). A grid of sites for computation of PSHA was defined. Source geometries were defined as a fault and an area source. The explanations for these input parameters are explained in the following bulleted list.

- A 0.005°-interval grid of sites was generated as shown in Figure 3.10.
- Line and area sources were defined as shown in Figure 3.8.
- Source seismicity for area source was defined according to Figure 3.9.
- The data table defining the attenuation relationship (GMPE) was defined by using Equation 2.3 for applicable ranges of the parameters a_c , V_{S30} , R_{jb} and M_w .

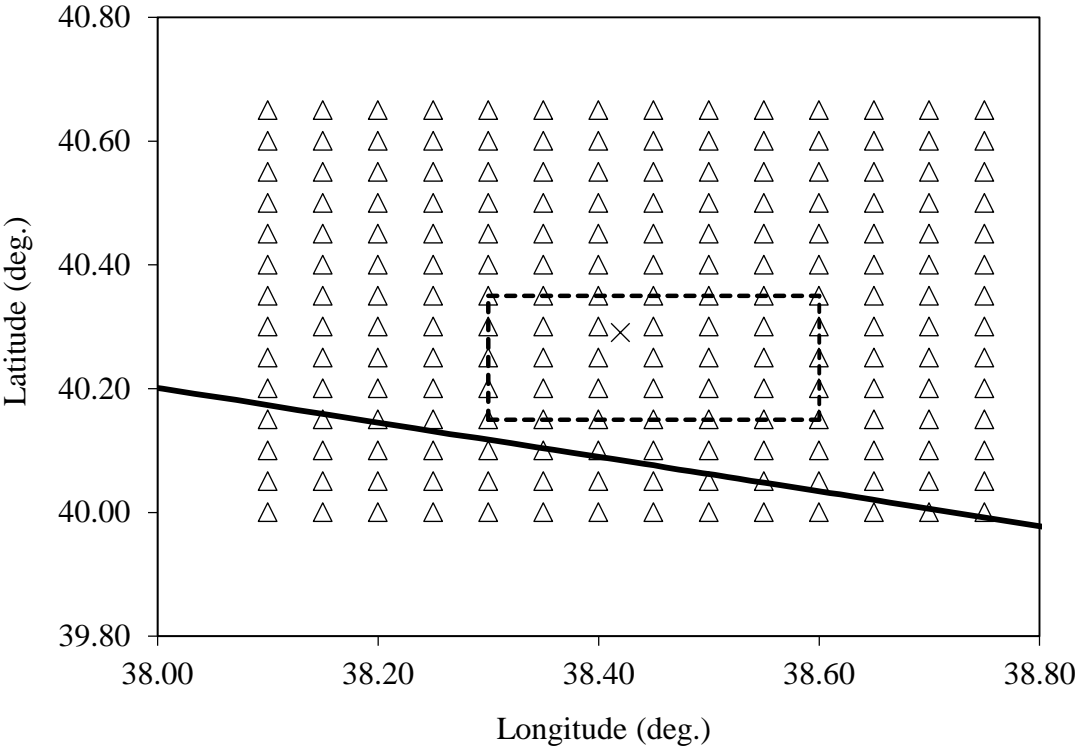


Figure 3.10 The calculation (grid) points shown by triangles

CRISIS basically computes the seismic hazard in terms of (spectral) acceleration. The ground-motion prediction equations predicting spectral acceleration amplitude for a regularly spaced set of magnitude, distance and oscillator period should be

defined numerically. Then the program uses interpolation techniques for calculation of acceleration for any arbitrary selection of these parameters. The use of magnitude and distance parameters for estimation of sliding block displacement D (Chapter 2) is similar to that for similar acceleration. Whereas the input for oscillator period was substituted by the parameter a_c . The parameter V_{S30} is explicitly defined, such that a new set of prediction equations is to be defined for any V_{S30} considered in analyses.

Eight different values of a_c were chosen for analysis: 0.05g, 0.075g, 0.10g, 0.15g, 0.20g, 0.30g, 0.40g, 0.50g. Seismic hazard was computed for nine levels of seismic intensity depicted by $T_R=98, 140, 475, 975, 2475, 4975, 9975, 14980, \text{ and } 24980$ years. This set of T_R respectively corresponds to 40%, 30%, 10%, 5%, 2%, 1% 0.333%, and 0.2% probabilities of exceedance in 50 years (Equation 3.11). The set of T_R is reasonable consistent with the set of Solomos (2008) shown in Table 3.1, and involves a set of large numbers for graphical completeness of hazard curves. Basically, $V_{S30}=300$ m/s, which represents the site conditions for stiff dense soils, was considered in all analyses except for those in which the effect of V_{S30} on seismic coefficient was investigated. The output file consists of hazard computed in terms of D on each grid point for the defined set of a_c . The hazard was computed for the grid shown in Figure 3.10. The results for the grid point on coordinates 38.40°E and 40.30°N are presented on Figure 3.11.b. The use of this figure is explained in the next section. In a separate PSHA, the ground motion prediction equation proposed by Akkar and Boomer (2007) was also used to compute the hazard in terms of PGA for a continued assessment of results. Sisi et al. (2017) also used this GMPE to compute PSHA on spectral coordinates closely located to eastern segments of NAF.

3.3.5 The selection of Seismic Coefficient

The seismic hazard expressed in terms of D on the coordinates 38.40°E and 40.30°N for a set of a_c , ranging from 0.05g to 0.50g, is shown in Figure 3.11.a. Figure 3.11.b is useful for selection of k_h , provided that D_{all} , and the probability (P_R) of exceeding this limit ($D > D_{all}$) in a duration, T_L have been prescribed. D_{all} is related to desired

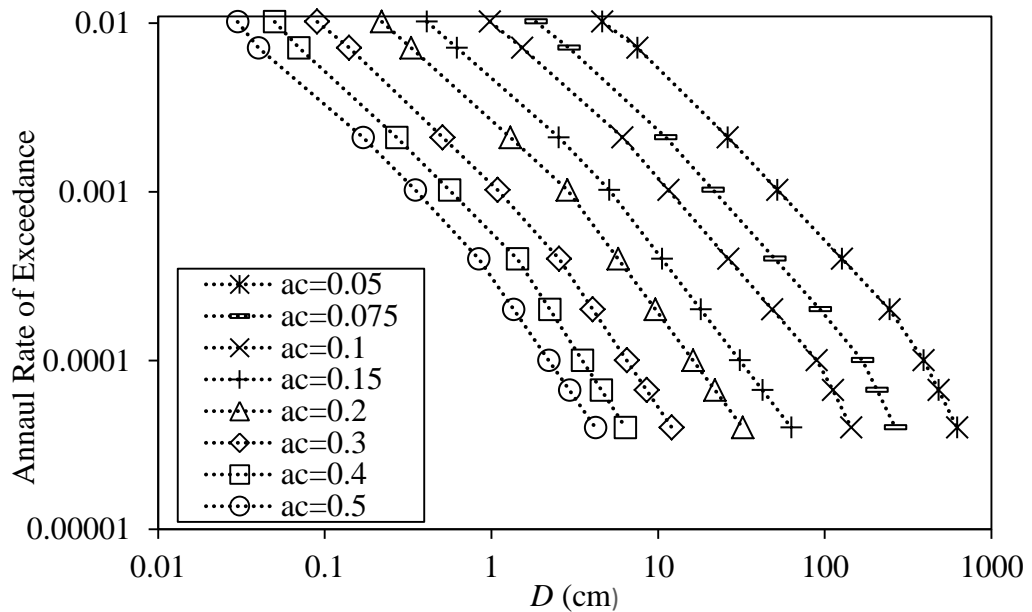
performance level for the facilities that can be effected by the sliding ground. T_L can be related to the service duration of effected facilities, and P_R can be related to the consequences of failure. In the absence of clear descriptions of T_L and P_R , a selection of T_R among widely used figures (e.g. Table 3.1) is possible, so that the level of seismic intensity can be compared with those specified for design of typical buildings. Reasonable limits for D employed in previous studies are presented in section 1.2.

An example for selection of k_h is shown in Figure 3.11.b. Two specific levels of D were supposed to be critical. The first is that slope is supposed to be unstable in case D exceeds a threshold around 1 cm. This limit can be considered if the shear strength on failure plane is very sensitive to D , or if the limit for D is related to the performance of a facility that is extremely sensitive to ground displacement such as a rail road. The second limit was chosen as 10 cm, which may be considered if there are buildings on mat foundations that can tolerate to relatively large foundation displacements (Wahls, 1981). T_R was chosen as 475 yr, which is typical in probabilistic estimation of spectral accelerations for design of dwellings. The parameter a_c was determined as 0.22g and 0.08g on Figure 3.11.b respectively, so that the probability of exceeding the displacement thresholds 1 cm and 10 cm in 50 years is 10%. Consequently, $k_h=0.22$ and $k_h=0.08$ are respectively the seismic coefficients to be considered in analysis of seismic safety of sloping ground on these coordinates according to the concept of performance based design.

A regional map of k_h can be prepared by using this procedure. First, the hazard curves in terms of D are computed for all grid points by considering specific V_{S30} . Second, the relationship between allowable limit for (i.e., $D=D_{all}$) and a_c is built for a range of T_R as shown in Figure 3.11.b. Finally, k_h is determined by considering a set of T_R and D_{all} . The contour maps are developed according to variation of k_h among grid points. The contour map of k_h around the area prone to landslides is shown in Figure 3.12 for the set of parameters: $T_R=475$ yr, $D=1$ cm and $V_{S30}=300$ m/s. The spatial variability of k_h in the case $D=10$ cm is shown in Figure 3.13 for comparisons.

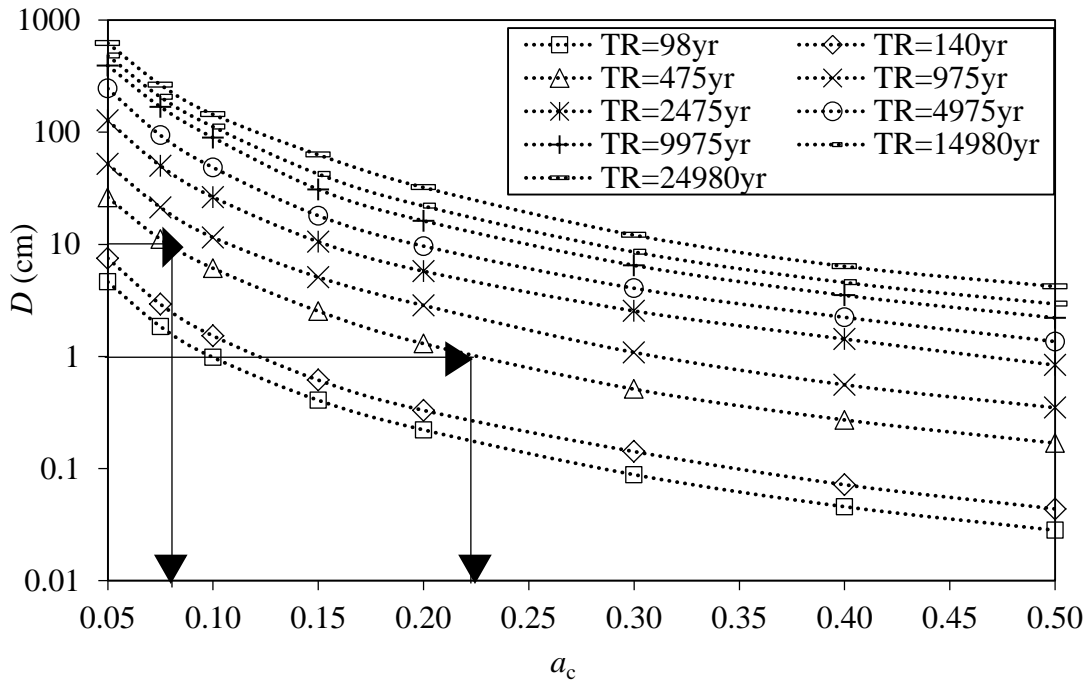
k_h decreases with increasing distance from NAF. The choice for D_{all} has a very pronounced effect on k_h , such that the figures for the case $D=1$ cm are almost three times the figures for the case $D=10$ cm.

Figure 3.14 shows k_h for the set of parameters $D=10$ cm, $T_R=2475$ yr and $V_{S30}=300$ m/s. The figures for k_h shown in Figure 3.14 are about two times those shown in Figure 3.13. This will correspond to $\gamma=2$ for $T_R=2475$ years if $\gamma=1$ is supposed for $T_R=475$ years. Certainly γ is dependent on the models of seismic activity and the variance of prediction equation.



(a)

Figure 3.11 The relationship between T_R , a_c and D for coordinates 38.40°E and 40.30°N a) to conversion b) to selection



(b)

Figure 3.11 (continued)

A set of γ is calculated is shown in Table 3.8 for comparison with Table 3.2. $\gamma=1.0$ is assigned for $T_R=475$ years in the cases $D_{all}=1$ cm and $D_{all}=10$ cm. Because $D_{all}=100$ cm yields practically very small figures for k_h in case $T_R=475$ years, the return period corresponding to $\gamma=1$ for this extreme limit of D all was chosen as 2475 years. The comparisons between Table 3.2 and Table 3.8 in terms of the relationship between T_R and γ suggest that $T_R=689$ years ($P_R=7\%$, $T_L=50$ years) for $\gamma=1.2$ and $T_R=975$ years ($P_R=5\%$, $T_L=50$ years) for $\gamma=1.4$ are reasonable for k_h in case D_{all} is limited with 10 cm. $T_R=2475$ years corresponds to $\gamma=2.0$. It is observed that the range $T_R \geq 2475$ years should be considered for unpredictable consequences of extremely large slope displacements.

Table 3.8. The calculated relationship between the importance factor (γ) and T_R for the coordinates 38.40°E and 40.30°N

γ	T_R (years)		
	$D_{all} = 1$ cm	$D_{all} = 10$ cm	$D_{all} = 100$ cm
0.80	322		
1.00	475	475	2475
1.20	713	709	3760
1.40	1011	1043	5173
2.00	2252	2689	14905

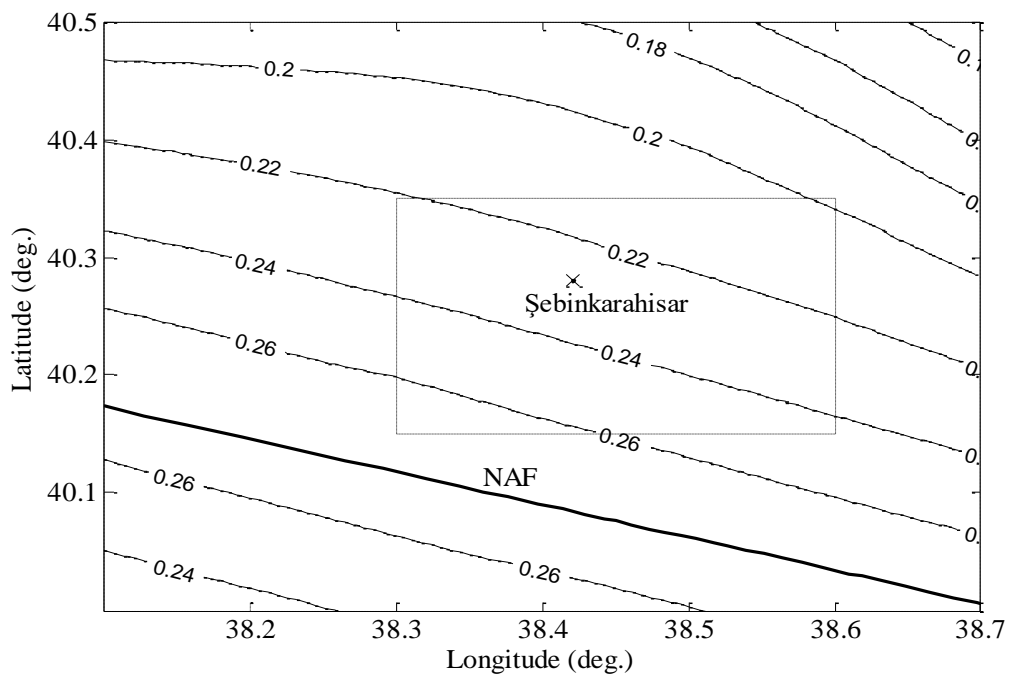


Figure 3.12 The spatial distribution of k_h for $D_{all} = 1$ cm, $T_R = 475$ yr and $V_{S30} = 300$ m/s

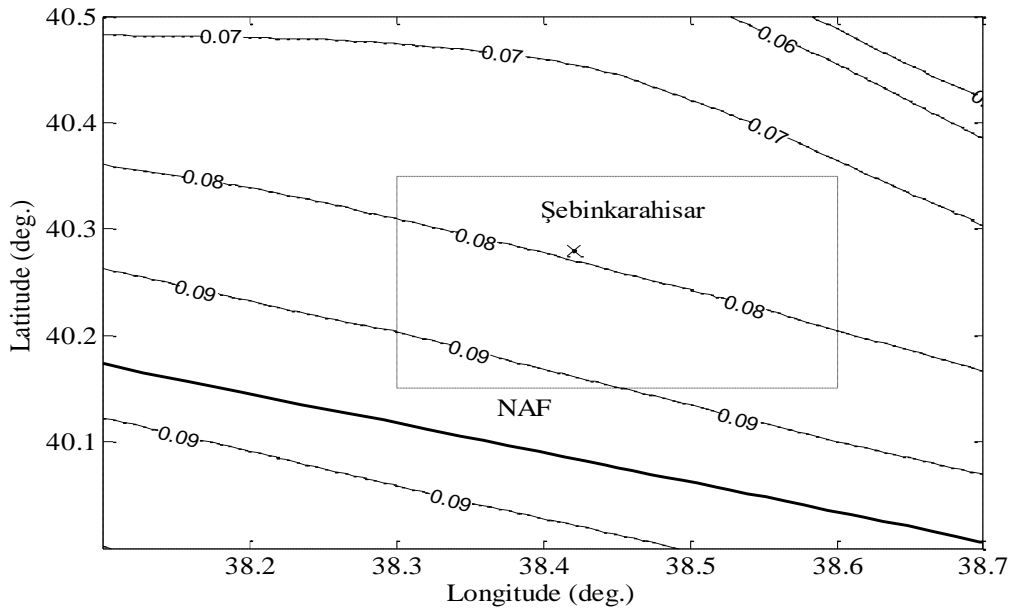


Figure 3.13 Spatial distribution of k_h for $D_{all}=10$ cm, $T_R=475$ yr, and $V_{S30}=300$ m/s

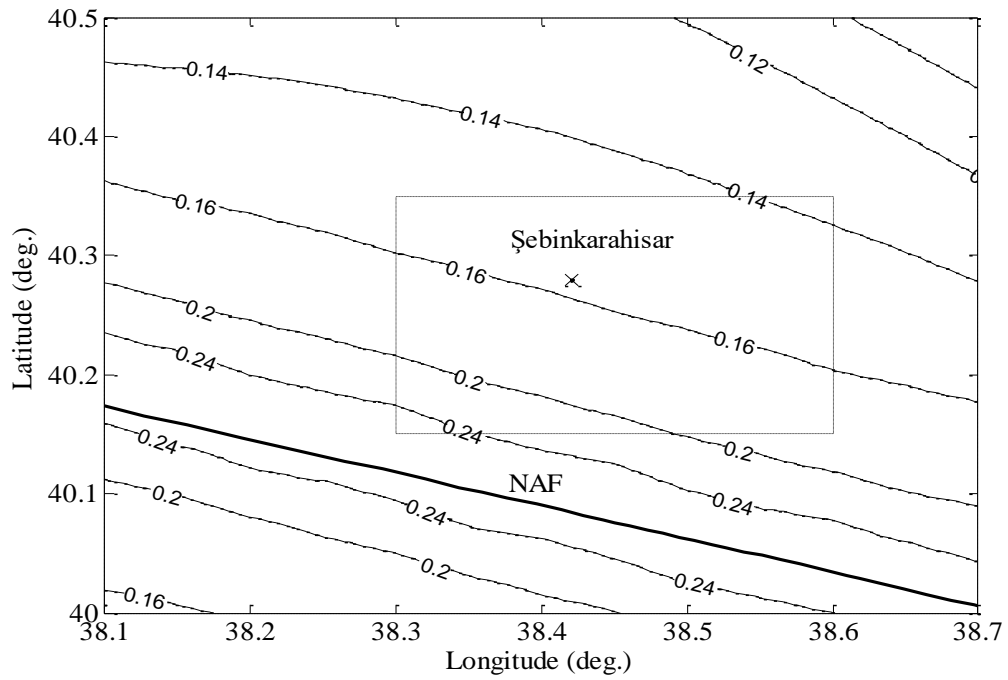


Figure 3.14 The spatial distribution of k_h for $D_{all}=10$ cm, $T_R= 2475$ yr and $V_{S30}=300$ m/s

The relationship between annual rate of exceeding D_{all} and a_c on the coordinates 38.40°E and 40.30°N is shown in Figure 3.15. Figure 3.15 is useful for a reasonable selection of k_h through a trade-off between T_R and D_{all} . The displacement limit for a specific performance is also relevant to the mobilized shearing resistance on the interface between sliding block and rigid support, representing the plane of failure on a possible landslide. For instance, if a system that is sensitive to residual ground displacements is of concern, a return period of 475 years will yield $k_h=0.22$. This k_h is close to 0.20, which has been practically used in regions of severe seismic activity (Table 1.1). On the other hand, a lower probability of exceeding this displacement threshold can be desired, because of the consequences of failure. In that case, $T_R=2475$ years will yield $k_h=0.47$, allowing considerably low slope angles in practice. Consequently, either geotechnical solutions that improve the shear strength on potential failure planes should be developed, or sensitivity of facilities to residual ground displacements should be reduced. $k_h=0.05$ can be reasonable choice for slopes that are not close to facilities hypothetically located on these spatial coordinates, because $D_{all}=100$ cm can be practical limit, possibly due to the unpredictable consequences of such large ground displacement and $T_R=2475$ years will a failure probability that is comparable to that considered for the design of critical structures such as hospitals.

The effect of V_{S30} on k_h was investigated by repeating the analysis for a set of V_{S30} . Figure 3.16 shows the effect of V_{S30} on D . The analysis show that V_{S30} has a pronounced effect on D , and consequently on k_h . This is explained by the significance of the coefficient of the term V_{S30} in the equation 2.3. D increases by a factor of 3.75 when V_{S30} is reduced from 700 m/s to 300 m/s. These figures can correspond to soft rock and stiff soil sites respectively. a_c should be greater than 0.30g in order to limit the displacement to figures less than 1 cm if V_{S30} is as low as 200 m/s. Therefore, a reasonable decision on V_{S30} is critically important before selection of k_h . Figure 3.17 shows the spatial variability of k_h for the sites characterized as $V_{S30}=700$ m/s in the case that the parameters are chosen as $D_{all}=1.0$ cm and $T_R=475$ years. The comparison of Figure 3.17 with Figure 3.12 shows that k_h

reduces almost by a factor of 2 for failure of discontinuous on rock that can show brittle response to displacements.

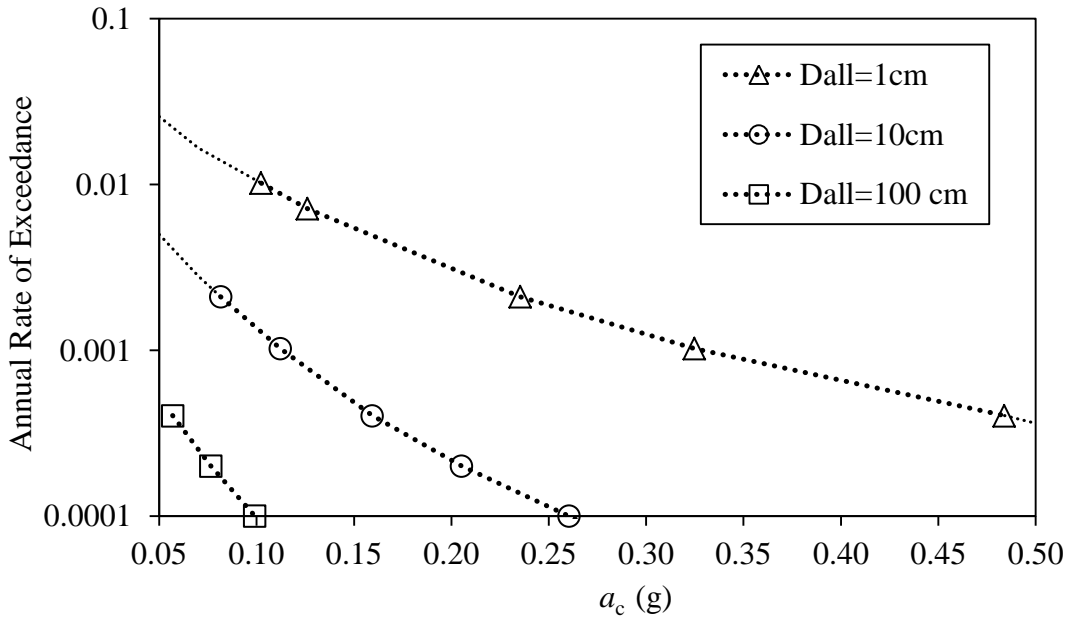


Figure 3.15 The annual rate of exceedance versus a_c for $D_{all}=1$ cm, $D_{all} =10$ cm and $D_{all} =100$ cm for the coordinates 38.40°E and 40.30°N

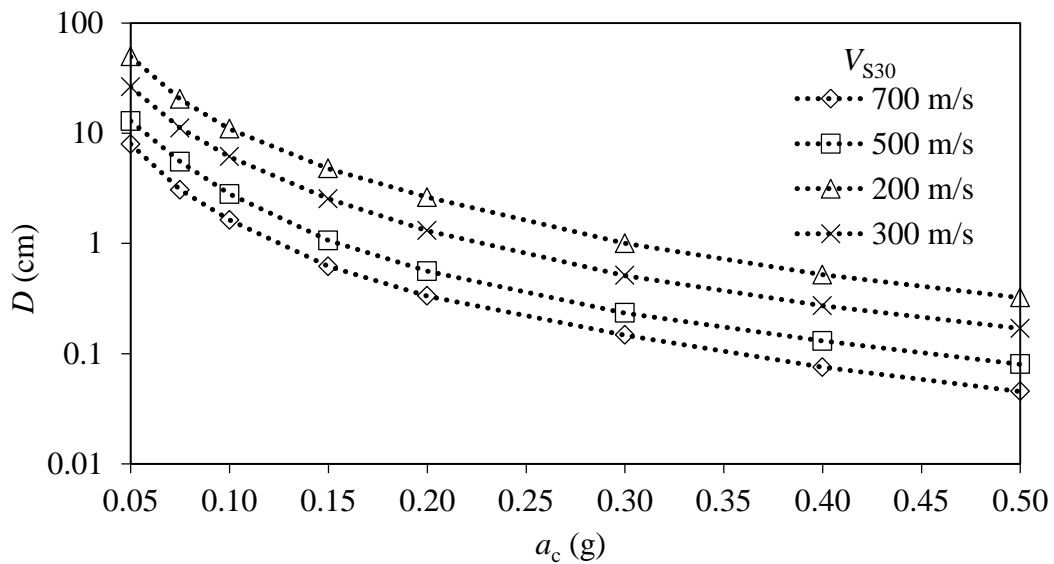


Figure 3.16 The relationship between D and V_{S30} on the coordinates 38.40°E and 40.30°N in case $T_R=475$ years

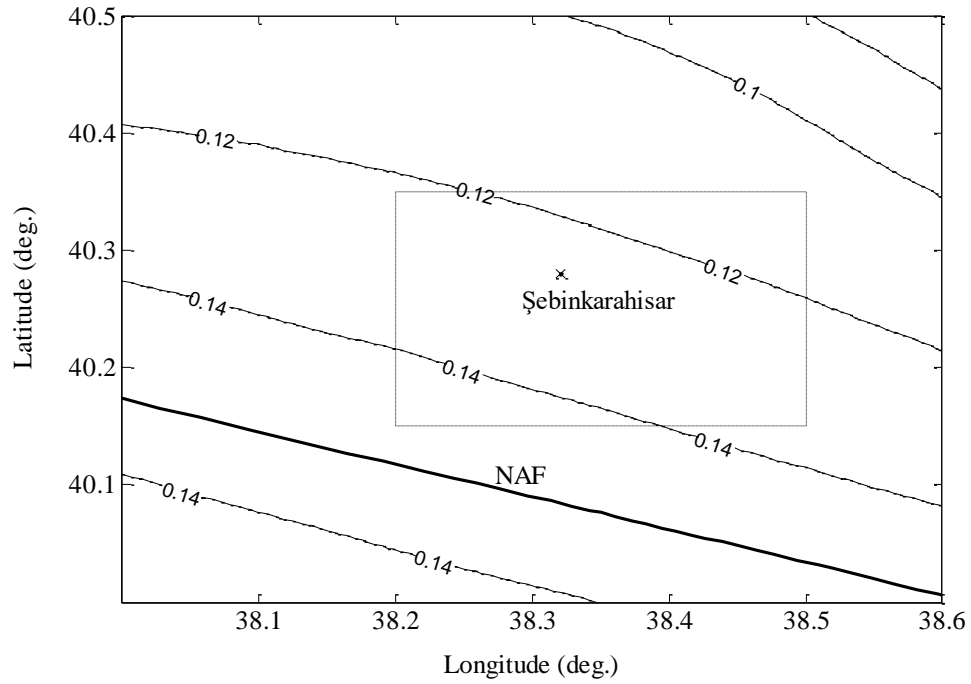


Figure 3.17 The spatial distribution of k_h for $D=1$ cm, $T_R=475$ yr and $V_{S30}=700$ m/s

3.3.6 Mapping Critical Slopes

A next step after mapping spatial distribution of k_h can be the identification of locations that are prone to seismic slope failure. The shear strength of geological materials is frequently modelled by Mohr-Columb failure criteria.

$$\tau_u = c + \sigma_n \cdot \tan(\phi) \quad (3.16)$$

where τ_u is ultimate shear resistance on a failure plane, c is cohesion, ϕ is internal friction angle, and σ_n is normal stress acting on a failure plane. However, a critical decision on the shear strength parameters c and ϕ is not straightforward, because mobilized shear strength of geological material depends on shear displacement (Skempton, 1964). This is illustrated in Figure 3.18. The peak strength is to be reached for initiation of failure. Whereas, the mobilized shear strength drops down to residual shear strength by increasing shear displacement. According to Skempton

(1964), the residual shear strength is mobilized in a ring shear or direct shear test, when the total shear displacement reaches to 5 cm approximately. The geological material shows almost no cohesion ($c=0$) during mobilization of residual strength. Therefore, the residual shear strength can be supposed to be mobilized if D_{all} is chosen as 10 cm in remoulded clays.

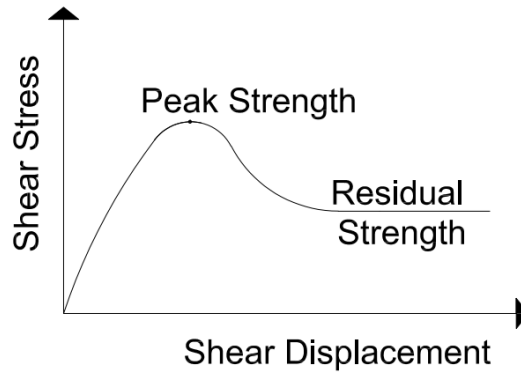


Figure 3.18 Residual shear strength of soil (after Skempton, 1964)

$$\tau_r = \sigma_n \cdot \tan(\phi_r) \quad (3.17)$$

where ϕ_r is defined as residual friction angle. Stark et al. (1994) stated that residual shear strength strongly depend on type of clay mineral and on quantity of clay-size particles. Therefore, ϕ_r is empirically related to plasticity index (PI) of clays. PI is the difference between Atterberg limits, liquid limit (LL) and plastic limit (PL), determined in laboratory (Knappett and Craig, 2012). Figure 3.19 shows a picture of the clayey soil deposits that were mobilized by a recent cut to open a path through a landslide route on approximately 5 km east of Şebinkarahisar. The specimens recovered from this site were tested for their Atterberg limits (Zemar, 2015). PI was reported to be ranging from 20 to 44 approximately for specimens recovered from first 15 m depth in three boreholes. The sample ranges for LL and PL was observed

to be 35-60 and 3-19 respectively. An empirical relationship between PI and ϕ_r is (Knappett and Craig, 2012)

$$\phi \cong 93 \cdot (PI)^{-0.56} \quad (3.18)$$



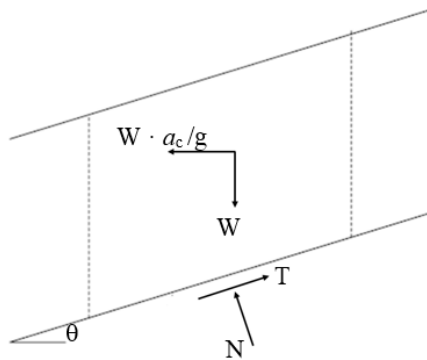
Figure 3.19 The clayey deposits on an unstable cut on landslide zone near Şebinkarahisar

Supposing that $PI > 30$ for soil deposits that are prone to landslides, $\phi_r \cong 14^\circ$ was considered as a reasonable first estimation for residual shear strength. It was also supposed that all such clay deposits in the area rest on failure planes that have been mobilized in the past during landslides. Because of the relatively high precipitation rates in the province of Giresun, the seepage of ground water was supposed to be a more important mechanism in triggering landslides than earthquakes.

In the absence of information about thickness of soil deposits and their geotechnical properties, a first order map showing the topographical opportunity for landslides can be prepared by simplifications. The infinite slope assumption (Abramson, 2001) provides simple formulas for threshold topographical slope. It was supposed that, either an excessive seepage in these soils or a severe seismic event can cause failure

of land masses but the probability of simultaneous occurrence of two events is negligible.

The infinite slope will be mobilized on the sliding plane that is extending parallel to the ground if horizontal inertial load, equal to $W \cdot a_c/g$ exceeds the ultimate shearing resistance on failure plane. According to principles of performance-based design, a level of displacement can be deemed as acceptable for a desired performance of facilities located on areas prone to landslides. A simplified regional analysis is possible by substituting $a_c/g = k_h$ and $\phi = \phi_r$ in the stability equations for an infinite slope (Figure 3.20), such that yielding



$$N = W \cdot \cos(\theta) - W \cdot k_h \cdot \sin(\theta)$$

$$T = W \cdot \sin(\theta) + W \cdot k_h \cdot \cos(\theta)$$

$$T \leq N \cdot \tan(\phi) \text{ for stability}$$

Figure 3.20 The forces acting on a section of an infinite slope

$$k_h \leq \frac{\cos(\theta) \cdot \tan(\phi) - \sin(\theta)}{\sin(\theta) \cdot \tan(\phi) + \cos(\theta)} \quad (3.19)$$

In equation 3.19 the parameter θ denotes the slope of ground. The upper limit for θ satisfying the inequality in Equation 3.19 can be considered as allowable range of topographical slope for a given k_h unless geotechnical data depict a more competent formation. It should be stated that, the soils are supposed to be unsaturated in derivation of Equation 3.19.

As a second assumption, it was supposed that soils deposits on sloping ground are marginally stable, and any increase in saturation of soil mass due to a rise in ground

water table after rainy seasons would result in temporary loss of stability. A criticism of this assumption can be the possible increase in shear strength on old failure planes (Stark and Mussain, 2005). Mesri and Huvaj-Sarihan (2012) showed that a change in σ_n due to compression or swelling after mobilization of residual shear strength causes formation of peak strength before remobilization at the residual. Nonetheless, this peak is often last after small shear displacements. Therefore $\phi=\phi_r$ was supposed to be reasonable assumption in the analysis of past landslides around Şebinkarahisar. Therefore, the limit for topographical slope is

$$\tan (\theta) < \tan (\phi) \quad (3.20)$$

according to the assumption of infinite slope. The simplified regional analysis proceeds with the following assumptions :

- 1) All soils in the landslide areas have already mobilized the residual shear strength ($\phi=\phi_r=14^\circ$) and marginally stable.
- 2) Equation 3.20 shows the criteria for locating clay deposits that have been moved to their location by landslides in the past.
- 3) $D \leq 10$ cm for $T_R=475$ years is an appropriate performance limit for facilities that can be affected by seismic slope failures.

Consequently, spatial distribution of k_h shown in Figure 3.13 was converted to the limit for topographical slope in percentages (i.e., $100 \cdot \tan(\phi)$) by using the inequality in Equation 3.19. The spatial distribution of this limit is shown in Figure 3.21. The topographical slopes steeper than 17% were supposed to be prone to severe displacements, and they are unacceptable for facilities nearby, provided that the shallow deposits consist of clays. The topographical slope is also limited by Equation 3.20, because any significant increase in ground water table after rainy seasons will trigger landslides, which will move deposits to flatter grounds.

Figure 3.21 shows the locations where topographical slope are flatter and steeper than $\tan 14^\circ (\cong 25\%)$. The topographical slopes were calculated by 250m resolution

SRTM digital elevation data (Jarvis et al., 2008). The computer tool Vertical Mapper v2.5 (Northwood Geoscience Ltd., 1999) was used for calculations of slope on each grid point of the digital elevation data. Basically, there are three important zones that can be identified on Figure 3.21.

- 1) The zones with topographic slopes greater than 25% are likely to involve more competent material than soft remoulded clays (i.e., $c > 0$ and $\phi > 9^\circ$).
- 2) The zones with topographical slopes less than 17% are not critical for assessment of seismic slope failure. The return period of $D > 10$ cm is longer than 475 years on these slopes grounds.
- 3) The zones with topographical slopes between 17% and 25% are critical for further investigation of seismic slope stability.

Further improvements in this approach will be possible, if the spatial analysis is supported by further geotechnical and geological data.

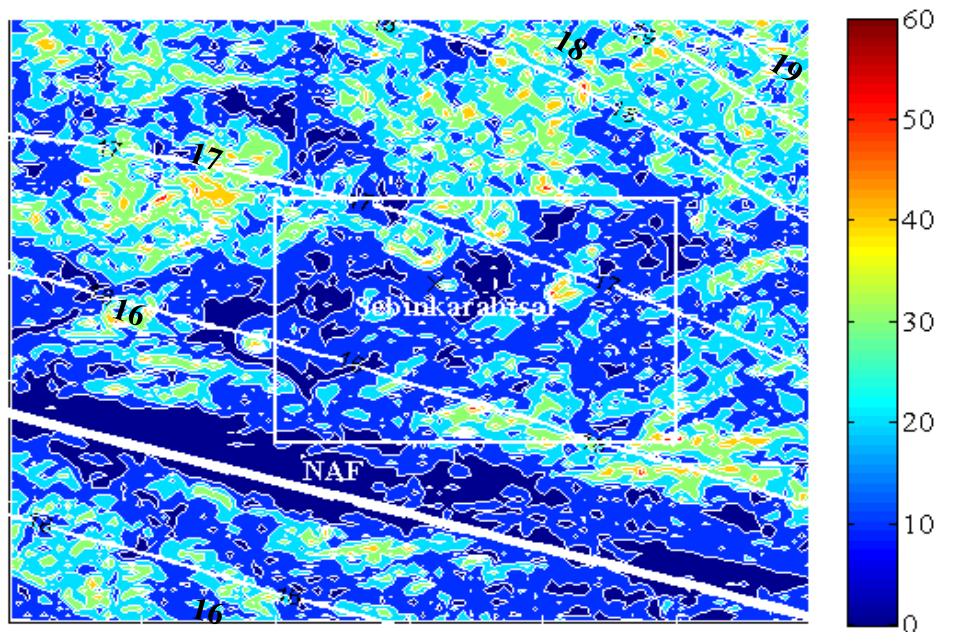


Figure 3.21 The limit for $\theta(\%)$ corresponding to k_h in Figure 3.13 (continuous black lines) and the spatial distribution of topographical slope (colored fill) around Sebinkarahisar.

3.4 Discussion

For an assessment of computed range of k_h in the case study, the seismic hazard in terms of peak ground acceleration, PGA, was computed for the coordinates 38.40° E and 40.30° N. The GMPE developed by Akkar and Bommer (2007) was implemented in computer program CRISIS2007 v7.6 for analysis. The site condition was supposed as soft soil corresponding to the range $180\text{m/s} \leq V_{S30} \leq 360\text{m/s}$. Consequently, PGA for $T_R=475$ years was computed as 0.31g. k_h was computed as 0.22 and 0.08 respectively for $D_{all}=1$ cm and for $D_{all}=10\text{cm}$ (Figures 3.12 and 3.13). Therefore, k_h is equal to 72% of estimated PGA/g in case 1.0 cm is the allowable limit for ground displacements. This ratio is above the range 1/2 - 1/3 suggested by Marcuson and Franklin (1983) and can be explained by the limitation in D_{all} . Whereas, k_h is equal to 25% of PGA/g, which is slightly lower than 1/3, in case $D_{all}=10$ cm. These figures for $k_h \cdot \text{g}/\text{PGA}$ also depend on GMPE implemented for calculation of PGA. On the other hand, the effect of magnitude-recurrence relationships on PGA, and that on duration of shaking, which has a significant effect on D , may not be very similar. This is supported by the studies involving event magnitude as a prediction parameter for D (Section 1.2). Hence, these results support that the determination of k_h through a PSHA in terms of D_{all} can be critically important to achieve a probabilistic uniformity in assessment of slopes.

In chapter 2, the very significant effect of V_{S30} was reported. The relationship between V_{S30} and D can be computed compared by the figures reported by Gülerce and Balal (2016), computing probabilistic seismic hazard in terms of D by using the vector-valued analysis method. This method was implicitly joining hazard expressed in terms of PGA and PGV with a relationship between PGA, PGV and D . Gülerce and Balal (2016) studied the hazard for 5 sites close to the western segments of NAF, located at about 530 km distance on the west of Şebinkarahisar. The effect of V_{S30} on hazard was demonstrated for the site #3, which is located at a distance of 5 km from NAF. For $T_R=2475$ years and $a_c=0.1\text{g}$, D was reported as 48cm, 88cm and more than 100 cm in the site conditions $V_{S30}=760$ m/s, $V_{S30}=560\text{m/s}$, and $V_{S30}=270$ m/s

respectively. Thus, the amplification factors for D with respect to the site condition described by $V_{S30}=760$ m/s are 1.83 and more than 2.0 for $V_{S30}=560$ m/s and $V_{S30}=270$ m/s respectively. The second factor is observed to be around 3.3 according to the extrapolation of the curves shown in Figure 2.5 of Gülerce and Balal (2016). For comparison, the grid point of coordinates 38.40°E and 40.15°N was chosen (Figure 3.10). The distance between NAF and this grid point is about 5 km. D was computed as 8.12 cm, 13.35 cm and 58.23 cm respectively in cases V_{S30} was set to 760 m/s, 560 m/s and 270 m/s respectively for $T_R=2475$ years and $a_c=0.1g$. Hence, the amplification factors are calculated 1.64 and 7.17 for $V_{S30}=560$ m/s and $V_{S30}=270$ m/s respectively. The first factor is consistent with the factor 1.83 calculated by the data of Gülerce and Balal (2016). However, the factor 7.17 is much larger than 3.3. Therefore, further studies are necessary for justification of amplification factors computed by implementing Equation 2.3 in PSHA. It is likely that this equation is under predict D for rock sites.

The eliminating the data in the range $D < 1$ cm yielded a pronounced effect on the prediction equation (Section 2.5). The consequences were also related to the sensitivity of k_h to $V_{S30}=300$ m/s and to the variance of prediction. Figure 3.22 shows the spatial distribution of k_h calculated by using Equation 2.4 instead of Equation 2.3 in the case T_R is 475 years, V_{S30} is 760 m/s and D_{all} is 10 cm. A comparison of Figure 3.22 with Figure 3.13 depicts that elimination of this range of D does not change k_h significantly. A similar comparison can be made between Figure 3.23 and Figure 3.14 by considering $T_R = 2475$ years. These two figures also show that k_h is not significantly affected by this elimination in the case D_{all} is 10 cm. However, this observation is not valid in case D_{all} is 1 cm as expected. The differences between Figure 3.24, based on Equation 2.4, and Figure 3.12, based on Equation 2.3, shows a factor of 2 approximately between the k_h ranges. That means that eliminating or truncating small displacements in the sample for D as done by Bray and Travararou (2007) can yield in biased estimations for k_h if D_{all} is small. Certainly, these conclusions are related to statistical method and the data employed for the development of prediction equation. Nevertheless, the difference between Equation

2.3 and Equation 2.4 is to be investigated further for their site amplification factors. In the case a_c is 0.1g and T_R is 2475 years, D will be computed as 65 cm, 22 cm and 15 cm respectively if V_{S30} is 270 m/s, 560 m/s and 760 m/s at a spatial coordinate that is 5 km away from NAF. Hence, the amplification of D will be 4.3 if V_{S30} is reduced from 760 m/s to 270 m/s. That amplification factor is more consistent with the factor 3.3, calculated according the results of Gülerce and Balal (2016), than the factor 7.17, computed by using Equation 2.3. Therefore, the site amplification factor for k_h that is calculated by using Equation 2.4 in PSHA can be more reasonable than those calculated by Equation 2.3. Further studies on site amplification factors for k_h are deemed as necessary. Nonetheless, the use Equation 2.4 is limited to the ranges of D that are greater than 1.0 cm due to the elimination of data.

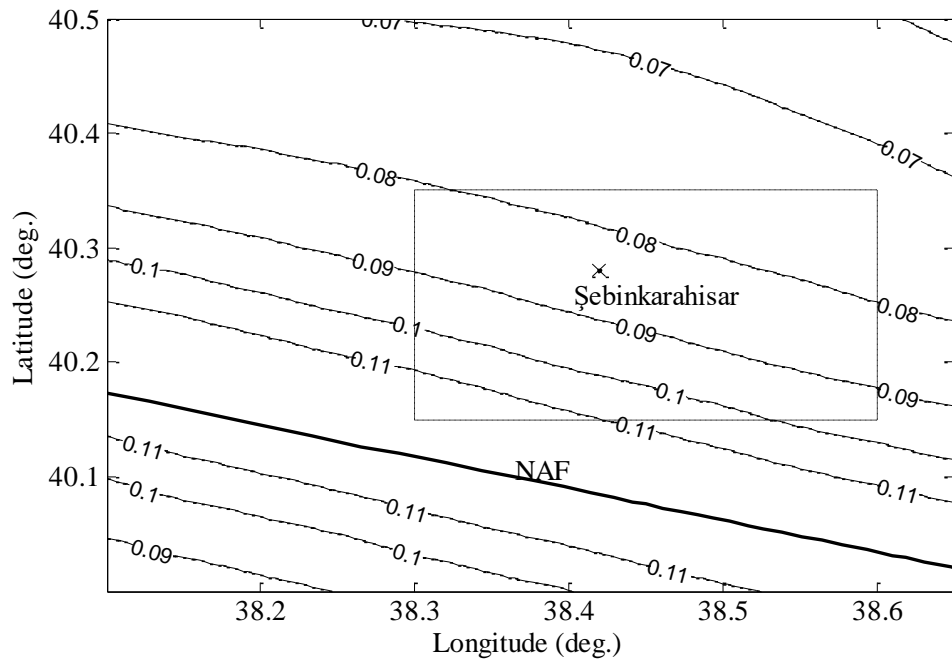


Figure 3.22 The spatial distribution of k_h for $D_{all}=10$ cm, $T_R=475$ yr, and $V_{S30}=300$ m/s

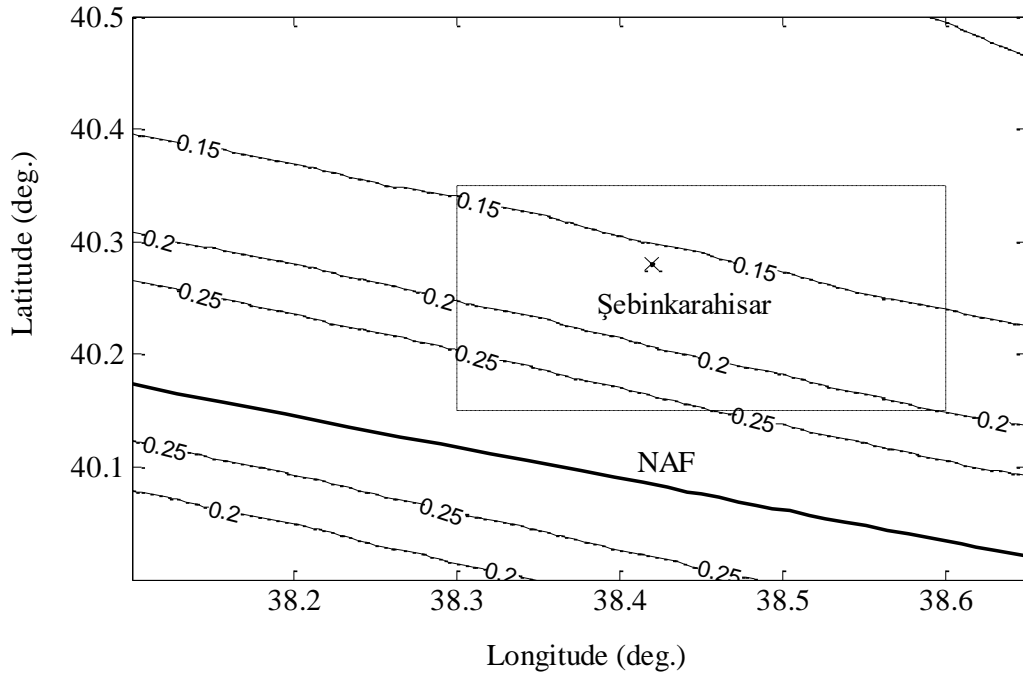


Figure 3.23 Spatial distribution of k_h for $D_{\text{all}}=10$ cm, $T_R=2475$ yr, and $V_{S30}=300$ m/s

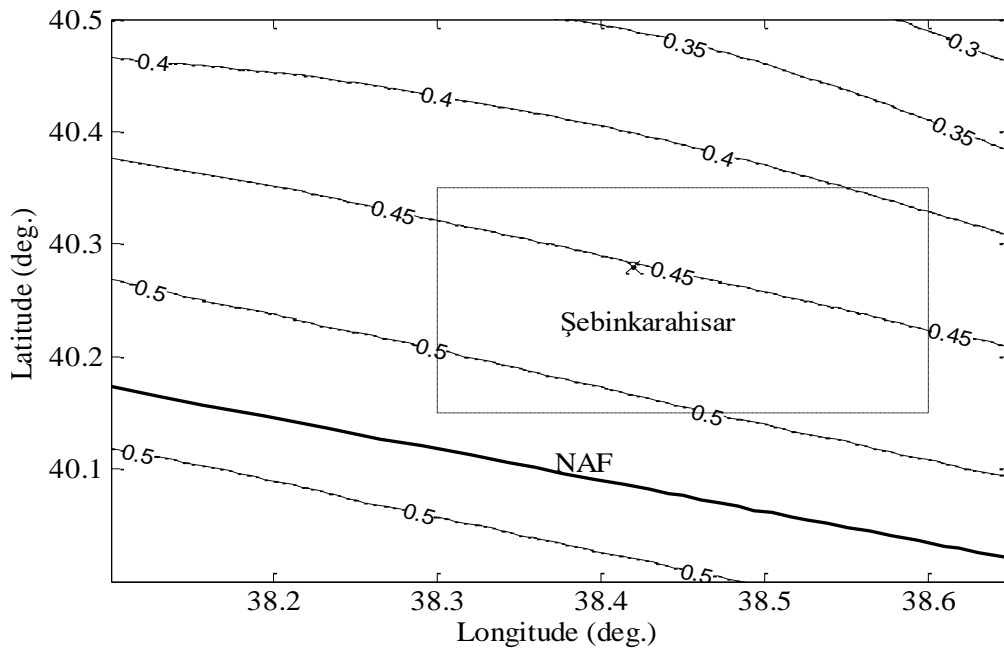


Figure 3.24 Spatial distribution of k_h for $D_{\text{all}}=1$ cm, $T_R=475$ yr, and $V_{S30}=300$ m/s

The hazard curves computed by implementing Equation 2.4 in PSHA are compared with those due to Equation 2.3 in Figure 3.25, for the spatial coordinates 38.40°E and 40.30°N, and for the site condition $V_{S30}=300$ m/s. The elimination of data for the range $D < 1$ cm yields a significant change in variance of prediction. Nonetheless, the hazard curves are similar in the range $5 \text{ cm} < D < 25 \text{ cm}$ approximately for $T_R=475$ years and for $T_R=2475$ years. Equation 2.3 yields greater hazard in the range $D > 25 \text{ cm}$ for these coordinates. It can be stated that Equation 2.3 can be used conservatively for higher ranges of D until a greater data set and a more rigorous prediction equation is made available for analysis. This study shows that k_h can be estimated by the principles of PBD by implementing the simple procedure explained in this study. Because the ultimate displacement of Newmark's sliding block is observed to be significantly dependent on magnitude, on site conditions, and on style of faulting, it is necessary to develop prediction equations that can be practically implemented in probabilistic seismic hazard analysis. The relationships between Newmark's analogy and true sliding displacements of deformable earth structures are certainly necessary for selection of D_{all} in the analyses of sloping ground.

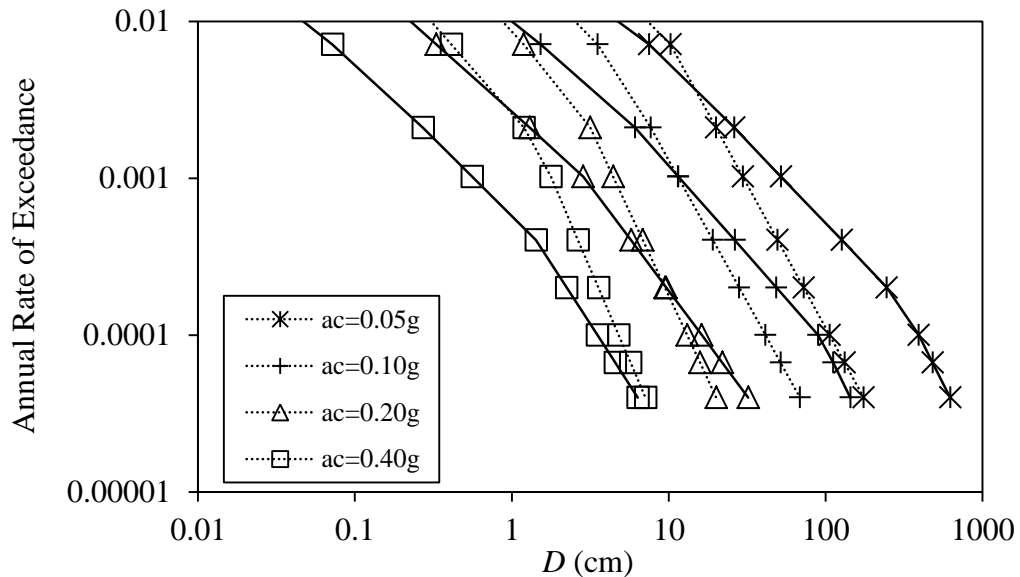


Figure 3.25 Relationship between T_R , a_c and D for coordinates 38.40°E and 40.30°N using Equation 2.3 and 2.4

CHAPTER 4

SUMMARY AND CONCLUSIONS

4.1 Summary

Newmark's sliding block analogy can be used for the selection of seismic coefficient (k_h), such that the principles of performance based design can be employed in assessment of seismic stability of sloping ground near to facilities, and in design of earth fill structures. A set of empirical equations were developed to predict the ultimate displacement of sliding block (D) by using moment magnitude (M_w), style of faulting (SoF), Joyner and Boore distance (R_{jb}), average shear wave velocity in top 30m of soil profile (V_{S30}), and the critical amplitude of acceleration that can be sustained without sliding of block (a_c). A set of unscaled ground motion accelerograms were compiled from the PEER database. The computer program SLAMMER was used to build a sample for D . The coefficients of prediction parameters were estimated by the method of least squares. One of the equations that provide a relatively high coefficient of determination (r^2), with a simple functional form was implemented in probabilistic seismic hazard analysis.

The magnitude recurrence relationships for seismic sources were modelled by considering the slip-rate estimations of NAF, and earthquake catalogs. The activity on NAF consisting of magnitudes in the range $6.5 \leq M_w \leq 8.0$ were modelled by a characteristic magnitude relationship, and the activity on unmapped faults, consisting of magnitudes in the range $4.5 \leq M_w < 6.5$ were modelled by truncated exponential model. The computer program CRISIS was used to computed the relationships

between D , and return period (T_R) for a given a_c . k_h was defined as the critical acceleration limiting D to a specific allowable value (D_{all}) for an intensity of ground motion that is specified by T_R . Consequently, the relationships between k_h and T_R for three specific D_{all} have been developed by considering specific coordinates near Şebinkarahisar town in Giresun province. These relationships allow a trade-off between seismic safety (i.e. the probability of exceeding D_{all}) and cost of geotechnical measures.

As an example for map applications, the spatial distribution of k_h around Şebinkarahisar was presented for a set of limit for T_R and D . The limits for topographic slopes (θ) were calculated and mapped by considering remolded clay deposits around Şebinkarahisar. The theoretical relationship between limits for θ and k_h was based on an infinite slope model. The results were compared with the slope data originating from 250m-resolution digital elevation data. The computed results for k_h was criticized by examining the effect of variance of the prediction equation on seismic hazard and by comparing k_h with other studies presented in literature.

4.2 Conclusions

The conclusions of this study are summarized in the following bulleted list.

- It is possible to calculate seismic hazard in terms of ultimate displacement of Newmark sliding block analogy for analysis of seismic stability of sloping ground and earth structures by implementing prediction equations for this displacement in conventional seismic hazard analysis.
- The earthquake magnitude and style of faulting was observed to have a very significant effect on block displacements. The sensitivity of block displacement to these source parameters depict the necessity for determination of k_h by probabilistic seismic hazard analysis.
- The site parameter V_{S30} has a pronounced effect on predictions for block displacements. Therefore, emphasis should be put on the estimations for

shear wave velocity in the competent geological formation beneath a sliding plane.

- The method for joining two components of block displacements that are computed separately for two horizontal components of ground motion is relatively unimportant with respect to uncertainties regarding prediction parameters.
- The concept of importance factor can be employed for practical seismicity if seismic hazard in terms of seismic coefficient is mapped on a large region.

4.3 Future Studies

- The prediction equation for estimation of ultimate block displacement can be improved by using larger database containing M_W up to 8.0.
- The coupled effect of vertical ground motion on ultimate block displacement can be investigated.
- The rules for appropriate selection of allowable block displacement can be developed.

REFERENCES

Akkar, S. and Bommer, J.J., (2007). Empirical prediction equations for peak ground velocity derived from strong-motion records from Europe and the Middle East. *Bulletin of the Seismological Society of America*, Vol. 97(2), 511-530.

Albarello, D., Camassi R., and Rebez A., (2001). Detection of space and time heterogeneity in the completeness level of a seismic catalogue by a «robust» statistical approach: an application to the Italian area. *Bulletin of Seismological Society of America*, 91 (6) 1694-1703.

Ambraseys N.N., and Jackson J.A., (1998). Faulting associated with historical and recent earthquakes in the Eastern Mediterranean region. *Geophysical Journal International*, 133, 2, 390-406.

Ambraseys, N and Srbulov, M., (1995). Earthquake induced displacements of slopes. *Soil Dynamics and Earthquake Engineering* 14. 59-71.

Anagnos, T., and Kiremidjian A.S., (1988). A Review of earthquake occurrence models for seismic hazard analysis. *Journal of Probabilistic Engineering Mechanics*, V3, 3-11.

Baker, J. W., Cornell, C. A., (2006a). Correlation of response spectral values for multicomponent ground motions, *Bulletin of Seismological Society of America*, 96 (1): 215-227.

Baker, J. W., Cornell, C. A., (2006b). Which spectral acceleration are you using? *Earthquake Spectra*, 22 (2):293-312.

Barka, A. A., (1992). The North Anatolian fault zone. *Annales Tectonicae*, 6, 164-195.

Barka, A. A., (1996). Slip distribution along the North Anatolian fault associated with the large earthquakes of the period 1939-1967. *BSSA*, 86, 5, 1238-1254.

Barka, A., Akyüz, H. S., Altunel E., Sunal, G., Çakir, Z., Dikbas, A., Yerli, B., Armijo, R., Meyer, B., de Chabalier, J. B., Rockwell, T., Dolan, J. R., Hartleb, R., Dawson, T., Christofferson, S., Tucker, A., Fumal, T., Langridge, R., Stenner, H., Lettis, W., Bachhuber, J., and Page, W., (2002). The Surface Rupture and Slip Distribution of the 17 August 1999 Izmit Earthquake (M 7.4), North Anatolian Fault, *Bulletin of the Seismological Society of America*, 92(1), 43–60.

Bommer J.J., Abrahamson N.A., (2006). Why do modern probabilistic seismic-hazard analyses often lead to increased hazard estimates?, *Bulletin of the Seismological Society of America*, Vol: 96, Pages: 1967-1977.

Bender, B., (1983). Maximum likelihood estimation of b values for magnitude grouped data, *Bulletin of the Seismological Society of America*, 73, 831-851.

Bender B. and Perkins D., (1982). SEISRISK II. A Computer program for seismic hazard estimation. U.S. Geological Survey, Open File Report: 82-293.

Bender B. and Perkins D., (1987) SEISRISK III: A Computer Program for Seismic Hazard Estimation, U.S. Geological Survey Bulletin 1772.

Bisch P., Carvalho E., Degee H., Fajfar P., Fardis M., Franchin P., Kreslin M., Pecker A., Pinto P., Plumier A., Somja H., Tsionis G., (2011). Eurocode 8: Seismic design of buildings worked examples. Luxembourg: Publications Office of the European Union.

Bommer, J. J., Stafford P. J., Alarcon J. E., and Akkar S., (2007). The Influence of magnitude range on empirical ground-motion prediction, *Bulletin of the Seismological Society of America*, 97 (6), 2152-2170.

Boore, D. M. and Atkinson G. M., (2007). Boore-Atkinson NGA ground motion relations for the geometric mean horizontal component of peak and spectral ground

motion parameters, PEER Report 2007/01, Pacific Earthquake Engineering Research Center, University of California, Berkeley.

Borcherdt, R. D., (1994). Estimates of site-dependent response spectra for design (Methodology and Justification), *Earthquake Spectra*, 10, 617-653.

Bozbey I. and Gündoğdu O., (2011). A methodology to select seismic coefficients based on upper bound “Newmark” displacements using earthquake records from Turkey, *Soil Dynamics and Earthquake Engineering* 31: 440–451.

Bray, J. D., Augello, A. J., Leonards, G. A., Repetto, P. C., and Byrne, R. J., (1995). Seismic stability procedures for solid-waste landfills, *Journal of Geotechnical and Geoenvironmental Engineering*, Vol.121, No.2, pp.139-151.

Bray, J.D., Rathje, E.M., Augello, A.J., and Merry, S.M., (1998). Simplified seismic design procedure for geosynthetic lined solid waste landfills, *Geosynthetics International*, Vol 5, Nos. 1-2, pp. 203-235.

Bray, J. D., and Travararou, T., (2007). Simplified procedure for estimating earthquake-induced deviatoric slope displacements, *Journal of Geotechnical and Geoenvironmental Engineering*, Vol. 133(4), pp. 381–392.

Bray, J. D., and Travararou, T., (2011). Pseudostatic slope stability procedure, 5th International Conference on Earthquake Geotechnical Engineering.

Chung, D.H., and Bernreuter, D.L., (1979). On the regionalization of ground motion attenuation in the conterminous United States. *Proc. of U.S. National Conf. on Earthquake Eng.*

Cornell, C.A., (1968). Engineering seismic risk analysis, *Bulletin of Seismological Society of America*, 58, 1583-1606.

Cornell, C. A., Banon, H., and Shakal, A. F., (1979). Seismic motion and response prediction alternatives, *Earthquake Engineering and Structural Dynamics*, 7(4), 295–315.

Cornell, C.A., and Winterstein S.R., (1986). Applicability of the poisson earthquake occurrence model. Eastern U.S. Seismic Hazard Assessment Project, Electric Power Research Institute, Palo Alto, CA.

Faccioli, E., (1979). Engineering seismic risk analysis of the Friuli region, *Bollettino di Geofisica Teorica ed Applicata*, XXI(83), 173–190.

Freeman, S.A., (1998). Development and use of capacity spectrum method, *Proceedings of 6th US National Conference on Earthquake Engineering*, Seattle, Washington, U.S.A., Paper No. 269.

Gazetas, G., and Uddin, N., (1994). Permanent deformation on preexisting sliding surfaces in dams, *Journal of Geotechnical Engineering*, 120(11), 2041– 2061.

Gipprich, T. L., Snieder, R. K., Jibson, R. W., and Kimman, W., (2008). The role of shear and tensile failure in dynamically triggered landslides, *Geophysical Journal International* 172, 770–778.

Hynes-Griffin ME., and Franklin AG., (1984). Rationalizing the seismic coefficient method. U.S, Army Corps of Engineers Waterways Experiment Station, Vicksburg, Mississippi, Miscellaneous Paper GL-84-13, 21 pp.

Jarvis A., Reuter HI., Nelson A., Guevara E., (2008). Hole filled seamless SRTM data. International Center for Tropical Agriculture (CIAT), <http://srtm.csi.cgiar.org> (last access November 1st , 2014).

Jibson, R.W., (1993). Predicting earthquake-induced landslide displacements using Newmark's sliding block analysis, *Transportation Research Record* 1411, 9-17.

Jibson, R.W., and Keefer, D.K., (1993). Analysis of the seismic origin of landslides: Examples from the New Madrid seismic zone, *Geological Society of America Bulletin* 105, 521-536.

Jibson, R. W., Harp, E. L., Michael, J. A., (1998). A Method for Producing Digital Probabilistic Seismic Landslide Hazard Maps: An Example from Los Angeles, California Area, USGS, Open file report 98-113.

Jibson, R.W., (2007). Regression models for estimating coseismic landslide displacement, *Engineering Geology*, 91, 209–218.

Jibson, R.W., Rathje, E.M., Jibson, M.W., and Lee, Y.W., (2013). SLAMMER - Seismic Landslide Movement Modeled using Earthquake Records (ver.1.1, November 2014), U.S. Geological Survey Techniques and Methods, book 12, chap. B1, unpagued.

Joyner, W. B., and Boore, D. M., (1981). Peak Horizontal Acceleration and Velocity from Strong Motion Records Including Records from the 1979 Imperial Valley, California, *Earthquake, Bulletin of the Seismological Society of America*, Vol. 71, No. 6, pp 2011-2038.

Kowalsky, M.J., Priestley, M.J.N., and MacRae G.A., (1995). Displacement-based design of RC bridge columns in seismic regions, *Earthquake Engineering and Structural Dynamics*, Vol. 24, No. 12 pp. 1623-1644.

Kramer, S. L., (1996). *Geotechnical earthquake engineering*, Prentice Hall, Upper Saddle River, N.J.

Kramer S. L., and Smith M. W., (1997). Modified Newmark model for seismic displacements of compliant slopes, *Journal of Geotechnical and Geoenvironmental Engineering*, Vol. 123, No. 7, 1997, pp. 635-644.

Krinitzsky, E. L., (1995). Deterministic versus probabilistic seismic hazard analysis for critical structures. *Engineering Geology* 40.1-7.

Lin, J.S., and Whitman R.V., (1983). Decoupling approximation to the evaluation of earthquake-induced plastic slip in earth dams, *Earthquake Engineering. and Structural Dynamics*, No. 11, pp. 667-678.

Makdisi F. H., Seed H. B., (1978). Simplified procedure for estimating dam and embankment earthquake-induced deformations, *Journal of Geotechnical Engineering Division, ASCE*, 104(7): 849-867.

Marin, S., Avouac, J.P., Nicolas, M., and Schlupp, A., (2004). A probabilistic approach to seismic hazard in metropolitan France, *Bulletin of the Seismological Society of America*, 94(6), 2137–2163.

McGuire, R.K., (1976). FORTRAN Computer Program for Seismic Risk Analysis. U.S. Geological Survey Open File Report 76-67, Washington, DC: Department of the Interior.

McGuire, R.K., (1978). FRISK-Computer program for seismic risk analysis using faults as earthquake sources, U.S. Geological Survey Open File Report 78-1007, Washington, DC: Department of the Interior.

McGuire, R. K., (1978). Seismic ground motion parameter relations, *Journal of the Geotechnical Engineering Division, ASCE*, 104(GT4), 481–490.

McGuire, R. K., (2004). Seismic hazard and risk analysis, Earthquake Engineering Research Institute, Oakland, CA.

Melo, C., and Sharma, S., (2004). Seismic coefficients for pseudostatic slope analysis, 13th World Conference on Earthquake Engineering, Canada, Paper ID No. 369.

Meteorological Service of Turkey (2017). <https://www.mgm.gov.tr/veridegerlendirme/yillik-toplam-yagis-verileri.aspx>, last access: July 8, 2017.

Ministry of Public Works (2007). The principles for buildings to be constructed in seismic zones (Deprem bölgelerinde yapılacak binalar hakkında esaslar), The Ministry of Public Works, Republic of Turkey.

Newmark, N., (1965). Effects of earthquakes on dams and embankments, Geotechnique, Vol. 15, No. 2, pp. 139-160. The Rankine Lecture.

Paradisopoulou P. M., Papadimitriou E. E., Karakostas V. G., Taymaz T., Kiliyas A., Yolsal S., (2010). Seismic hazard evaluation in western Turkey as revealed by stress transfer and time-dependent probability calculations. Pure and Applied Geophysics, volume 167, number 8-9, page 1013.

Priestley, M.J.N., (2000). Performance based seismic design, Bulletin of the New Zealand Society for Earthquake Engineering. V.33, N.3. pp 325-346.

Rampello, S., Callisto, L. and Fagnoli, P., (2010). Evaluation of slope performance under earthquake loading conditions, Italian Geotechnical Journal, XLIV, No 4, 29-41.

Rathje E.M., and Bray J.D., (2000). Nonlinear coupled seismic sliding analysis of earth structures, Journal of Geotechnical and Geoenvironmental Engineering, 126(11): 1002-1014.

Rathje, E. M., and Saygılı, G., (2008). Probabilistic seismic hazard analysis for the sliding displacement of slopes: scalar and vector approaches, *Journal of Geotechnical and Geoenvironmental Engineering*, 134 (6), 804-814.

Rathje, E.M. and Saygili G., (2009). Probabilistic assessment of earthquake-induced sliding displacements of natural slopes, *Bulletin of the New Zealand Society for Earthquake Engineering*, 42(1), pp. 18-27.

Rousset B., Jolivet R., Simons M., Lasserre C., Riel B., Milillo P., Çakir Z., and Renard F., (2016). An aseismic slip transient on the North Anatolian Fault. *Geophysical Research Letters*, 43, 3254-3262.

Sarma K., and Free M., (1995). The comparison of attenuation relationships for peak horizontal acceleration in intraplate regions, In *Pacific Conference on Earthquake Engineering*, volume 2, pages 175–184.

Sarma S.K., (1988). Seismic response and stability of earth dams, *Seismic risk assessment and design of building structures*, Ed. A. Koridze, Omega Scientific, 143-160.

Saygili G. and Rathje E.M., (2008). Empirical predictive models for earthquake-induced sliding displacements of slopes, *Journal of Geotechnical and Geoenvironmental Engineering* 134(6), 790.

Strasser, F. O., Abrahamson N. A., and Bommer J. J., (2009). Sigma: Issues, insights, and challenges, *Seismological Research Letters* 80, 41–56.

Seed, H. B., Idriss, I. M. and Kiefer, F. W., (1969). Characteristics of rock motions during earthquakes, *Journal of Soil Mechanics and Foundations Division, ASCE*, v. 95, no. SM5, September, pp 1199- 1218.

Seed H. B., (1979). Consideration in the earthquake-resistant design of earth and rockfill dams, *Geotechnique*, Vol. 29, No. 3, pp. 215-263.

Sesetyan, K., Demircioglu, M., Rovida, A., Albini, P., Stucchi M., (2013). SHARE-CET, the SHARE earthquake catalogue for Central and Eastern Turkey complementing the SHARE European Earthquake Catalogue (SHEEC).

Sharma, M.L., Douglas, J., Bungum, H., and Kotadia, J., (2009). Ground-motion prediction equations based on data from the Himalayan and Zagros regions, *Journal of Earthquake Engineering* 13(8),1191–1210.

Skempton, A. W., (1964). Long-term Stability of Slopes. *Geotechnique*, 14(2), 75-102.

Sisi, A.A., Askan, A., Erberik M.A., (2017). Site-specific uniform hazard spectrum in Eastern Turkey based on simulated ground motions including near-field directivity and detailed site. *Acta Geophysics*, 65: 309-330.

Stucchi M., Rovida A., Gomez Capera A.A., Alexandre P., Camelbeeck T., Demircioglu M.B., Gasperini P., Kouskouna V., Musson R.M.W., Radulian M., Sesetyan K., Vilanova S., Baumont D., Bungum H., Fäh D., Lenhardt W., Makropoulos K., Martinez Solares J.M., Scotti O., Živcic M., Albini P., Batllo J., Papaioannou C., Tatevossian R., Locati M., Meletti C., Viganò D., Giardini D., (2012). The SHARE European Earthquake Catalogue (SHEEC) 1000-1899. *Journal of Seismology* 17, 523-544.

UDIM (2016). *Tarihsel depremler* (Historical Earthquake), <http://www.koeri.boun.edu.tr>, last access: January 20th 2016.

Wahls, H.E., (1981). Tolerable settlement of Buildings. Journal of the Geotechnical Engineering Division, American Society of Civil Engineers, 107: 1489-1504.

Watson-Lamprey, J., and Abrahamson, N. A., (2006). Selection of ground motion time series and limits on scaling, Soil Dynamics and Earthquake Engineering, 26 (5), 477-482.

Whitman, R.V., and Liao, S., (1985). Seismic design of gravity retaining walls, US Army Engineer Waterways Experiment Station, Vicksburg, Mississippi.

Wieczorek, G.F., Wilson, R.C., and Harp, E.L., (1985). Map showing slope stability during earthquakes in San Mateo County, California. U.S. Geological Survey Miscellaneous Investigations Map I-1257-E, scale 1:62.500.

Wilson, R. C., (1993). Relation of arias intensity to magnitude and distance in California, U.S. Geological Survey Open-File Report, 93-556 42 pp.

Yegian M.K., Marciano E.A., and Ghahraman V.G., (1991). Earthquake-induced permanent deformations: probabilistic approach, ASCE, Journal of Geotechnical Engineering, vol. CXVII, n. 1, pp. 35- 50.

ZEMAR (2015). *Giresun-Şebinkarahisar Burçak -2 HES Heyelan Sahası Etüd Raporu*, ZEMAR Zemin Araştırma ve Mühendislik, İstanbul.

APPENDIX A

THE LIST OF SEISMIC EVENTS

Table A.1. List of declustered events

No	Event Name	Date (M/D/Y)	Time (H:M)	<i>M</i>	<i>SoF</i>
1	ANZA	02/25/80	10:47	5.19	SS
2	BIGBEAR	06/28/92	15:05	6.46	SS
3	CAPE MENDOCINO	04/25/92	18:06	7.01	R
4	CHALFANT	07/31/86	07:22	5.44	SS
5	CHI-CHI	09/20/99	17:47	7.62	RQ
6	COALINGA	05/02/83	23:42	6.36	R
7	COALINGA	05/09/83	02:49	5.09	R
8	COALINGA	07/09/83	07:40	5.18	R
9	COALINGA	07/22/83	02:39	5.77	R
10	COALINGA	07/22/83	03:43	4.89	R
11	COYOTE LAKE	08/06/79	17:05	5.74	SS
12	DUZCE	11/12/99	16:57	7.14	SS
13	FRIULI	05/06/76	20:00	6.50	R
14	FRIULI	09/15/76	03:15	5.91	R
15	GILROY	05/13/02	05:00	4.90	SS
16	HECTOR MINE	11/16/99	02:46	7.13	SS
17	IMPERIAL VALLEY	10/15/79	23:16	6.53	SS
18	IMPERIAL VALLEY	10/15/79	23:19	5.01	SS
19	IRPINIA	11/23/80	19:35	6.20	N
20	KOBE	01/16/95	20:46	6.90	SS
21	KOCAELI	08/17/99	03:01	7.51	SS
22	LIVERMORE	01/24/80	19:00	5.80	SS
23	LIVERMORE	01/27/80	02:33	5.42	SS
24	LOMA PRIETA	10/18/89	00:05	6.93	RQ
25	LYTLE CREEK	09/12/70	14:30	5.33	RQ
26	MAMMOTH LAKES	01/07/83	01:38	5.34	SS

Table A.1. (continued)

No	Event Name	Date (M/D/Y)	Time (H:M)	<i>M</i>	<i>SoF</i>
27	MAMMOTH LAKES	01/07/83	03:24	5.31	SS
28	MAMMOTH LAKES	05/25/80	16:34	6.06	NQ
29	MAMMOTH LAKES	05/25/80	16:49	5.69	SS
30	MAMMOTH LAKES	05/25/80	20:35	5.91	SS
31	MAMMOTH LAKES	05/27/80	19:01	4.73	SS
32	MAMMOTH LAKES	05/31/80	15:16	4.50	SS
33	MAMMOTH LAKES	05/27/80	14:51	5.94	SS
34	MANAGUA	12/23/72	06:29	6.24	SS
35	N. PALM SPRINGS	07/08/86	09:20	6.06	RQ
36	NORTHRIDGE	01/17/94	04:30	5.13	RQ
37	NORTHRIDGE	03/20/94	21:20	5.28	R
38	OROVILLE	08/08/75	07:00	4.70	N
39	PARKFIELD	06/28/66	04:26	6.19	SS
40	PTMUGU	02/21/73	14:45	5.65	R
41	SAN FERNANDO	02/09/71	14:00	6.61	R
42	SAN FRANCISCO	03/22/57	19:44	5.28	R
43	VICTORIA	06/09/80	03:28	6.33	SS
44	WESTMORELAND	04/26/81	12:09	5.90	SS
45	WHITTIER	10/01/87	14:42	5.99	RQ
46	WHITTIER NARROWS	10/04/87	10:59	5.27	RQ

APPENDIX B

THE LIST OF *D* SAMPLES

Table B.1. List of *D* samples

Event No	Station Name	R_{jb} (km)	V_{S30} (km)	PGA _x (g)	PGA _y (g)
1	PINYON FLAT	12.0	724.9	0.11	0.13
1	RANCHO DE ANZA	18.1	345.4	0.10	0.09
2	SAGE - FIRE STATION	63.1	622.9	0.17	0.17
2	WINCHESTER	58.4	684.9	0.08	0.06
3	CAPE MENDOCINO	0	513.7	1.50	1.04
3	PETROLIA	0	712.8	0.59	0.66
4	BISHOP LADWP SOUTH ST	24.0	271.4	0.18	0.12
5	CHY080	0.1	680	0.97	0.90
5	HWA003	52.5	1525.8	0.14	0.05
5	TAP012	100.1	201	0.10	0.06
6	PARKFIELD	23.8	271.4	0.21	0.27
7	ANTICLINE RIDGE FF	2.2	376.1	0.58	0.67
7	ANTICLINE RIDGE PAD	2.2	376.1	0.45	0.41
8	ANTICLINE RIDGE PAD	5.3	376.1	0.38	0.26
9	CHP	7.0	338.5	0.32	0.61
9	OIL CITY	2.4	376.1	0.87	0.45
10	CHP	7.9	338.5	0.15	0.20
11	GILROY ARRAY #1	10.2	1428.0	0.10	0.13
12	LAMONT STATION 375	3.9	424.8	0.97	0.51
12	LAMONT STATION 531	8.0	659.6	0.16	0.12
13	TOLMEZZO	15.0	424.8	0.35	0.30
14	FORGARIO CORNINO	14.7	412.4	0.26	0.21
15	GAVILAN COLLEGE	2.0	729.6	0.21	0.25
16	AMBOY	41.8	271.4	0.18	0.15
16	FRINK	118.5	345.4	0.07	0.07
16	HEC	10.3	684.9	0.27	0.34
17	BONDS CORNER	0.5	223	0.59	0.77
17	CHIHUAHUA	7.3	274.5	0.27	0.25

Table B.1. (continued)

Event No	Station Name	R_{jb} (km)	V_{S30} (km)	PGA_x (g)	PGA_y (g)
17	EL CENTRO ARRAY 5	1.8	205.6	0.52	0.38
17	EL CENTRO ARRAY 8	3.9	206.1	0.60	0.45
18	EL CENTRO ARRAY 5	8.6	205.6	0.24	0.24
18	EL CENTRO ARRAY 6	7.4	203.2	0.19	0.37
19	BISACCIA	14.7	1000.0	0.07	0.08
19	RIONERO IN VULTURE	22.7	530.0	0.10	0.09
20	TOT	119.6	609	0.08	0.08
21	DUZCE	13.6	276	0.31	0.36
21	EREGLI	141.4	659.6	0.11	0.09
22	DEL VALLE DAM	23.0	338.5	0.13	0.23
23	LIVERMORE FAGUNDES RANCH	0.6	338.5	0.26	0.23
24	EMERYVILLE - 6363 CHRISTIE	76.9	198.7	0.26	0.21
24	POINT BONITA	83.4	1315.9	0.07	0.07
24	SF INTERN AIRPORT	58.5	190.1	0.24	0.33
25	DEVILS CANYON	17.9	684.9	0.15	0.15
25	WRIGHTWOOD	10.9	486.0	0.16	0.20
26	CONVICT CREEK	6.5	338.5	0.15	0.17
27	CONVICT CREEK	7.4	338.5	0.10	0.15
28	CONVICT CREEK	1.1	338.5	0.34	0.44
29	MAMMOTH LAKES HS	1.4	370.8	0.39	0.44
30	LONG VALL DAM UPP L	8.6	345.4	0.48	0.19
31	GREEN CHURCH	2.9	338.5	0.17	0.17
32	FIS	3.8	338.5	0.28	0.15
32	MAMMOTH ELEM SCHOOL	7.5	338.5	0.10	0.09
33	FIS	6.8	338.5	0.40	0.40
34	MANAGUA, ESSO	3.5	288.8	0.33	0.42
35	TEMECULA CDF FIRE	64.7	370.8	0.12	0.10
36	CASTAIC OLD RIDGE ROUTE	20.3	450.3	0.11	0.06
37	LOS ANGELES	17.7	316.5	0.29	0.11
38	DWR GARAGE	0.0	622.9	0.14	0.21
38	JOHNSON RANCH	7.4	438.3	0.19	0.10
38	OROVILLE AIRPORT	8.6	438.3	0.05	0.06
39	CHOLAME 5	9.6	289.6	0.37	0.44
40	PORT HUENEME	14.7	297.9	0.11	0.08
41	CASTAIC OLD RIDGE ROUTE	19.3	450.3	0.32	0.27
41	LAKE HUGHES 12	14.0	602.1	0.37	0.28
41	SANTA ANITA DAM	30.7	684.9	0.15	0.21
42	GOLDEN GATE	9.6	874.0	0.10	0.11

Table B.1. (continued)

Event No	Station Name	R_{jb} (km)	V_{S30} (km)	PGA_x (g)	PGA_y (g)
43	CERRO PRIETO	13.8	659.6	0.29	0.29
44	FIRE STATION	6.2	193.7	0.37	0.50
45	STUDIO CITY-COLDWATER	26.9	294.2	0.18	0.23
46	116TH ST SCHOOL	18.9	301.0	0.17	0.15

APPENDIX C

UDIM CATALOG FOR EVENTS

Table C.1. List of UDIM catalog for events

Event No	Station No	a_c (g)	D_x (cm)	D_y (cm)	D_{SRSS} (cm)
1	1	0.05	0.04	0.08	0.09
1	2	0.05	0.20	0.07	0.21
2	3	0.1	0.04	0.07	0.08
2	3	0.05	1.27	1.22	1.76
2	4	0.05	0.02	0.00	0.02
3	5	0.05	170.62	21.64	171.98
3	5	0.1	53.82	8.02	54.42
3	5	0.15	32.04	4.11	32.30
3	5	0.2	22.53	2.30	22.64
3	5	0.3	13.30	1.02	13.34
3	5	0.4	9.85	0.61	9.87
3	5	0.5	7.74	0.37	7.75
3	5	0.6	6.11	0.21	6.11
3	5	0.7	4.83	0.13	4.83
3	5	1	2.15	0.01	2.15
3	5	1.2	0.94	0.00	0.94
3	6	0.05	77.91	86.71	116.57
3	6	0.1	35.40	41.21	54.33
3	6	0.15	18.68	22.17	28.99
3	6	0.2	9.65	13.53	16.62
3	6	0.3	1.63	5.88	6.10
3	6	0.4	0.24	2.19	2.20
3	6	0.5	0.05	0.35	0.35
3	6	0.6	0.00	0.04	0.04
4	7	0.05	1.98	0.38	2.01
4	7	0.1	0.32	0.01	0.32
4	7	0.15	0.03	0.00	0.03
5	8	0.05	300.16	219.79	372.03

Table C.1.(continued)

Event No	Station No	a_c (g)	D_x (cm)	D_y (cm)	D_{SRSS} (cm)
5	8	0.1	165.18	125.65	207.54
5	8	0.15	104.08	84.93	134.33
5	8	0.2	71.88	61.26	94.44
5	8	0.3	35.96	34.64	49.93
5	8	0.4	18.34	18.82	26.27
5	8	0.5	9.96	8.48	13.08
5	8	0.6	5.05	3.16	5.96
5	8	0.7	2.02	0.96	2.24
5	9	0.05	8.91	0.00	8.91
5	9	0.1	0.93	0.00	0.93
5	10	0.05	0.12	0.04	0.13
6	11	0.05	13.35	24.61	27.99
6	11	0.1	2.56	9.36	9.70
6	11	0.15	0.53	3.96	3.99
6	11	0.2	0.01	1.28	1.28
7	12	0.05	5.25	7.10	8.83
7	12	0.1	2.48	3.76	4.50
7	12	0.15	1.04	2.22	2.45
7	12	0.2	0.25	1.23	1.25
7	12	0.3	0.00	0.28	0.28
7	12	0.4	0.00	0.01	0.01
7	13	0.05	7.62	7.22	10.50
7	13	0.1	4.16	3.42	5.38
7	13	0.15	2.32	1.90	3.00
7	13	0.2	1.15	0.98	1.51
7	13	0.3	0.23	0.10	0.25
7	13	0.4	0.02	0.00	0.02
8	13	0.05	8.04	4.78	9.36
8	13	0.1	3.42	1.49	3.73
8	13	0.15	1.24	0.37	1.29
8	13	0.2	0.37	0.06	0.37
8	13	0.3	0.01	0.00	0.01
9	14	0.05	4.87	8.88	10.13
9	14	0.1	1.82	4.36	4.72
9	14	0.15	0.53	2.53	2.58
9	14	0.2	0.13	1.59	1.59
9	14	0.3	0.00	0.77	0.77
9	14	0.4	0.00	0.28	0.28

Table C.1. (continued)

Event No	Station No	a_c (g)	D_x (cm)	D_y (cm)	D_{SRSS} (cm)
9	14	0.5	0.00	0.06	0.06
9	15	0.05	32.07	14.59	35.23
9	15	0.1	19.51	6.54	20.58
9	15	0.15	13.58	3.56	14.04
9	15	0.2	9.54	1.78	9.70
9	15	0.3	4.97	0.28	4.98
9	15	0.4	2.63	0.00	2.63
9	15	0.5	1.21	0.00	1.21
9	15	0.6	0.40	0.00	0.40
9	15	0.7	0.06	0.00	0.06
10	14	0.05	0.15	0.79	0.80
10	14	0.1	0.00	0.30	0.30
10	14	0.15	0.00	0.07	0.07
11	17	0.05	0.22	0.09	0.24
12	18	0.05	23.94	104.65	107.35
12	18	0.1	7.66	58.10	58.61
12	18	0.15	3.00	34.76	34.89
12	18	0.2	1.38	21.37	21.42
12	18	0.3	0.30	6.99	7.00
12	18	0.4	0.04	1.59	1.59
12	18	0.5	0.00	0.08	0.08
12	19	0.05	3.16	3.73	4.89
12	19	0.1	0.10	0.22	0.24
13	20	0.05	13.04	30.97	33.61
13	20	0.1	3.71	13.64	14.14
13	20	0.15	1.41	4.98	5.18
13	20	0.2	0.52	0.89	1.03
13	20	0.3	0.03	0.00	0.03
14	21	0.05	2.84	4.01	4.91
14	21	0.1	0.88	0.71	1.13
14	21	0.15	0.29	0.13	0.32
14	21	0.2	0.07	0.01	0.07
15	22	0.05	0.26	0.39	0.47
15	22	0.1	0.01	0.12	0.12
15	22	0.15	0.00	0.04	0.04
15	22	0.2	0.00	0.01	0.01
16	23	0.05	8.49	6.04	10.42
16	23	0.1	0.44	0.21	0.48

Table C.1. (continued)

Event No	Station No	a_c (g)	D_x (cm)	D_y (cm)	D_{SRSS} (cm)
16	23	0.15	0.03	0.00	0.03
16	24	0.05	0.76	0.19	0.78
16	25	0.05	17.73	61.42	63.93
16	25	0.1	3.22	17.78	18.07
16	25	0.15	0.61	3.72	3.77
16	25	0.2	0.13	0.80	0.81
16	25	0.3	0.00	0.02	0.02
17	26	0.05	66.80	117.08	134.80
17	26	0.1	26.54	55.35	61.38
17	26	0.15	11.43	33.26	35.17
17	26	0.2	5.22	21.37	21.99
17	26	0.3	1.12	8.66	8.73
17	26	0.4	0.15	3.70	3.71
17	26	0.5	0.00	1.56	1.56
17	26	0.6	0.00	0.49	0.49
17	26	0.7	0.00	0.09	0.09
17	27	0.05	24.20	25.47	35.14
17	27	0.1	3.75	4.18	5.62
17	27	0.15	0.43	0.86	0.96
17	27	0.2	0.00	0.17	0.17
17	28	0.05	29.31	102.03	106.16
17	28	0.1	7.53	29.54	30.49
17	28	0.15	2.62	12.84	13.11
17	28	0.2	0.98	3.97	4.09
17	28	0.3	0.04	0.17	0.18
17	29	0.05	67.23	31.52	74.25
17	29	0.1	25.50	8.28	26.81
17	29	0.15	8.48	3.39	9.13
17	29	0.2	3.68	1.25	3.89
17	29	0.3	0.96	0.11	0.97
17	29	0.4	0.36	0.01	0.36
17	29	0.5	0.09	0.00	0.09
18	28	0.05	1.28	1.64	2.08
18	28	0.1	0.16	0.05	0.17
18	28	0.15	0.02	0.00	0.02
18	30	0.05	1.61	6.93	7.12
18	30	0.1	0.23	3.11	3.12
18	30	0.15	0.02	1.70	1.70

Table C.1. (continued)

Event No	Station No	a_c (g)	D_x (cm)	D_y (cm)	D_{SRSS} (cm)
18	30	0.2	0.00	0.94	0.94
18	30	0.3	0.00	0.13	0.13
19	31	0.05	0.43	0.28	0.51
19	32	0.05	0.96	43.45	43.47
20	33	0.05	0.44	0.32	0.55
21	34	0.05	41.02	43.54	59.82
21	34	0.1	9.64	18.78	21.12
21	34	0.15	1.48	7.18	7.33
21	34	0.2	0.03	2.80	2.80
21	34	0.3	0.00	0.13	0.13
21	35	0.05	0.59	0.32	0.67
22	36	0.05	0.27	2.00	2.02
22	36	0.1	0.00	0.84	0.84
22	36	0.15	0.00	0.30	0.30
22	36	0.2	0.00	0.04	0.04
23	37	0.05	2.31	2.46	3.38
23	37	0.1	1.01	0.67	1.22
23	37	0.15	0.36	0.22	0.42
23	37	0.2	0.07	0.03	0.08
24	38	0.05	50.63	10.35	51.68
24	38	0.1	15.43	1.77	15.54
24	38	0.15	2.95	0.44	2.98
24	38	0.2	0.23	0.01	0.23
24	39	0.05	0.03	0.89	0.89
24	40	0.05	13.12	18.26	22.48
24	40	0.1	3.61	4.72	5.95
24	40	0.15	0.99	1.23	1.58
24	40	0.2	0.07	0.18	0.19
25	41	0.05	0.37	0.72	0.81
25	41	0.1	0.02	0.03	0.04
25	42	0.05	1.59	1.35	2.09
25	42	0.1	0.16	0.04	0.16
26	43	0.05	3.25	3.85	5.04
26	43	0.1	0.43	0.36	0.56
27	43	0.05	0.68	0.37	0.77
27	43	0.1	0.01	0.00	0.01
28	43	0.05	30.37	25.25	39.49
28	43	0.1	10.47	8.53	13.51

Table C.1. (continued)

Event No	Station No	a_c (g)	D_x (cm)	D_y (cm)	D_{SRSS} (cm)
38	54	0.15	0.01	0.00	0.01
38	55	0.05	0.00	0.01	0.01
39	56	0.05	14.66	8.51	16.95
39	56	0.1	5.19	3.72	6.39
39	56	0.15	2.53	1.95	3.19
39	56	0.2	1.41	1.07	1.77
39	56	0.3	0.37	0.11	0.39
39	56	0.4	0.02	0.00	0.02
40	57	0.05	1.89	0.04	1.89
40	57	0.1	0.07	0.00	0.07
41	58	0.05	7.13	16.72	18.18
41	58	0.1	2.41	4.31	4.94
41	58	0.15	0.96	1.20	1.53
41	58	0.2	0.35	0.21	0.41
41	58	0.3	0.01	0.00	0.01
41	59	0.05	8.21	5.90	10.11
41	59	0.1	2.41	2.32	3.35
41	59	0.15	0.95	0.71	1.18
41	59	0.2	0.37	0.12	0.39
41	59	0.3	0.03	0.00	0.03
41	60	0.05	1.00	1.43	1.75
41	60	0.1	0.06	0.18	0.19
41	60	0.15	0.00	0.02	0.02
42	61	0.05	0.07	0.25	0.26
43	62	0.05	29.96	12.75	32.56
43	62	0.1	6.18	2.95	6.85
43	62	0.15	1.49	0.69	1.64
43	62	0.2	0.25	0.22	0.33
44	63	0.05	57.68	41.18	70.88
44	63	0.1	22.53	18.07	28.88
44	63	0.15	7.36	8.69	11.38
44	63	0.2	1.54	4.12	4.40
44	63	0.3	0.00	0.64	0.64
44	63	0.4	0.00	0.05	0.05
45	64	0.05	4.11	4.73	6.27
45	64	0.1	0.71	1.14	1.35
45	64	0.15	0.03	0.36	0.36
45	64	0.2	0.00	0.05	0.05

Table C.1. (continued)

Event No	Station No	a_c (g)	D_x (cm)	D_y (cm)	D_{SRSS} (cm)
46	65	0.05	1.45	0.57	1.56
46	65	0.1	0.34	0.08	0.35
46	65	0.15	0.01	0.00	0.01

APPENDIX D

THE LIST OF DECLUSTERED EVENTS FOR BACKGROUND SEISMICITY

Table D.1. List of declustered events

Longitude (deg.)	Latitude (deg.)	Year	Month	Day	Chosen M_w	Depth (km)	Hour	Min
38.4	40.3	1904	2	16	5.3	30.0	3	45
39.0	39.0	1905	12	4	6.5	30.0	7	4
40.4	39.3	1907	4	6	5.2	30.0	0	0
38.0	40.0	1909	2	9	6.2	60.0	11	24
37.0	39.0	1909	2	22	5.8	30.0	14	14
40.0	39.0	1909	3	5	5.5	30.0	12	16
36.8	40.3	1916	1	24	6.7	10.0	6	55
36.4	40.1	1923	4	29	5.9	10.0	9	34
37.9	40.2	1929	5	18	6.0	10.0	6	37
37.0	41.0	1929	8	21	4.6	5.0	1	24
38.8	40.3	1929	9	15	5.3	50.0	13	10
39.3	39.6	1930	4	9	5.3	10.0	5	27
39.2	39.7	1930	12	10	5.7	30.0	10	31
39.6	41.0	1931	7	31	5.2	10.0	0	25
36.6	40.3	1934	2	25	4.7	40.0	16	26
40.4	39.9	1937	12	7	4.9	60.0	9	31
38.0	39.0	1938	11	25	4.9	30.0	4	10
39.5	39.8	1939	12	26	7.7	20.0	23	57
38.1	40.0	1939	12	27	5.6	50.0	2	48
37.0	40.5	1939	12	28	5.8	40.0	3	25
38.5	40.5	1940	1	21	4.7	10.0	16	5
38.5	41.5	1940	1	26	4.9	10.0	20	56
36.5	40.9	1942	12	20	6.7	10.0	14	3
38.1	41.9	1945	11	29	4.8	40.0	12	3

Table D.1. (continued)

Longitude (deg.)	Latitude (deg.)	Year	Month	Day	Chosen M_w	Depth (km)	Hour	Min	
40.6	39.6	1949		8	17	5.4	60.0	20	45
38.3	39.8	1951		5	8	4.9	30.0	13	28
38.4	40.0	1953		10	8	5.2	10.0	10	26
40.0	40.0	1954		10	24	4.8	30.0	0	44
39.7	38.7	1957		4	18	4.9	10.0	5	25
40.5	39.4	1957		7	7	5.3	60.0	5	58
38.8	39.8	1959		12	13	4.7	10.0	2	7
38.8	40.2	1960		1	26	5.9	20.0	9	52
36.4	39.4	1960		3	12	4.7	5.0	21	25
39.1	39.6	1960		4	24	4.5	10.0	6	0
37.8	38.9	1960		6	19	4.7	70.0	2	29
37.3	40.6	1960		7	26	4.8	40.0	12	36
38.8	41.4	1963		4	22	5.5	60.0	15	38
38.3	39.0	1963		8	25	4.9	50.0	6	11
40.3	39.9	1964		2	24	4.7	57.0	11	32
37.6	41.1	1964		9	21	4.5	33.0	18	7
40.3	39.5	1964		11	16	5.2	16.0	5	27
36.5	39.5	1964		12	15	4.6	30.0	7	0
40.4	39.5	1967		7	26	5.9	30.0	18	53
40.2	39.8	1969		1	10	4.6	56.0	1	23
37.2	38.9	1969		9	5	4.5	47.0	17	53
38.8	39.6	1970		9	3	5.4	22.0	5	32
37.1	41.2	1971		4	17	4.9	33.0	16	37
40.0	39.3	1971		5	29	4.5	33.0	12	6
40.3	40.0	1973		3	19	4.5	33.0	12	20
39.2	38.8	1974		6	23	4.8	75.0	21	6
38.8	38.8	1974		8	21	4.6	11.0	13	36
40.0	39.5	1976		10	2	4.9	53.0	10	6
38.9	40.1	1976		10	19	4.5	39.0	23	8
40.1	39.9	1977		2	21	5.0	33.0	13	2
39.9	39.7	1978		2	15	4.7	48.0	3	17
39.6	39.9	1979		1	19	5.1	11.0	23	36
40.2	39.6	1980		4	30	4.7	33.0	2	28
40.3	39.9	1980		10	18	5.3	37.0	3	14

Table D.1. (continued)

Longitude (deg.)	Latitude (deg.)	Year	Month	Day	Chosen M_w	Depth (km)	Hour	Min
38.0	40.0	1981	6	23	4.6	33.0	17	3
40.4	39.5	1983	1	1	4.6	33.0	23	6
39.4	39.8	1983	11	18	5.0	37.0	1	15
39.4	39.8	1984	5	15	4.7	10.0	17	41
38.0	38.8	1984	7	15	4.7	10.0	20	0
40.0	40.2	1985	6	28	5.1	0.0	18	19
40.2	41.2	1986	11	1	4.9	29.0	3	18
40.2	40.0	1987	5	14	5.0	10.0	22	24
40.2	39.6	1989	5	20	5.4	34.0	20	44
40.1	40.1	1990	4	20	4.9	22.0	23	30
38.4	39.6	1990	5	3	4.7	24.0	21	5
39.6	39.7	1992	3	13	6.6	23.0	17	18
38.4	39.6	1993	6	14	4.7	26.0	19	59
36.5	39.5	1995	7	31	4.7	0.0	3	26
40.2	39.4	1995	12	5	5.7	33.0	18	49
39.6	39.1	1995	12	6	4.6	0.0	7	49
38.0	39.6	1996	6	6	4.5	0.0	15	33
36.4	40.5	1997	3	3	5.2	0.0	16	0
40.2	39.1	1998	11	10	4.8	1.0	8	42
38.2	39.3	1999	4	6	5.3	0.0	0	8
39.2	38.5	1999	4	13	4.9	10.0	9	47
36.7	39.5	1999	6	11	5.0	9.0	5	25
40.1	39.1	1999	8	22	4.5	10.0	11	12
40.2	39.3	2002	10	22	4.9	10.0	15	52
39.8	39.5	2003	1	27	6.1	10.0	5	26
38.2	39.6	2003	9	24	4.6	2.0	8	13
38.5	39.6	2004	9	30	4.5	10.0	9	42
37.3	40.4	2005	5	12	5.1	9.6	9	25
39.1	38.8	2005	10	18	4.6	5.0	7	17
38.9	41.2	2008	6	20	4.5	12.0	8	23
40.0	40.0	2008	9	17	4.9	5.0	12	8
40.5	40.4	2009	4	15	4.5	10.1	22	21
39.8	39.6	2009	7	30	5.0	3.3	7	37
38.0	39.6	2010	2	1	4.5	5.9	4	1

Table D.1. (continued)

Longitude (deg.)	Latitude (deg.)	Year	Month	Day	Chosen M_w	Depth (km)	Hour	Min
40.0	39.5	2011	8	24	4.5	5.0	15	47
38.9	39.8	2011	9	22	5.5	5.0	3	22
37.4	38.6	2012	2	16	5.0	5.0	11	1